Aspects of Conformal and Thermal Field Theories

A Thesis

Submitted to the

Tata Institute of Fundamental Research, Mumbai

for the degree of

Doctor of Philosophy

in

Physics

by

Kasi Jaswin

International Center for Theoretical Sciences, Bengaluru

Tata Institute of Fundamental Research

Bengaluru

November 2020

Final Version Submitted in September 2021

Declaration

This thesis is a presentation of my original research work. Wherever contributions of others are involved, every effort is made to indicate this clearly, with due reference to the literature, and acknowledgement of collaborative research and discussions.

The work was done under the guidance of Prof. Loganayagam R, at the International Centre for Theoretical Sciences, Tata Institute of Fundamental Research, Bangalore.

Kasi Jaswin

Kasi Jaswin
20/09/2021

In my capacity as supervisor of the candidate's thesis, I certify that the above statements are true to the best of my knowledge.

R. Loganayagam
Prof. Loganayagam R
Date: 20TH SEP 2021

Collaborators

- The first two chapters in the thesis was advised by my thesis supervisor Dr. Pallab Basu. The first chapter was in collaboration with Dr. Anosh Joseph.
- The last chapter was in collaboration with Dr. Sudip Ghosh, Dr. Amin Nizami and Dr. Rajesh Gupta.

List of publications

1. *Complex Langevin Dynamics in Large N Unitary Matrix Models*, with Pallab Basu and Anosh Joseph - [1].

2. *Higher point OTOCs and the bound on chaos*, with Pallab Basu - [2].

3. *ϵ-Expansion in the Gross-Neveu model from conformal field theory*, with Sudip Ghosh, Rajesh Gupta and Amin A. Nizami - [3].

Contents

To Family

Acknowledgments

First and foremost, I would like to sincerely thank my PhD advisor and mentor Pallab Basu. Without his constant guidance, mentor-ship and support, my pursuit of PhD would not have been complete.

I would like to thank all the members of ICTS-TIFR String Theory department, especially Loganayagam R, Sudip Ghosh, Anosh Joseph and Amin Nizami, for collobarotion and for stimulating discussions in Physics. Also I must thank the entire ICTS-TIFR family, for helping me in academics and a smooth stay during my PhD days.

I would like to thank my parents and my brother for being the constant pillar of emotional support in my tough PhD journey, which was a wild roller coaster full of emotions - hopes, dreams, frustrations, anxiety and euphoria! They were my inspiration and role models in my pursuit of higher education.

Some very dear friends, have played an important role in my PhD journey. They have always been available to listen to my ideas, grievances, etc. and provide useful inputs. I must thank them all, especially Jitendra Prakash, Arun Kumar, Amit Kumar, Aritra Kundu, Subiya Fathima, Sai Rohit and Phanindra.

I would like to thank Ziroh Labs, Bangalore where I am currently employed, for financially supporting me while writing the thesis. In Ziroh Labs, I especially thank Sweta Dey and Hrishikesh Dewan for a friendly, cordial environment and making my transition from academia-to-industry a total breeze.

1

Introduction

1.1 Motivation

A deeper understanding of Quantum Gravity(QG) is an important goal in theoretical physics. In the past century, interesting research was conducted in Semi-Classical Gravity employing perturbative tools in physics. In this regime, the gravitational force is much weaker as compared to other fundamental forces, the perturbative calculations prove to be insightful and threw in interesting questions and puzzles. This led physicists to explore new avenues and pursue for a full Quantum Gravity theory. Various ideas were tried out to quantize gravity, ranging from treating space-time as discrete, or to giving a geometric picture to remaining fundamental forces. Nonetheless, most of these approaches had limited success, and needs further research for concreteness. But, String Theory has emerged to be the most successful candidate in capturing some important aspects of QG. It's central idea of considering fundamental particles as excited states of tiny extended objects naturally encapsulate the massless spin-two state, gravitons which is the quanta of gravitational force. Amongst various successes it had, it's most important achievement is giving a well-defined example of QG - Gauge-Gravity duality [4, 5].

The Gauge-Gravity duality also famously referred to as the AdS/CFT correspondence is a nice toy example of Quantum Gravity. Over past two decades it has been theorist's favorite "laboratory" setup to test QG. It proposes that large N limits of certain Conformal Field Theories(CFT) in d dimension can be described in terms of (super-)gravity on $d+1$-dimensional Anti-de-sitter (AdS) space-time. Maldacena [4] gave the first complete example of this correspondence from Superstring Theory, where it was shown that Type IIB Superstring Theory on $AdS_5 \times S^5$ is dual to

$\mathcal{N} = 4$ super Yang-Mills theory in four dimensions with gauge group $SU(N)$, in the large N limit. Although, the main idea is not that supergravity, or string theory to be present, but any suitable theory on AdS_{d+1} space which would be equivalent to a CFT in d dimensions. This correspondence was more mathematically established in [5, 6] by equating correlation functions both sides. Interestingly the quantum effects which come from $1/N$ corrections of the correspondence were computed, and agreeable matching was found. Therefore this correspondence is true in the quantum regime and not strictly a classical-correspondence statement. This opened the flood-gates of research on QG for past couple of decades. And has possibly revealed an important nature of QG - the "Holographic principle", i.e QG could be described by a Quantum Field Theory(QFT), which usually exists in one lower dimension.

AdS/CFT had an enormous success in understanding the Black Holes(BH), especially in the study of entanglement entropy, phase-transitions and other thermodynamical properties. Also this framework has led to a lot of open problems which wasn't accessible earlier. Some of the important open problems are the Quantum Information Paradox, equivalent de-Sitter/CFT correspondence and phase-space of Quantum-Chromo-Dynamics(QCD). Although, to have a significant progress in these problems there are various challenges. Amongst many, two major stumbling blocks turn out to be our lack of understanding of open Quantum Field Theories(QFT) and strongly-coupled QFTs. Though they existed before, discovery of AdS/CFT correspondence has given us sharper questions to pursue.

Open QFTs stand as interesting open problem in itself. Any physical system in the world, strictly speaking is an open system, as it exchanges energy and matter with the environment. Even the act of measurement can be thought of as forcing the environmental variables to interact with the physical system. A lot of paradoxes that arose in quantum mechanics, like the Schrodinger's cat or the Quantum Zeno Paradox could be traced to open QFTs. Recent technological advancement in Quantum Information and Quantum Computation would also need a better understanding of open QFTs. Also as our Universe is undergoing an accelerated expansion, we can only access a patch of space-time. Hence the study of large space-time structure of Universe fall under the regime of open QFTs. Possibly, one of the greatest unsolved problems in Physics - the mismatch of Cosmological constant and zero-point energy predicted by QFT which of order 10^{120}, could be addressed

if one understood open QFTs better! In the context of AdS/CFT, it appears naturally when we want to address the Black-Hole Information paradox. The paradox arises while reconciling notions of general relativity with quantum mechanics. Since a region of space-time behind the horizon isn't accessible, the dual field theory can be thought of as attached to a heat bath, where the temperature is a function of the area of the horizon. Also if matter falls into the BH, the dual field theory is an open QFT. Although Schwinger-Keldysh formalism is a formalism to study open QFT, but there are technical difficulties in doing calculations. Therefore it is interesting to invent new methods to deal with open QFT.

Challenges in understanding strongly coupled field theory are ubiquitous, ranging from Condensed matter physics to QCD. It has been an age-old problem in theoretical physics which has inspired new techniques routinely. In some special cases, like large-N limit of field theories or Supersymmetric field theories, strongly-coupled systems have been exactly solved, but the generic case still remains an open problem. In the context of AdS/CFT conjecture, strongly coupled theories naturally appear as they are expected to be dual to a weak gravitational theory. In this regime the usual perturbative expansion is not helpful. But interestingly, few examples of AdS/CFT have emerged in lower dimensions, where exploiting the symmetries of the field theory, many calculations are doable. For instance, in AdS_3/CFT_2 correspondence, we have a good mathematical understanding of two-dimensional CFT(as it has infinite symmetries). These infinite symmetries allow for exact computations in the CFT side, and has shed light on the dual gravitational theory. Inspired by the success of AdS/CFT in lower dimensions, recently a new model was discovered in one further lower dimension. It is a (conformal)-quantum mechanical (QM) model called the Sachdev-Ye-Kitaev (SYK) [7, 8] model, and is thought to have a bulk dual in two-dimensions. It has generated an excitement, as it a non-trivial example of strongly-coupled QM model which could be analytically solved. Also, it has led to discovery of few similar solvable QM models, like the Gurau-Witten [9, 10] and Klebanov-Tarnopolsky [11] tensor models.

1.2 Problems addressed in the Thesis

During my graduate studies, I had the opportunity of studying a few aspects of open and strongly-coupled QFTs. I have worked on three different projects, which I describe in the following sections. These projects are motivated by recent approaches to address aforementioned problems of physics.

1.2.1 Complex Langevin Dynamics in Large N Unitary Matrix Models

Exploring the QCD matter phase diagram has been important quest for both theoretical and experimental high-energy physicist alike. The known phase diagram remains mostly conjectural because it is difficult to perform calculations, as it is a strongly coupled theory at finite density and temperature. The only available calculational tool is Lattice QCD which involves brute computational power. Lattice QCD uses Monte-Carlo simulations to explore various configurations in the ensemble with a probability weight which is positive definite. But in the case of QCD, the effective action on integrating out fermionic degrees of freedom becomes complex and so does the measure. Because of this technical obstacle, known as the "Fermion Sign" problem, Lattice QCD can only be used at low density and high temperature. Sign problem often arises when we numerically simulate open QFTs and non-equilibrium physics.

An alternative approach has been invented recently based on "Complex Langevin Dynamics". The complex Langevin method was proposed in the early 1980s by Klauder [12] and Parisi [13]. Though it became popular in the beginning certain problems were found immediately after. First one was the problem of runaways, where the simulations would not converge and the second one was the problem of convergence to a wrong limit. In recent years the complex Langevin method has been revived, with sometimes cases of impressive success [14, 15, 16]. It has been shown recently that complex Langevin simulations produce seemingly correct answer, even when the fermion sign problem is severe, for one-, three- and four-dimensional field theories with nonzero chemical potential [17, 18]. The central idea is "Stochastic Quantization" where expectation values of observables are obtained as equilibrium values of a stochastic process. In order to achieve this we evolve the system in a fictitious time τ, subject to a stochastic noise. That is, the system evolves according

to Langevin dynamics. When the action is complex it is still possible to consider Langevin dynamics. The force (gradient of the action) becomes complex in this case making the fields also complex during the evolution.

In this project we consider simple QFTs, large N Unitary Matrix Models with complex actions and we make use of complex Langevin dynamics with stochastic quantization to study them. They exhibit sign problem due to the fact that the action is complex. Standard Monte Carlo methods fail to produce the correct equilibrium distributions of these models. We can use discretized complex Langevin equation with Euler method (which is a first order algorithm) to find the equilibrium field distributions of these models. If there is only one unitary matrix we can go the diagonal gauge, and the fields/degrees of freedom can be expressed in angles θ_i. Then let us take $\theta_i(\tau)$ with $i = 1, \cdots, N$ as the complexified angle variables of the gauge link $U(\tau)$ at a Langevin time τ. We have the discrete Langevin evolution equation

$$\theta_i(\tau + \Delta\tau) \;=\; \theta_i(\tau) - \left[\frac{\partial S}{\partial \theta_i(\tau)}\right] \Delta\tau + \sqrt{\Delta\tau}\, \eta_i(\tau), \tag{1.2.1}$$

where $\Delta\tau$ is the Langevin time step, and $\eta_i(\tau)$ is a Gaussian random variable satisfying the conditions

$$\langle \eta_i(\tau) \rangle = 0, \quad \langle \eta_i(\tau)\eta_j(\tau') \rangle = 2\delta_{ij}\delta_{\tau\tau'}. \tag{1.2.2}$$

We also need to impose the $SU(N)$ constraint on the complexified angular variables after each Langevin time step. That is,

$$\sum_{i=1}^{N} \theta_i(\tau) = 0. \tag{1.2.3}$$

This can be easily implemented by subtracting the average value $\theta_{\text{av}}(\tau)$ from each $\theta_i(\tau)$ variable.

To demonstrate the effectiveness of Complex Langevin Dynamics, we begin by studying a simple, yet non-trivial model – a complexified version of Gross-Witten-Wadia (GWW) Model [19, 20]. We refer to our model as *ab-Model*. It has two phases, confined and deconfined, exhibiting a third-

order phase transition. The action is given by

$$S = N\left(a\,\mathrm{Tr}\,U + b\,\mathrm{Tr}\,U^{\dagger}\right) \tag{1.2.4}$$

where, $a, b \in \mathbb{C}$, U is an element of $SU(N)$, and $a = b$ is the Gross-Witten-Wadia model. We have analytically solved the model in the Large N limit and compared Complex Langevin simulations and found agreement. For instance, considering $b = 2a$, we have plotted the expectation value of Polyakov Loop, $\langle \mathrm{Tr}(U) \rangle$, we find a good match at different values of a.

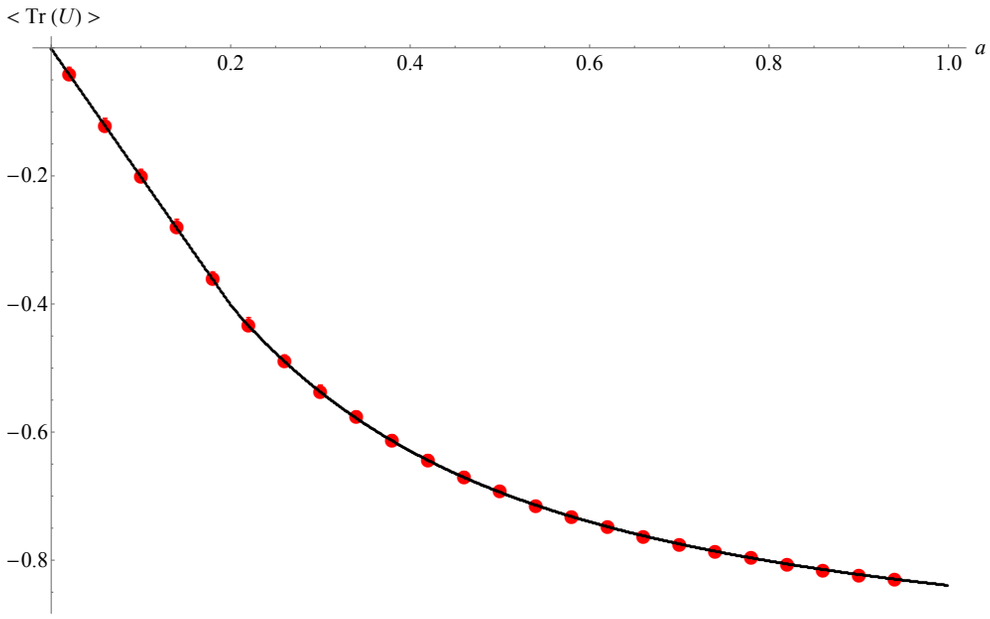

Then we turn to a more physical example; if we consider a a one-loop formulation of QCD (and analogous $SU(N)$ gauge theories) on compact spaces $S_1 \times S_3$, a unitary matrix model arises. The one-loop effective action of QCD on $S^1 \times S^3$ with chemical potential μ and quark mass m has the form [21], with thermal Polyakov loop as the unitary matrix model

$$\begin{aligned} S \;=\; & \sum_{n=1}^{\infty} \frac{1}{n} z_b\left(\frac{n\beta}{R}\right) \mathrm{Tr}\,U^n \;\mathrm{Tr}\,U^{\dagger n} \\ & + \sum_{n=1}^{\infty} \frac{(-1)^n}{n} N_f z_f\left(\frac{n\beta}{R}, mR\right)\left[e^{n\beta\mu}\,\mathrm{Tr}\,U^n + e^{-n\beta\mu}\,\mathrm{Tr}\,U^{\dagger n}\right]. \end{aligned} \tag{1.2.5}$$

The quadratic term in Polyakov loop is the contribution from adjoint fields and the linear term is the contribution from the fundamental matter fields. Here, we have taken the adjoint contribution to be bosonic and the contribution from fundamental fields to be fermionic. In free theory the

effective action is determined in terms of single particle partition function

$$z_b\left(\frac{\beta}{R}\right) = 2\sum_{l=1}^{\infty} l(l+2)e^{-\beta(l+1)/R}, \tag{1.2.6}$$

and

$$z_f\left(\frac{\beta}{R}, mR\right) = 2\sum_{l=1}^{\infty} l(l+1)e^{-\frac{\beta}{R}\sqrt{(l+\frac{1}{2})^2+m^2R^2}} \tag{1.2.7}$$

In the above equations R is the radius of S^3 and m is the mass of the fundamental fermions. We use dimensionless variables β/R, μR and mR in numerical simulations. In the low temperature limit, $\beta \to \infty$, we have $z_b(\infty) = 0$ and so the gluonic contribution is negligible. Thus the action is

$$S = S_{\mathrm{Vdm}} + S_f, \tag{1.2.8}$$

where, S_{Vdm} is the van der Monde term and S_f is the fundamental fermionic contribution. The fermionic part could be summed in a logarithm

$$S[U] = -\sum_{l=1}^{\infty} \sigma_l \left(\log\left[\det\left(1+e^{\beta(\mu-\epsilon_l)}U\right)\det\left(1+e^{\beta(-\mu-\epsilon_l)}U^{-1}\right)\right]\right). \tag{1.2.9}$$

Truncating the above action to a single level, in a double scaling limit:

$$\begin{aligned} \beta &\to \infty, \\ \mu &\to \epsilon_0, \\ \exp(\beta(\mu-\epsilon_l)) &= \xi, \end{aligned} \tag{1.2.10}$$

where ϵ_0 is a fixed quark energy level and ξ the effective fugacity, the action becomes

$$S[U] = -\sigma \log\left(1+\xi U\right) \tag{1.2.11}$$

which can be solved analytically. Comparing complex Langevin simulations against analytic results we get a good match. For instance, the expectation value of Polyakov Loop and Inverse Polyakov Loops are evaluated for different values of N.

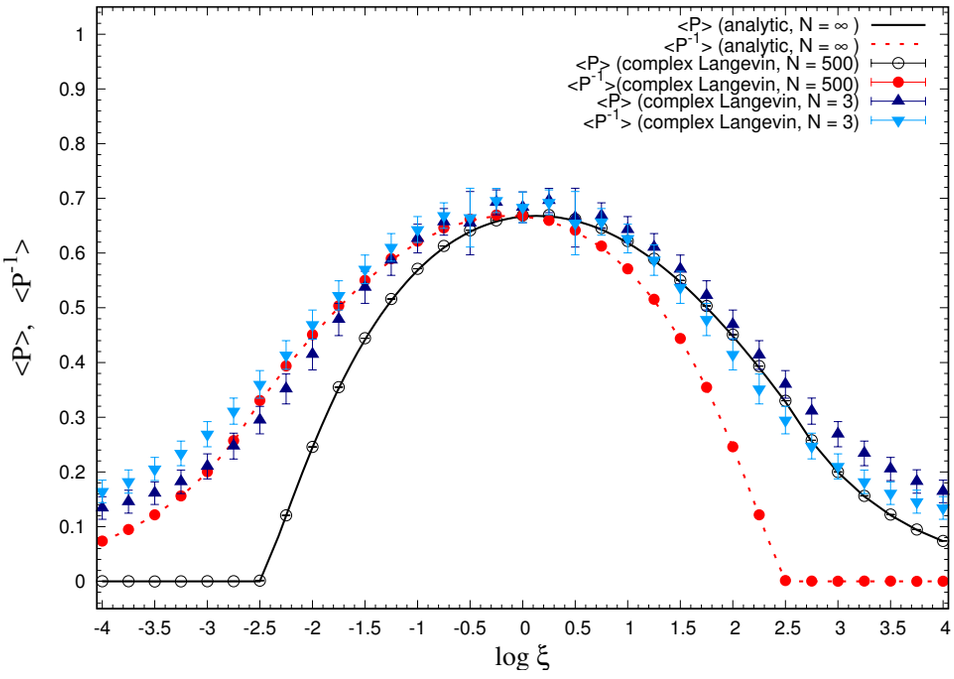

1.2.2 Bound on higher-point Out-of-time-ordered-correlators (OTOCs)

Recent attempts to reconcile Quantum Gravity and Quantum Mechanics, has led to interesting developments. Since the space-time behind the horizon is classically inaccessible in a Black Hole geometry it becomes interesting to invoke the notions of Quantum information and computation(QIQC) in such a setup. In the past decade, many creative questions have been posed using QIQC which has led to interesting revelations of QG. One such question arising from quantum information theory was to quantify the speed at which scrambling of information happens in a given system. Applying it in the context of Black Hole, it was conjectured that there is a universal bound on information scrambling [22, 23]. Using AdS/CFT, the information scrambling bounds translated to a universal bound on the growth of quantum chaos [24].

Quantum Chaos was inspired by the definition of classical chaos, which quantified the behaviour of dynamical systems that are highly sensitive to initial conditions. In mathematical terms, given two starting trajectories in the phase space that are infinitesimally close, with initial separation δx_0, at late times diverge exponentially as,

$$|\delta x(t)| = e^{\lambda t}|\delta x_0| \tag{1.2.12}$$

where λ is known as the Lyapunov exponent. Schematically the above equation can be expressed in terms of Poisson Bracket,

$$\frac{\partial x(t)}{\partial x_0} = \{x(t), p\}_{PB} \tag{1.2.13}$$

Now lifting the observables to operators, and Poisson bracket to a commutator, we get a diagnostic of quantum chaos. But in the thermal ensemble the commutator is often zero and one may need to consider the square of it,

$$\begin{aligned} C &= \left\langle [W(t), V(0)]^2 \right\rangle_\beta , \\ &= \mathrm{Tr}\left[e^{-\beta H} [W(t), V(0)]^2 \right] . \end{aligned} \tag{1.2.14}$$

Here we have generalized $\hat{x}, \hat{p}$ operators to generic Hermitian operators W, V. On expanding the commutator square we get two pieces,

$$C = \left\langle [W(t), V(0)]^2 \right\rangle_\beta = -2 \left\langle W(t)W(t)V(0)V(0) \right\rangle_\beta + 2 \left\langle W(t)V(0)W(t)V(0) \right\rangle_\beta . \tag{1.2.15}$$

The first term in the above expression is a time-ordered-correlator (TOC) and the second term is an out-of-time-ordered-correlator (OTOC). The first term in the above expression goes to zero at large time due to usual diffusion/relaxation. At a time scale of the order of diffusion time t_d, we have, $W(t)V(0) \sim e^{-\frac{t}{t_d}}$. Hence diffusion with large N factorization gives thermal factorization of TOCs, i.e. all time ordered thermal correlators factorizes to a product of thermal expectations. For our particular example in hand, we have,

$$\left\langle W(t)W(t)V(0)V(0) \right\rangle \approx \left\langle W(0)W(0) \right\rangle \left\langle V(0)V(0) \right\rangle , \tag{1.2.16}$$

at large time. Hence the large time behavior of the commutator is given by the OTOC.

At a first look, OTOC may apparently seem to have a similar large N factorization as TOC,

$$F \approx 2 \left\langle W(t)V(0) \right\rangle^2 + \left\langle W(t)W(t) \right\rangle \left\langle V(0)V(0) \right\rangle + O(1/N_d) \tag{1.2.17}$$

However, the catch is that the sub-leading part of $F(t)$ grows with time. One may argue that for a system with a large number of degrees of freedom, F tends to zero asymptotically. This could be understood as following: in an chaotic system, at an intermediate time much larger than the diffusion time $t \gg t_d$, behavior of C is given by

$$C \propto \epsilon e^{2\lambda t}, \tag{1.2.18}$$

where ϵ is a small parameter related to the number of degrees freedom and λ is the Lyapunov exponent. Hence, F at an intermediate time would then behave like,

$$F \approx f_0 - \epsilon f_1 e^{2\lambda t}. \tag{1.2.19}$$

The second term become important at time scale $t_* \approx -\frac{1}{\lambda}\log\epsilon$, which is known as the scrambling time.

Using complex analytic techniques, [24] proves that maximum possible value of Lyapunov exponent has an upper bound proportional to the temperature,

$$\lambda_{max} \leq \frac{2\pi}{\beta}. \tag{1.2.20}$$

This maximum value of Lyapunov exponent is also known to saturate in holographic models with gravity [25], certain two dimensional CFTs [26] and also in SYK model ([7, 8, 27]).

In our work [2], we continued the same logic as that of the previous paragraph, considered the higher power of the commutator,

$$C = \left\langle \prod_{i=1}^{r} [V(T), V(0)]^{2n} \right\rangle \tag{1.2.21}$$

and found the chaos bound of such a correlation function. For that purpose, we considered the most generic n-point OTOC with a given scheme of regulation may be expressed as,

$$\mathcal{F}_\beta(t_i, \tau_i) = \mathrm{Tr}\left(e^{-\beta_1 \hat{H}} V_1(t_1) e^{-\beta_2 \hat{H}} V_2(t_2) \dots e^{-\beta_n \hat{H}} V_n(t_n) \right) \tag{1.2.22}$$

where, $\hat{H}$ is the Hamiltonian of the system, $\beta_i > 0$ are separations between two consecutive operator insertions along the thermal circle, and therefore satisfy the constraint,

$$\sum_{i=1}^{n} \beta_i = \beta \tag{1.2.23}$$

where β is the inverse temperature of the heat bath i.e the circumference of the thermal circle. $\mathcal{F}_\beta(t_i, \tau_i)$ can visualized as

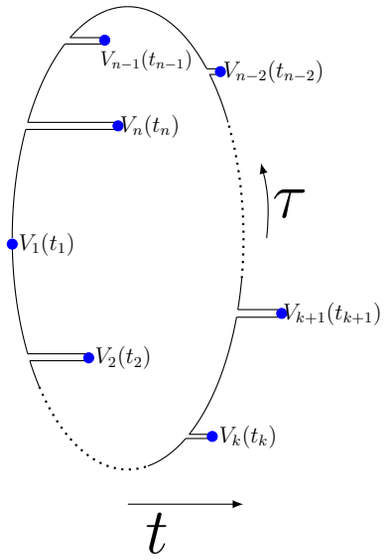

Figure 1.1: Generic n-point correlator on a thermal circle of radius β

where $V_i(t_i)$'s are thermal ordered along τ direction and time is perpendicular to the thermal circle. We restrict ourselves to increasing linear functions.

$$t_i \equiv f_i(t) = \omega_i t \qquad ; \omega_i \geq 0 \tag{1.2.24}$$

and under analytic continuation $t \to t + i\tau$, we find the domain of analyticity to be a half-strip $\mathcal{D} = (0, \infty) \times i(-\tau_-, \tau_+)$,

$$\tau_- = \text{min.} \left\{ \frac{\beta_j}{\omega_{j,j-1}} \right\} < \tau < \text{min.} \left\{ \frac{\beta_i}{\omega_{i-1,i}} \right\} = \tau_+. \tag{1.2.25}$$

Choosing an appropriate normalization factor $\mathcal{N}_\beta$, we show that $\mathcal{F}_\beta(t_i, \tau_i)$ decays at late times as,

$$|\mathcal{F}_\beta| \lesssim \mathcal{N}_\beta - |\mathcal{F}_\beta(t_0)| e^{\frac{\pi}{\tau_+ + \tau_-} t} \tag{1.2.26}$$

and the Lyapunov exponent can be read-off as $\lambda_L = \dfrac{\pi}{\tau_+ + \tau_-}$ thus, it is just a function of the width of the strip $\mathcal{D}$. Therefore considering a correlators which is has a form $\langle (V(t)W(0))^n \rangle$, choosing a equispaced regulator,

$$F^n(t) = \mathrm{Tr}\left(\hat{\rho}^{\frac{1}{2n}} V(t) \hat{\rho}^{\frac{1}{2n}} W(0)\right)^n \tag{1.2.27}$$

we show that the Lyapunov exponent $\lambda_l = \frac{n\pi}{\beta}$ for such correlators.

1.2.3 $\epsilon-$Expansion in the Gross-Neveu model from Conformal Field Theory

Symmetries have played an important role in studying strongly-coupled field theories. Instead of working with a Lagrangian and doing tedious Feynman diagrams computation, the idea was to study correlators and S-matrix. This emerged in the 1960's known as the S-matrix bootstrap program. The philosophy was to derive as much information as possible about the strong interaction from plausible assumptions about the S-matrix which were analyticity, crossing symmetry and unitarity. In early days, much of the success was in the context of two-dimensional conformal field theories, i.e Conformal bootstrap program. Very recently there has been a revival of Conformal bootstrap program in higher dimensional field theories.

In higher dimensions, conformal bootstrap was developed in [28, 29] numerically using semi-definite programming. The method has been used to obtain many general results in conformal and superconformal field theories in three, four, five and six dimensions. Applied to the conformal field theory describing the critical point of the three-dimensional Ising model, it produced the most precise predictions [30, 31] for its critical exponents. An analytical approach using Mellin space representation of CFT was introduced in [32].

Based on the techniques introduced by Rychkov and Tan [33], in this project [3], we study a

certain non-Lagrangian description of fermionic CFTs. The underlying idea is, as a consequence of equations of motion of Gross-Neveu model, the conformal multiplets ψ and $\psi(\bar{\psi}\psi)$ combine at the Gross-Neveu fixed point. Using this fact and other conformal properties we compute the leading order - in the epsilon expansion - anomalous dimensions of a class of composite operators in the Gross- Neveu model in $2+\epsilon$ dimensions. And it was accomplished without relying on Feynman diagrams and conventional perturbation theory techniques.

The Gross-Neveu model is a renormalizable field theory in two dimensions. It is described by a $U(\tilde{N})$ symmetric action for $\tilde{N}$ massless self-interacting Dirac fermions $\{\psi^I, \bar{\psi}^I\}$. We will consider the Gross-Neveu model in $2+\epsilon$ dimensions

$$S = \int d^{2+\epsilon}x \left[\bar{\psi}^I \partial\!\!\!/ \psi^I + \frac{1}{2} g\mu^{-\epsilon} \left(\bar{\psi}^I \psi^I\right)^2\right], \quad I = 1, ..., \tilde{N}. \tag{1.2.28}$$

Here g is the coupling constant which is dimensionless in two dimensions. This theory has a weakly coupled UV fixed point given by the non-trivial zero of the beta function,

$$\beta(g) = \epsilon g - (N-2)\frac{g^2}{2\pi}, \qquad N = \tilde{N}\,\mathrm{Tr}\{\mathbb{I}\}\,. \tag{1.2.29}$$

Here $\mathrm{Tr}\{\mathbb{I}\}$ is the trace of identity in Dirac fermion space, and in two dimensions $N = 2\tilde{N}$. The fixed point occurs at

$$g_* = \frac{2\pi\epsilon}{N-2} + \mathcal{O}(\epsilon^2)\,. \tag{1.2.30}$$

The dimensions of the fermion ψ^I, Δ_1, and composite scalar $\bar{\psi}^I\psi^I$, Δ_2, are given by

$$\begin{aligned} \Delta_1 &= \frac{d-1}{2} + \gamma_1 = \frac{1}{2} + \frac{\epsilon}{2} + \gamma_1\,, \\ \Delta_2 &= d - 1 + \gamma_2 = 1 + \epsilon + \gamma_2\,. \end{aligned} \tag{1.2.31}$$

The anomalous dimensions of the fundamental fermions and the composite scalar in the ϵ-expansion have been computed in perturbation theory using the standard Feynman diagram techniques and,

to leading order in ϵ, are given by

$$\gamma_1 = \frac{N-1}{16\pi^2} g_*^2 = \frac{(N-1)\,\epsilon^2}{4\,(N-2)^2}\,,$$
$$\gamma_2 = -\frac{N-1}{2\pi} g_* = -\frac{N-1}{N-2}\epsilon\,. \tag{1.2.32}$$

Assuming that the fixed point is a conformal fixed point, we derive the above expressions and for higher dimensional composite operators using CFT techniques. Starting with the equations of motion at Gross-Neveu fixed point,

$$\not{\partial}\psi^I = -\frac{g\mu^{-\epsilon}}{2\pi}\psi^I\left(\bar{\psi}^J\psi^J\right)\,, \tag{1.2.33}$$
$$\partial_\mu\bar{\psi}^I\Gamma^\mu = \frac{g\mu^{-\epsilon}}{2\pi}\bar{\psi}^I\left(\bar{\psi}^J\psi^J\right)\,. \tag{1.2.34}$$

In the free theory the fermions satisfy $\not{\partial}\psi^I = 0,\ \partial_\mu\bar{\psi}^I\Gamma^\mu = 0$ which are the shortening conditions for the multiplets $\{\psi^I\}_{\text{free}}$ and $\{\bar{\psi}^I\}_{\text{free}}$. In addition all other bilinears of ψ^I and $\bar{\psi}^I$ are primary operators. At the interacting fixed point $\{\psi^I\}_{\text{fixed pt}}$ and $\{\bar{\psi}^I\}_{\text{fixed pt}}$ are no longer short multiplets. The primary operators in the free theory $\psi^I\left(\bar{\psi}^J\psi^J\right)$ and $\bar{\psi}^I\left(\bar{\psi}^J\psi^J\right)$ now become descendants of the $\{\psi^I\}_{\text{fixed pt.}}$ and $\{\bar{\psi}^I\}_{\text{fixed pt.}}$ respectively. Now assuming that every operator $\mathcal{O}$ in the free theory has a counterpart $V_\mathcal{O}$ at the interacting fixed point. The operators $V_\mathcal{O}$ and their correlation functions in the interacting theory, approach, respectively, $\mathcal{O}$ and their free correlation function in the $\epsilon \to 0$ limit. In the Gross Neveu model at the IR free point, various operators are constructed out of products of elementary operators ψ and $\bar{\psi}$. Denoting these operators in the interacting theory as V_{2p}, V_{2p+1} and $\bar{V}_{2p+1}$ such that in the limit $\epsilon \to 0$ (IR free point)

$$V_{2p} \to (\bar{\psi}\psi)^p, \quad V^I_{2p+1} \to (\bar{\psi}\psi)^p\psi^I\,, \quad \bar{V}^I_{2p+1} \to (\bar{\psi}\psi)^p\bar{\psi}^I\,. \tag{1.2.35}$$

And requiring the multiplet recombination as

$$\not{\partial}V^I_1 = \alpha V^I_3, \quad \partial_\mu\bar{V}^I_1\Gamma^\mu = -\alpha\bar{V}^I_3\,, \tag{1.2.36}$$

for some unknown function $\alpha \equiv \alpha(\epsilon)$, which is determined by OPE expansion and three-point

functions. Demanding in $\epsilon \to 0$ limit,

$$\left\langle V_{2p}(x_1) V^I_{2p+1}(x_2) \bar{V}^J_3(x_3) \right\rangle \to \left\langle \left(\bar{\psi}\psi\right)^p (x_1) \left(\bar{\psi}\psi\right)^p \psi^I(x_2) \left(\bar{\psi}\psi\right) \bar{\psi}^J(x_3) \right\rangle \,. \tag{1.2.37}$$

and,

$$\left\langle V^I_3(x_2) \bar{V}^J_3(x_3 \right\rangle \to \left\langle \left(\bar{\psi}\psi\right) \psi^I(x_2) \left(\bar{\psi}\psi\right) \bar{\psi}^J(x_3) \right\rangle \tag{1.2.38}$$

the scaling dimensions of the following composite operators are,

$$\Delta_{(\bar{\psi}\psi)^p} \equiv \Delta_{2p} = p + p\epsilon - \frac{p(N-p)}{(N-2)}\epsilon + O(\epsilon^2)\,, \tag{1.2.39}$$

$$\Delta_{(\bar{\psi}\psi)^p\psi} \equiv \Delta_{2p+1} = (p+\frac{1}{2}) + (p+\frac{1}{2})\epsilon - \frac{p(N-p-1)}{(N-2)}\epsilon + O(\epsilon^2) \tag{1.2.40}$$

and the leading order anomalous dimension of scalar primary of the form,

$$\mathcal{O}^{(IJ)} = \bar{\psi}^I \psi^J - \frac{\delta^{IJ}}{\tilde{N}} \bar{\psi}^K \psi^K \tag{1.2.41}$$

to be,

$$\gamma_{\mathcal{O}^{(IJ)}} = \frac{1}{N-2}\epsilon\,. \tag{1.2.42}$$

2

Complex Langevin Dynamics in Large N Unitary Matrix Models

2.1 Introduction

A nonperturbative study of the phase structure of QCD at finite temperature and nonzero baryon chemical potential still remains an outstanding problem [34, 35]. This is due to the fact that the fermion determinant becomes complex and the theory has a sign problem. The standard methods to study the theory, lattice QCD algorithms based on importance sampling, fail to produce reliable simulations. There have been recent developments in tackling this problem. One method is the use of complex Langevin dynamics with stochastic quantization [36, 13]. This method is not based on importance sampling but instead on a stochastic exploration of an enlarged (complexified) field configuration space. Another recently proposed method is the Lefschetz thimble method [37, 38, 39, 40, 41, 42], which is also based on complexification of the original real field variables.

The complex Langevin method was proposed in the early 1980s by Klauder [12, 43, 36] and Parisi [13]. Though it became popular in the beginning certain problems were found immediately after. First one was the problem of runaways, where the simulations would not converge and the second one was the problem of convergence to a wrong limit. In recent years the complex Langevin method has been revived, with sometimes cases of impressive success [44, 45, 46, 47, 14, 15]. It has been shown recently that complex Langevin simulations produce seemingly correct answer, even when the fermion sign problem is severe, for one-, three- and four-dimensional field theories with nonzero chemical potential [17, 48, 49, 18]. There have also been studies of supersymmetric matrix

models based on complex Langevin dynamics. See Refs. [16, 50, 51].

In this work, we consider a large N unitary matrix model at low temperature with a finite quark chemical potential and quark mass. This model is obtained from the one-loop formulation of QCD on $S^1 \times S^3$ at finite temperature with finite quark chemical potential μ, quark mass m, and with N number of colors and N_f number of quark flavors. After integrating out the quark and gauge degrees of freedom we obtain the model of our interest – a conventional unitary matrix model with a complex action. The unitary matrix U in this model is the holonomy (Wilson loop) of the gauge field around the thermal time circle in Euclidean space. We can use the expectation value of the trace of Polyakov line in the fundamental representation as order parameter for the phase transitions. It is zero in the confined phase and non-zero in the deconfined phase. The model is interesting as it exhibits a rich thermal phase structure. When the chemical potential passes one of the quark energy levels there is a third order Gross-Witten-Wadia (GWW) transition from a confined to a deconfined phase and back again. This model also exhibits another interesting feature known as the *Silver Blaze* behavior. When the quark mass is nonvanishing the bulk observables of the model are nearly zero until the onset transition to the deconfined phase, which occurs when the chemical potential reaches the value of the lightest quark mass.

In the matrix model with complex action, the dominant contributions to the functional integral come from complexified gauge field configurations. Due to this reason, the saddle point eigenvalues of the unitary matrix U lie off the unit circle, on a contour in the complex plane. The eigenvalues of U can be written as $\exp(i\theta_i)$ with θ_i the angle variables and $i = 1, \cdots, N$. We can make a change of variables such that the functional integral reduces to an integral over $\{\theta_i\}$. At large N, the functional integral is dominated by a single saddle point but since the action is complex this saddle point configuration lies out in the complex plane where the θ_i are no longer real. As a consequence, the Polyakov line and the inverse Polyakov line are not equal, that is, $\langle P \rangle \neq \langle P^{-1} \rangle$. Through complex Langevin simulations we indeed confirm this behavior. In fact the behavior of inverse Polyakov line precedes that of the Polyakov line as a function of chemical potential. This feature was observed analytically in an earlier work by Hands, Hollowood and Myers in Ref. [21].

In this work, we examine this large N unitary matrix models using complex Langevin simulations. It is possible to generate representative field configurations by integrating a stochastic differ-

ential equation, known as the complex Langevin equation. The drift terms arising from the complex action force the field variables to evolve in an extended (complexified) field space, in which the large regions where the observables are plagued by phase fluctuations are avoided [14].

When N is large, we can consider the gauge field, corresponding to the angles of the Polyakov line, as a distribution on a contour. From the equation of motion, the saddle point distribution of the Polyakov line eigenvalues can be calculated analytically and plotted by mapping the angles from an arc on the unit circle to a contour over the same range of angles in the complex plane [21]. The theory is said to be in a confined phase when the contour on which the Polyakov line eigenvalues are distributed is closed. The contour opens up in between quark energy level transitions giving rise to a deconfined phase in the theory. The third derivative of the grand potential is discontinuous at each energy level crossing. These are characteristic features of a third order, GWW transition [19, 20].

This chapter is organized as follows, in Sec. 2.2 we give a brief outline of complex Langevin dynamics and stochastic quantization. In Sec. 2.3 we discuss a simple yet nontrivial matrix model called the ab-Model, which is a complexified version of the Gross-Witten-Wadia (GWW) model. This model has two phases, confined and deconfined, and it exhibits a third-order phase transition. In Sec. 2.4 we discuss another interesting large N unitary matrix model which arises in the one-loop formulation of QCD on compact spaces. The model possess a tower of quark energy levels due to compactification and is defined for positive and negative chemical potential values. We then focus on to a truncated cousin of this model - a single quark energy level matrix model with positive chemical potential. This model also has a complex action and captures the physics we are interested in without loss of generality. We can define an effective fugacity in this model, and as we change the fugacity, the model exhibits confinement/deconfinement phase transitions. We show the eigenvalue distributions corresponding to the confined (closed) and deconfined (gapped) phases of the theory using complex Langevin simulations. We also simulate the behaviors of Polyakov lines and fermion number density as a function of effective fugacity. We simulate the model for a range of temperatures and chemical potentials to study its phase structure. We also show the phase diagram of the model, at low temperature, on the (μ, β) plane, in the vicinity where quark energy level equals the chemical potential. Our simulation results agree well with the schematic prediction given

by Hands, Hollowood and Myers in Ref. [21]. We then simulate the model at large quark mass and show that the bulk observables exhibit the Silver Blaze behavior – the observables are roughly zero until the onset transition to the deconfined phase, which occurs when the chemical potential equals quark mass. We then move on to discuss the single-level model with a simple non-trivial gauge interaction turned on. We study the behavior of observables as a function of the interaction parameter. We see that the model prefers to stay in the confined phase as the interaction strength is increased. In Sec. 2.5 we provide conclusions and discussions.

2.2 Complex Langevin Dynamics

The central idea of stochastic quantization is that expectation values of observables are obtained as equilibrium values of a stochastic process [52, 53]. In order to achieve this we evolve the system in a fictitious time τ, subject to a stochastic noise. That is, the system evolves according to Langevin dynamics. When the action is complex it is still possible to consider Langevin dynamics. The force (gradient of the action) becomes complex in this case making the fields also complex during the evolution.

In this work we make use of complex Langevin dynamics with stochastic quantization to study large N unitary matrix models with complex actions. They exhibit sign problem due to the fact that the action is complex. Standard Monte Carlo methods fail to produce the correct equilibrium distributions of these models. We can use discretized complex Langevin equation with Euler method (which is a first order algorithm) to find the equilibrium field distributions of these models.

Let us take $\theta_i(\tau)$ with $i = 1, \cdots, N$ as the complexified angle variables of the gauge link $U(\tau)$ at a Langevin time τ. We have the discrete Langevin evolution equation

$$\theta_i(\tau + \Delta\tau) \;=\; \theta_i(\tau) - \left[\frac{\partial S}{\partial \theta_i(\tau)}\right] \Delta\tau + \sqrt{\Delta\tau}\, \eta_i(\tau), \tag{2.2.1}$$

where $\Delta\tau$ is the Langevin time step, and $\eta_i(\tau)$ is a Gaussian random variable satisfying the conditions

$$\langle \eta_i(\tau) \rangle = 0, \quad \langle \eta_i(\tau) \eta_j(\tau') \rangle = 2\delta_{ij}\delta_{\tau\tau'}. \tag{2.2.2}$$

We also note that strictly at infinite N the fluctuation term in Eq. (2.2.1) could be safely dropped.

To reduce excursions in the imaginary directions of the field configurations, which would spoil the validity of the method, we should use real Gaussian random variables [54, 55, 56].

We also need to impose the $SU(N)$ constraint on the complexified angular variables after each Langevin time step. That is,

$$\sum_{i=1}^{N} \theta_i(\tau) = 0. \tag{2.2.3}$$

This can be easily implemented by subtracting the average value $\theta_{\text{av}}(\tau)$ from each $\theta_i(\tau)$ variable.

We note that there also exists another complementary method in which one could implement complex Langevin dynamics directly on the matrix variables $U(\tau)$. In this case the evolution equation takes the form

$$U(\tau + 1) = R(\tau)U(\tau) \tag{2.2.4}$$

where the matrix R is a stochastic unitary matrix. We note that this method can be used for studying similar models in higher spacetime dimensions.

In this paper, we use the first method described above where the link field U is diagonalized and the $SU(N)$ constraint is imposed.

2.3 ab-Model

To demonstrate the effectiveness of Complex Langevin Dynamics, we begin by studying a simple, yet non-trivial model – a complexified version of Gross-Witten-Wadia (GWW) Model [57, 19, 20, 58]. We refer to our model as *ab-Model*. It has two phases, confined and deconfined, exhibiting a third-order phase transition. The action is given by

$$S = N \left(a \operatorname{Tr} U + b \operatorname{Tr} U^\dagger \right) \tag{2.3.1}$$

where, $a, b \in \mathbb{C}$, U is an element of $SU(N)$, and $a = b$ is the Gross-Witten-Wadia model.

Before proceeding further let us make a few generic comments. A linear term in $\operatorname{Tr} U$ breaks the center symmetry. Furthermore, the above action (or other polynomial generalization of it) is complex. If $a \neq b$, then the $\mathbb{Z}_2$ symmetry $U \to U^\dagger$ is broken. This implies $\langle \operatorname{Tr} U \rangle \neq \langle \operatorname{Tr} U^\dagger \rangle$.

One may ask, that what it means in terms of manifestly gauge invariant operators. This means that the contribution from baryon and anti-baryon is different. Another related observation is one may naively expand Eq. (2.3.1) in series,

$$Z = \int DU e^{-S} = \int DU \left(1 + N^2 ab \,\mathrm{Tr}\, U \,\mathrm{Tr}\, U^\dagger + \frac{N^4}{4}(ab)^2 (\mathrm{Tr}\, U \,\mathrm{Tr}\, U^\dagger)^2 \cdots\right) - \left(Na \,\mathrm{Tr}\, U + b \,\mathrm{Tr}\, U^\dagger - \frac{N^2}{2} a^2 (\mathrm{Tr}\, U)^2 - \frac{N^2}{2} b^2 (\mathrm{Tr}\, U^\dagger)^2\right) + \cdots \tag{2.3.2}$$

Here we have separated the "mesonic" and "baryonic" contributions. Due to the center symmetry only a gauge invariant combination of $\mathrm{Tr}\, U$ and $\mathrm{Tr}\, U^\dagger$ contributes. By mesonic contribution we mean product of traces for which sum of powers all the occurrence of unitary matrix and its inverse sum to zero. For baryonic operator, the sum is only zero up to modulo N, i.e., proportional to a non-zero integral power of N. If baryonic contributions are neglected then Eq. (2.3.1) is equivalent to a model with parameters, $a = b = \sqrt{(ab)}$. We will later see that for gauge invariant operators, this equivalence is actually held in the ungapped phase.

Expressing the action in diagonal gauge, the effective action becomes

$$\begin{aligned} S_{eff} &= \sum_{i,j=1, i\neq j}^{N} -\frac{1}{2} \ln\left(\sin^2\left(\frac{\theta_i - \theta_j}{2}\right)\right) + iN\mathcal{M} \sum_{i=1}^{N} \theta_i \\ &\quad + N\left(a \sum_{i=1}^{N} e^{i\theta_i} + b \sum_{i=1}^{N} e^{-i\theta_i}\right), \end{aligned} \tag{2.3.3}$$

where the first term is the Vandermonde piece, and $\mathcal{M}$ is the Lagrange multiplier which ensures that $\det(U) = 1$.

At large N, the theory is dominated by the saddle-point equation

$$\frac{\partial S_{eff}}{\partial \theta_i} = 0, \tag{2.3.4}$$

which gives the equation of motion

$$i\mathcal{M} + i\left(ae^{i\theta_i} - be^{-i\theta_i}\right) = \frac{1}{N} \sum_{j\neq i} \cot\left(\frac{\theta_i - \theta_j}{2}\right). \tag{2.3.5}$$

On substituting $z_i = e^{i\theta_i}$ the equation of motion becomes

$$i\mathcal{M} + iaz_i - i\left(\frac{b}{z_i}\right) = \frac{i}{N}\sum_{j\neq i}\left(\frac{z_i + z_j}{z_i - z_j}\right), \tag{2.3.6}$$

and $\mathcal{M}$ is given by

$$\mathcal{M} = \frac{1}{N}\sum_{i=1}^{N}\left(\frac{b}{z_i} - az_i\right). \tag{2.3.7}$$

In the saddle point, $\mathcal{M}$ may have a non-zero value and could be thought as effective baryon number.

At $N \to \infty$ limit, we can replace the summation by an integral over a non-decreasing function

$$\frac{1}{N}\sum_{i=1}^{N} \to \int_{-\pi}^{\pi}\frac{ds}{2\pi}, \tag{2.3.8}$$

and performing a change of variables from s to complex variables $z(s)$

$$\frac{ids}{dz} = \rho(z), \tag{2.3.9}$$

the equation of motion becomes

$$\mathcal{M} + az - \left(\frac{b}{z}\right) = P\oint_c \frac{d\omega}{2\pi i}\rho(\omega)\left(\frac{z+\omega}{z-\omega}\right), \tag{2.3.10}$$

and P implies we are taking the principal value of the integral.

2.3.1 Ungapped Phase

In GWW model, it is known that for small potential, i.e., $a < 0.5$, the theory is in an ungapped phase. Assuming a similar picture also holds for the *ab-Model*, we solve it by taking an ansatz for $\rho(z)$ in ungapped phase as,

$$\rho(\omega) = A_0 + \frac{A_1}{\omega} + \frac{A_2}{\omega^2} + \cdots \tag{2.3.11}$$

then

$$P\oint_C \frac{d\omega}{2\pi i}\rho(w)\left(\frac{z+\omega}{z-\omega}\right) = -A_0 z + \frac{A_2}{z} + \cdots \tag{2.3.12}$$

Comparing with the LHS of Eq. (2.3.10)

$$A_0 = -a \text{ and } A_2 = -b. \tag{2.3.13}$$

Therefore ρ becomes,

$$\rho(z) = -a + \frac{A_1}{z} - \frac{b}{z^2} + \cdots \tag{2.3.14}$$

We also find

$$\mathcal{M} = \oint_C \frac{dz}{2\pi i}\rho(z)\left(\frac{b}{z} - az\right) = 0, \tag{2.3.15}$$

which indicates that the theory is in an ungapped phase. Demanding normalization of $\rho(z)$

$$\oint \frac{dz}{2\pi i}\rho(z) = 1, \tag{2.3.16}$$

we fix $A_1 = 1$.

Therefore,

$$\rho(z) = \frac{1}{z} - a - \frac{b}{z^2} + \cdots \tag{2.3.17}$$

We can solve for the contour, where $\rho(z)$ is positive definite, by integrating Eq. (2.3.9)

$$is = \ln(z) - az + \frac{b}{z} + c. \tag{2.3.18}$$

Since s is purely real, and assuming that

$$z = r(\theta)e^{i\theta}, \;\; a = |a|e^{i\phi_1} \text{ and } b = |b|e^{i\phi_2}, \tag{2.3.19}$$

the above equation is satisfied only if the real part of the RHS is zero. That is,

$$\ln(r(\theta)) - |a|r(\theta)\cos(\theta + \phi_1) + \frac{|b|}{r(\theta)}\cos(\theta - \phi_2) + Re(c) = 0. \tag{2.3.20}$$

To fix c, we invoke the condition that $\det(U) = 1$, i.e., $\sum_{i=1}^{N}\theta_i = 0$, which translates to

$$\int_C \frac{dz}{2\pi i}\ln(z)\rho(z) = 0, \tag{2.3.21}$$

where the branch-cuts are taken from $z = 0$ to the point $z(\pm\pi)$. Replacing $\ln(z)$ using Eq. (2.3.18), the above equation becomes

$$\begin{aligned}
&\int \frac{dz}{2\pi i}\left(is + az - \frac{b}{z} - c\right)\rho(z) = 0 \\
&\quad \Rightarrow -c + \oint \frac{dz}{2\pi}\rho(z)s = 0 \\
&\quad \Rightarrow -c + i\int_{-\pi}^{\pi} \frac{ds}{2\pi}s = 0 \\
&\quad \Rightarrow c = 0.
\end{aligned} \tag{2.3.22}$$

Hence the contour is got by solving the transcendental equation

$$\ln(r(\theta)) - |a|r(\theta)\cos(\theta + \phi_1) + \frac{b}{r(\theta)}\cos(\theta - \phi_2) = 0. \tag{2.3.23}$$

Now we can compare the distribution of eigenvalues from complex Langevin dynamics with the analytic result for any (a, b) combination. In Fig. 2.1 we show the analytical result and the data obtained through complex Langevin simulations without noise for parameters $a = 0.35, b = 0.2$ and $N = 100$. In Fig. 2.2 we show the result with Gaussian noise turned on. We see an excellent agreement between the analytical and numerical results [*].

[*]These images were produced using Mathematica Plot function and the code was written from scratch.

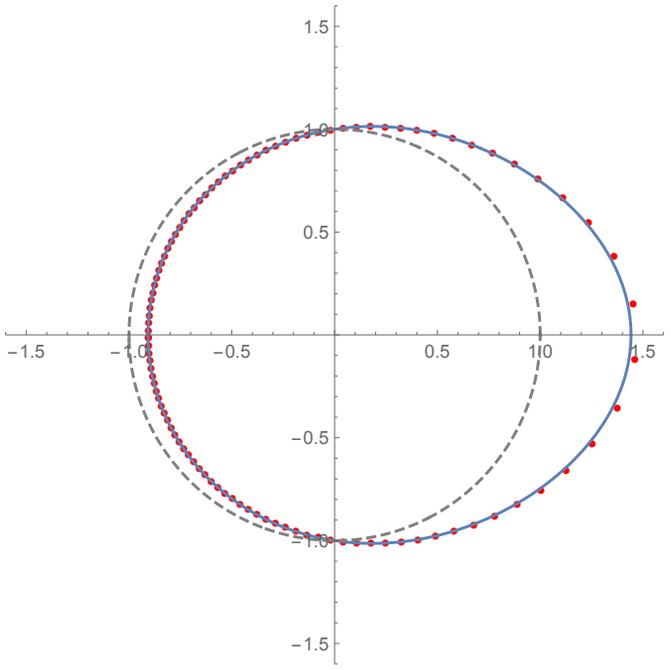

Figure 2.1: The distribution of eigenvalues of ab-model with parameters $a = 0.35, b = 0.2$ and $N = 100$. The solid curve is the analytical result and the data points are obtained through complex Langevin simulations without introducing the Gaussian noise. The dashed curve is a unit circle.

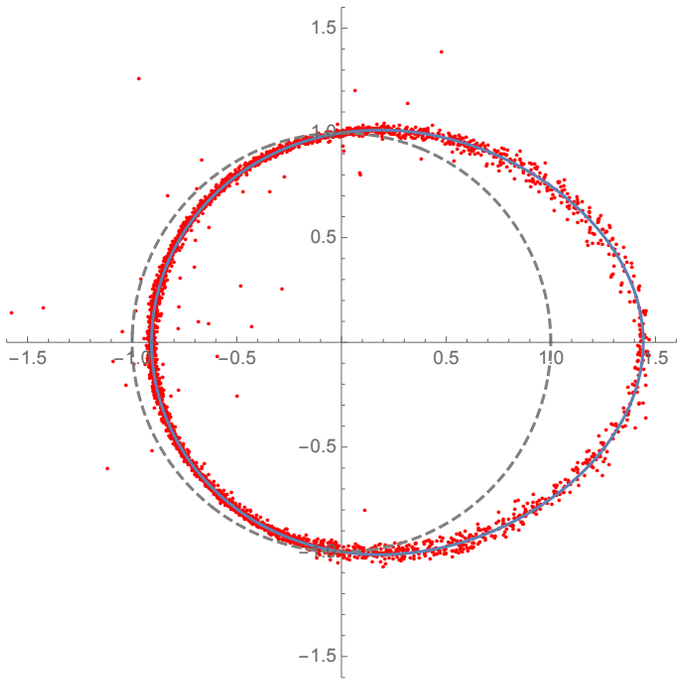

Figure 2.2: The distribution of eigenvalues of ab-model with parameters $a = 0.35, b = 0.2$ and $N = 100$. The solid curve is the analytical result and the data points are obtained through complex Langevin simulations. The dashed curve is a unit circle.

We also note that the complex Langevin simulations show excellent agreement with analytical results when the parameters are also complex. In Fig. 2.3 we show the analytical result and the data obtained through complex Langevin simulations without noise for parameters $a = 0.2 + i0.2$, $b = -0.1 + i0.1$ and $N = 100$. In Fig. 2.4 we show the result with Gaussian noise turned on.

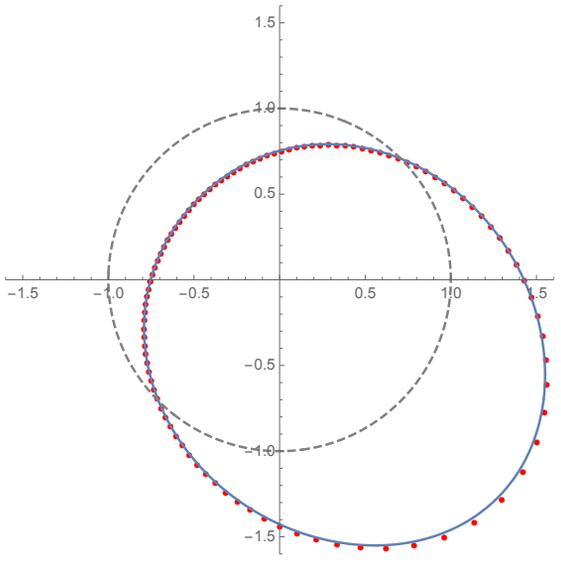

Figure 2.3: The distribution of eigenvalues of ab-model with parameters $a = 0.2 + i0.2, b = -0.1 + i0.1$ and $N = 100$. The solid curve is the analytical result and the data points are obtained through complex Langevin simulations without introducing the Gaussian noise. The dashed curve is a unit circle.

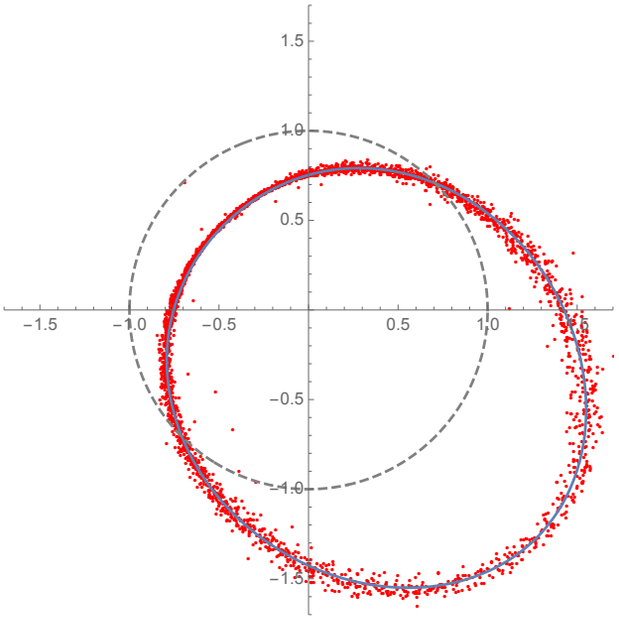

Figure 2.4: The distribution of eigenvalues of ab-model with parameters $a = 0.2 + i0.2, b = -0.1 + i0.1$ and $N = 100$. The solid curve is the analytical result and the data points are obtained through complex Langevin simulations. The dashed curve is a unit circle.

2.3.2 Gapped Phase

In the gapped phase, similar to GWW model, the eigenvalues lie on an open contour C.

To study this phase, we employ resolvent/spectral-curve method used in Ref. [21], and reviewed

in Ref. [59]. The resolvent is defined as

$$\omega(z) = -\frac{1}{N}\sum_j \left(\frac{z+z_j}{z-z_j}\right). \tag{2.3.24}$$

At large N limit, $\omega(z)$ is analytic everywhere in the complex plane, except along a square-root branch cut running along C, and expressed as

$$\omega(z) = -\int_C \frac{dz'}{2\pi i}\rho(z')\frac{z+z'}{z-z'}. \tag{2.3.25}$$

For a given potential $V(z)$, the equation of motion (similar to Eq. (2.3.10))

$$zV'(z) = P\oint_C \frac{dz'}{2\pi i}\rho(z')\frac{z+z'}{z-z'} \tag{2.3.26}$$

can be expressed in terms of $\omega(z)$ using the Plemelj formulae

$$zV'(z) = \frac{1}{2}\left[\omega(z+\epsilon)+\omega(z-\epsilon)\right], \;\; z\in C, \tag{2.3.27}$$

where $z\pm\epsilon$ lies on either side of the branch cut and $\epsilon\to 0$ limit is taken.

We can also express $\rho(z)$ as the discontinuity of $\omega(z)$ across the cut C as

$$z\rho(z) = \frac{1}{2}\left[\omega(z+\epsilon)-\omega(z-\epsilon)\right]. \tag{2.3.28}$$

The expectation value of any function $G(z)$ can be found as

$$\int_C \frac{dz}{2\pi i}\rho(z)G(z) = \oint_{\tilde{C}} \frac{dz}{4\pi i z}\omega(z)G(z). \tag{2.3.29}$$

For ab-model

$$\omega(z) = -\mathcal{M} - az + \frac{b}{z} + f(z)\sqrt{(z-\tilde{z})(z-\tilde{z}^*)}, \tag{2.3.30}$$

where $\tilde{z}$, $\tilde{z}^*$ are the end points of branch cut C and $f(z)$ is an unknown function, which remains to be fixed. Since $\omega(z)$ has to be regular over the entire plane except along C and the origin we can

fix the form of $f(z)$ as

$$f(z) = c + \frac{d}{z}. \tag{2.3.31}$$

Therefore $\omega(z)$ becomes (substituting $\tilde{z} = Re^{i\phi}$)

$$\omega(z) = -\mathcal{M} - az + \frac{b}{z} + \left(c + \frac{d}{z}\right)\sqrt{z^2 + R^2 - 2Rz\cos(\phi)}. \tag{2.3.32}$$

Normalization of $\rho(z)$, from Eq. (2.3.25), translates to

$$\lim_{|z|\to 0} \omega(z) = 1 \tag{2.3.33}$$

and

$$\lim_{|z|\to \infty} \omega(z) = -1. \tag{2.3.34}$$

This fixes $f(z)$ as

$$f(z) = a - \frac{b}{Rz}. \tag{2.3.35}$$

We also get two more relations between R, $\mathcal{M}$ and $\cos(\phi)$

$$aR + \frac{b\cos(\phi)}{R} = 1 + \mathcal{M}, \tag{2.3.36}$$

and

$$a\cos(\phi)R + \frac{b}{R} = 1 - \mathcal{M}. \tag{2.3.37}$$

To fix the three unknowns completely, we need a third equation, which comes from invoking the $\det(U) = 1$ condition, from Eq. (2.3.29)

$$\int_{\tilde{C}} \frac{dz}{4\pi i z}\omega(z)\ln(z) = 0, \tag{2.3.38}$$

where $\tilde{C}$ is a contour encircling the branch cut C, and the branch cut of $\ln(z)$ ranges from $(-\infty, 0)$. Deforming the contour Fig. 2.5 to the one in Fig. 2.6

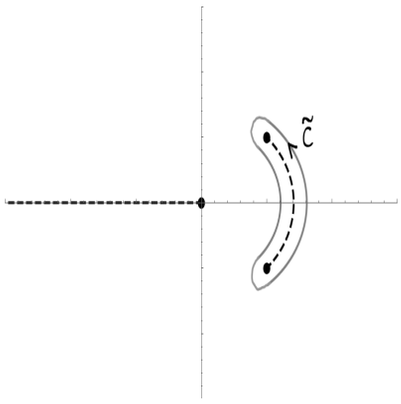

Figure 2.5: Actual contour over which Eq. (2.3.38) needs to be performed.

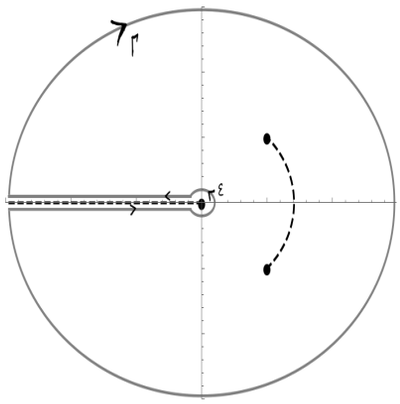

Figure 2.6: Deformed contour over which the integral was performed.

and evaluating in $\epsilon \to 0$ and $\Gamma \to \infty$ limits, we find that the divergences arising from the cutoffs Γ and ϵ cancel separately and we arrive at the following condition

$$\left(aR - \frac{b}{R}\right)\left[\left(\frac{1-\cos(\phi)}{2}\right)\ln\left(\frac{1-\cos(\phi)}{2}\right) + \left(\frac{1+\cos(\phi)}{2}\right)\right] = \left(aR + \frac{b}{R}\right)\left(\frac{1+\cos(\phi)}{2}\right)\ln(R). \tag{2.3.39}$$

Now for a given a, b we can numerically solve the Eqs. (2.3.36), (2.3.37), and (2.3.39) for R, $\mathcal{M}$ and $\cos(\phi)$, and hence fix $\omega(z)$ completely. Also from Eq. (2.3.28) we can fix $\rho(z)$

$$\rho(z) = \left(\frac{a}{z} - \frac{b}{Rz^2}\right)\sqrt{z^2 + R^2 - 2Rz\cos(\phi)}. \tag{2.3.40}$$

From Eq. (2.3.15), we can numerically compute $\mathcal{M}$, both in ungapped and gapped phases, and compare it against analytical results. Choosing $b = 2.0a$ and varying a from 0 to 1.2, we find that it matches very well both in ungapped and gapped regimes – see Fig. 2.7. (Gap opening point can be found from Fig. 2.10.)

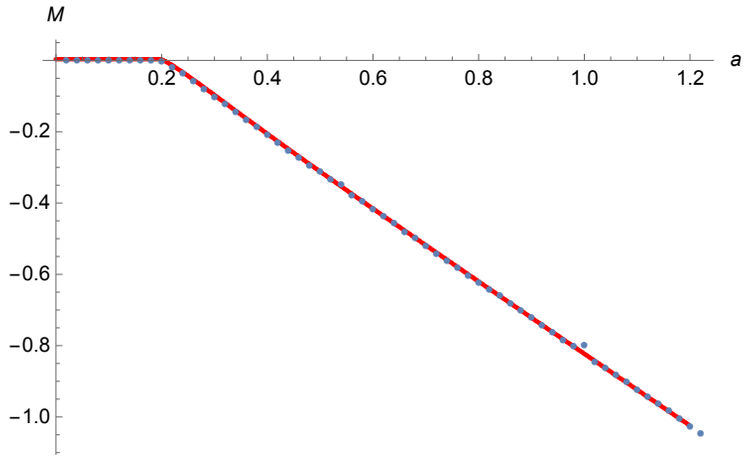

Figure 2.7: The value of $\mathcal{M}$ at $(a, 2a)$ for the ab-model with $N = 100$. The solid curve is analytical result and the data points are obtained through complex Langevin simulations.

Similarly we compare other observables, $\langle \operatorname{Tr}(U)\rangle$ and $\langle \operatorname{Tr}(U^{-1})\rangle$. Analytically $\langle \operatorname{Tr}(U)\rangle$ is given by,

$$\begin{aligned}\langle \operatorname{Tr}(U)\rangle &= \oint \frac{dz}{2\pi i}\left(\frac{1}{z} - a - \frac{b}{z^2}\right) z = -b && \text{(Ungapped)}\\ &= \oint_{\tilde{C}} \frac{dz}{4\pi i}\frac{w(z)}{z} z = \left(\frac{\cos\phi + 1}{4}\right)\left(a(\cos\phi - 1)R^2 - 2b\right) && \text{(Gapped)}\end{aligned} \tag{2.3.41}$$

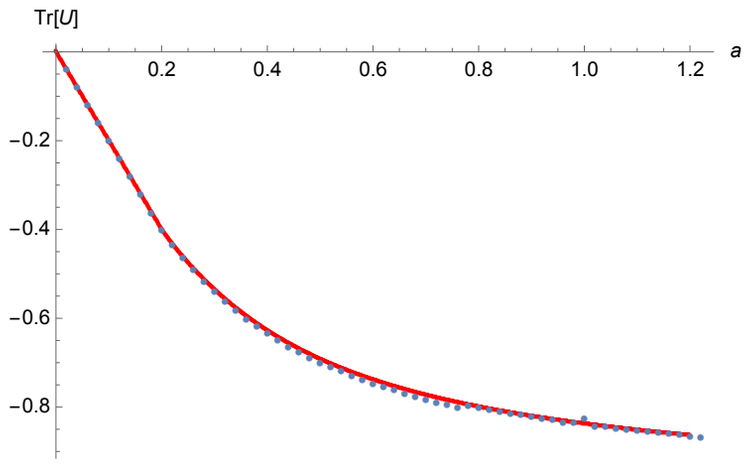

Figure 2.8: The value of $\operatorname{Tr}(U)$ at $(a, 2a)$ for the ab-model with $N = 100$. The solid curve is analytical result and the data points are obtained through complex Langevin simulations.

and $\langle \operatorname{Tr}(U^{-1})\rangle$ by,

$$\begin{aligned}\langle \operatorname{Tr}\big(U^{-1}\big)\rangle &= \oint \frac{dz}{2\pi i}\left(\frac{1}{z}-a-\frac{b}{z^2}\right)\frac{1}{z} = -a && \text{(Ungapped)}\\ &= \oint_{\tilde{C}} \frac{dz}{4\pi i}\frac{\omega(z)}{z}\frac{1}{z} = \left(\frac{\cos\phi+1}{4}\right)\left(\frac{b(\cos\phi-1)}{R^2}-2a\right) && \text{(Gapped)}\end{aligned} \tag{2.3.42}$$

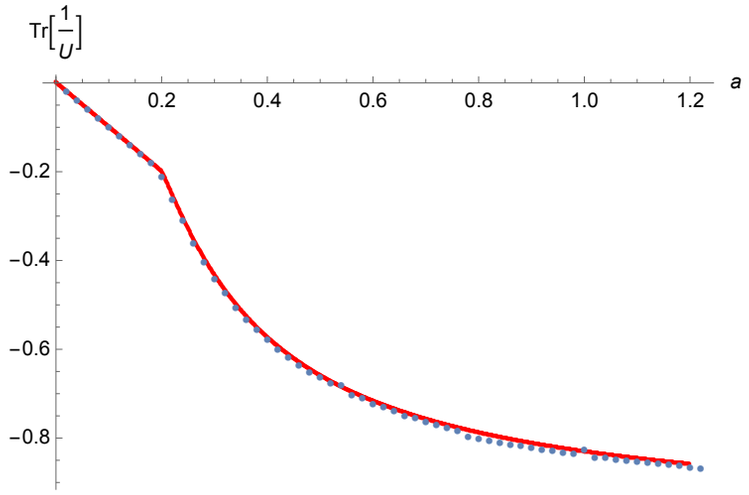

Figure 2.9: The value of $\operatorname{Tr}\big(U^{-1}\big)$ at $(a, 2a)$ for the ab-model with $N = 100$. The solid curve is analytical result and the data points are obtained through complex Langevin simulations.

In Fig. 2.8 and Fig. 2.9 we show the observables $\langle \operatorname{Tr}(U)\rangle$ and $\langle \operatorname{Tr}(U^{-1})\rangle$, respectively. The analytical and numerical results show excellent agreement.

2.3.3 Phase transition of ab-Model

The eigenvalue density Eq. (2.3.17) on contour Eq. (2.3.23), is proportional to ds, which in terms of $r(\theta)$ is given by

$$\begin{aligned} ds &= \frac{d}{d\theta}\left[\theta - |a|\sin(\theta+\phi_1)r(\theta) - \frac{|b|}{r(\theta)}\sin(\theta-\phi_2)\right]d\theta \\ &= \Big[1 - |a|\cos(\theta+\phi_1)r(\theta) - |a|\sin(\theta+\phi_1)r'(\theta) \\ &\qquad - \frac{|b|}{r(\theta)}\cos(\theta-\phi_2) + \frac{|b|r'(\theta)}{r(\theta)^2}\sin(\theta-\phi_2)\Big]d\theta \end{aligned} \tag{2.3.43}$$

which is not positive definite for all (a, b) combinations. It fails to do so, when the function inside the brackets, $[\dots]$, becomes negative. Restricting to $a, b \in \mathbb{R}$, the condition simplifies as the gap opens about $\theta = 0$

$$\begin{aligned} 1 - ar(0) - \frac{b}{r(0)} \quad &\leq 0 \\ \Rightarrow \quad \exp\left\{\left(ar(0) + \frac{b}{r(0)}\right)\right\} \quad &\geq e. \end{aligned} \tag{2.3.44}$$

From Eq. (2.3.23) $r(0)$ is given by

$$r(0) = \exp\left\{\left(ar(0) - \frac{b}{r(0)}\right)\right\}. \tag{2.3.45}$$

The phase diagram of the model is shown in Fig. 2.10.

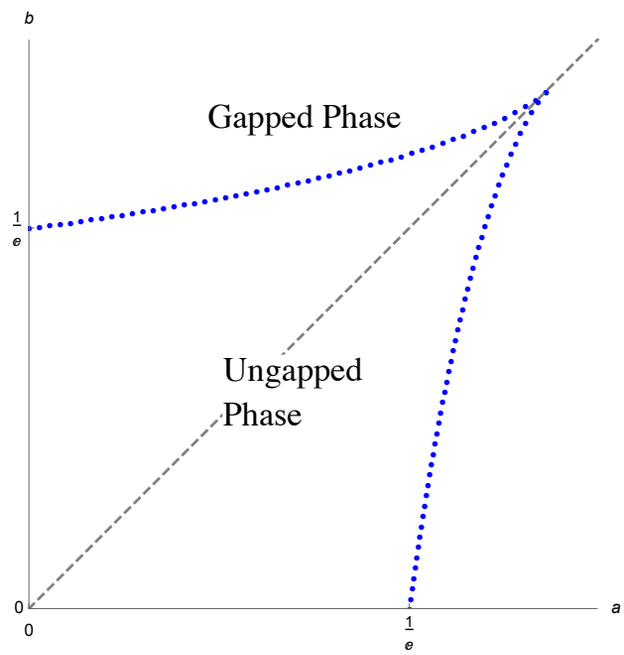

Figure 2.10: The phase diagram of the ab-model in the a-b plane.

It would be interesting to know how quantities change across the gap opening transition and also the order of the phase transition. To study that we first restrict ourselves to a special case, $b = 0$ in our model. Then from Eqs. (2.3.44) and (2.3.45) the gap opens about $a = \frac{1}{e}$, $R = e$, and since the ungapped phase has no branch cuts in the eigenvalue distributions, ϕ should start from zero,

about the gap-opening point. And the conditions Eqs. (2.3.36) and (2.3.37) simplifies to

$$aR\left(\frac{\cos(\phi)+1}{2}\right)=1 \tag{2.3.46}$$

and Eq. (2.3.39) to

$$\left(\frac{1-\cos(\phi)}{2}\right)\ln\left(\frac{1-\cos(\phi)}{2}\right)=\left(\frac{1+\cos(\phi)}{2}\right)\ln\left(\frac{R}{e}\right). \tag{2.3.47}$$

The observable $\langle\,\mathrm{Tr}(U)\rangle$ becomes

$$\begin{aligned}\langle\,\mathrm{Tr}(U)\rangle =&0 && \text{(Ungapped)}\\ =&\left(\frac{a(\cos(\phi)^2-1)R^2}{4}\right) && \text{(Gapped)}\end{aligned} \tag{2.3.48}$$

Since the first derivative of free-energy $F[a]$ given by

$$\frac{\partial F[a]}{\partial a}=\frac{\partial \ln Z[a]}{\partial a}=\frac{1}{Z[a]}\int[DU]\,\mathrm{Tr}(U)\exp(a\,\mathrm{Tr}(U))=\langle\,\mathrm{Tr}(U)\rangle \tag{2.3.49}$$

is the expectation value of $\mathrm{Tr}(U)$, we find that it is continuous across the gap.

Upon expanding about

$$a=\frac{1}{e}+\delta a,\quad \cos(\phi)=1-2\delta p \text{ and } R=e+\delta R \tag{2.3.50}$$

the variation of $\delta\langle\,\mathrm{Tr}(U)\rangle$ is given by

$$\delta\langle\,\mathrm{Tr}(U)\rangle=\delta\left(\frac{a(\cos(\phi)^2-1)R^2}{4}\right)=-e\delta p. \tag{2.3.51}$$

From Eqs. (2.3.46) and (2.3.47) we get

$$\delta p=e\delta a+\frac{\delta R}{e}, \tag{2.3.52}$$

and

$$\delta p \ln(\delta p) = \frac{\delta R}{e}. \tag{2.3.53}$$

Eliminating δR from above two equations we get the equation

$$\delta p(1 - \ln(\delta p)) = e\delta a. \tag{2.3.54}$$

To invert the above equation let us substitute $\delta p \to e^k$. Then we have

$$(k-1)e^{(k-1)} = -\delta a. \tag{2.3.55}$$

The above equation is of the form, $xe^x = y$, which can be inverted to express x as a function of y and it is known as the Lambert-W function [60]. (It is often expressed as $W_c(y)$.) This function is in general a multivalued-complex function, where $c \in \mathbf{Z}$, chooses each branch. Since $\delta a > 0$ and $\delta p \in \mathbf{R}$ we have two real valued branches: $W_0(y)$ (the principal branch) and $W_{-1}(y)$.

Therefore,

$$\delta p = e^{W_0(-\delta a)+1} \text{ or } e^{W_{-1}(-\delta a)+1}. \tag{2.3.56}$$

For small values of δa we know that

$$\lim_{\delta a \to 0} W_0(-\delta a) = 0, \quad \lim_{\delta a \to 0} W_{-1}(-\delta a) \approx \ln(\delta a). \tag{2.3.57}$$

Therefore, δp will vanish as $\delta a \to 0$ only if we choose the second branch, i.e., $\delta p = e^{W_{-1}(-\delta a)+1}$. Hence

$$\delta \langle \operatorname{Tr}(U) \rangle = -e^{W_{-1}(-\delta a)+2}. \tag{2.3.58}$$

Now the second derivative of free energy

$$\frac{\partial^2 F}{\partial(\delta a)^2} = \frac{\partial \left(\delta \langle \operatorname{Tr}(U) \rangle\right)}{\partial(\delta a)} \frac{e^2}{W_{-1}(-\delta a) + 1} \tag{2.3.59}$$

goes to zero as $\delta a \to 0$ and is continuous across the gap. But the third derivative

$$\frac{\partial^3 F}{\partial(\delta a)^3} = -\frac{e^2 W_{-1}(-\delta a)}{\delta a (W_{-1}(-\delta a)+1)^3} \tag{2.3.60}$$

diverges as $\delta a \to 0$. Hence it has a third order phase transition. It can also be shown that similar arguments hold in the generic case $b \neq 0$. Thus we conclude that the ab-Model displays a third order phase transition.

2.4 Gauge Theory to Unitary Matrix Model

A unitary matrix model arises in a one-loop formulation of QCD (and analogous $SU(N)$ gauge theories) on compact spaces (often $S^1 \times S^3$). This was originally derived in [61, 62, 63, 64] for theories with more general matter content.

The one-loop effective action of QCD on $S^1 \times S^3$ with chemical potential μ and quark mass m has the form [21], with thermal Polyakov loop as the unitary matrix model

$$\begin{aligned} S &= \sum_{n=1}^{\infty} \frac{1}{n} z_b\left(\frac{n\beta}{R}\right) \operatorname{Tr} U^n \operatorname{Tr} U^{\dagger n} \\ &\quad + \sum_{n=1}^{\infty} \frac{(-1)^n}{n} N_f z_f\left(\frac{n\beta}{R}, mR\right) \left[e^{n\beta\mu} \operatorname{Tr} U^n + e^{-n\beta\mu} \operatorname{Tr} U^{\dagger n}\right]. \end{aligned} \tag{2.4.1}$$

The quadratic term in Polyakov loop is the contribution from adjoint fields and the linear term is the contribution from the fundamental matter fields. Here, we have taken the adjoint contribution to be bosonic and the the contribution from fundamental fields to be fermionic.

To be noted is that in the free theory the effective action is determined in terms of single particle partition function

$$z_b\left(\frac{\beta}{R}\right) = 2\sum_{l=1}^{\infty} l(l+2) e^{-\beta(l+1)/R}, \tag{2.4.2}$$

and

$$z_f\left(\frac{\beta}{R}, mR\right) = 2\sum_{l=1}^{\infty} l(l+1) e^{-\frac{\beta}{R}\sqrt{(l+\frac{1}{2})^2 + m^2R^2}}. \tag{2.4.3}$$

In the above equations R is the radius of S^3. We use dimensionless variables β/R, μR and mR in numerical simulations.

An analogous action, for the simpler $0+1$ dimensional case would be,

$$z_b = 0, \tag{2.4.4}$$

$$z_f = 2e^{-\beta m}, \tag{2.4.5}$$

where the parameter m is the mass of the fundamental fermions.

In the low temperature limit, $\beta \to \infty$, we have $z_b(\infty) = 0$ and so the gluonic contribution is negligible. Thus the action is

$$S = S_{\mathrm{Vdm}} + S_f, \tag{2.4.6}$$

where S_f is the fundamental fermionic contribution. The fermionic part could be summed in a logarithm

$$S[U] = -\sum_{l=1}^{\infty} \sigma_l \left(\log \left[\det \left(1 + e^{\beta(\mu - \epsilon_l)} U \right) \det \left(1 + e^{\beta(-\mu - \epsilon_l)} U^{-1} \right) \right] \right). \tag{2.4.7}$$

2.4.1 Observables

We can study several interesting observables in the model described above. We briefly describe them below

1. The most natural set of observables are Polyakov line and inverse Polyakov line.

3. Fermion number f_N

   It gives the number of fermions minus the number of anti-fermions in a given volume

$$f_N = \frac{1}{\beta} \left(\frac{\partial \log Z}{\partial \mu} \right). \tag{2.4.8}$$

   In the model we study here we have a single chemical potential μ. In general there can be chemical potential for each fermion flavor.

   The quark number susceptibility χ_f measures the response of the fermion number density

to infinitesimal changes in the chemical potential,

$$\chi_f = \frac{1}{\beta}\frac{\partial f_N}{\partial \mu}. \tag{2.4.9}$$

This observable follows the behavior of the Polyakov line. Thus, it also serves as an indicator of confinement-deconfinement transitions for nonzero chemical potential.

4. Pressure p

$$p = \frac{1}{\beta}\left(\frac{\partial \log Z}{\partial V_3}\right), \tag{2.4.10}$$

with V_3 denoting the spatial volume.

5. Energy E

It can be constructed from pressure and fermion number density

$$E = -pV_3 + \mu f_N. \tag{2.4.11}$$

It is also possible to compute the chiral condensate and average phase, though we will not compute them in this work. The chiral condensate $\langle\overline{\psi}\psi\rangle$ is given by

$$\langle\overline{\psi}\psi\rangle = -\frac{1}{\beta V_3}\lim_{m\to 0}\left(\frac{\partial \log Z}{\partial m}\right), \tag{2.4.12}$$

and the average phase $\langle e^{i\phi}\rangle_{pq}$ has the form

$$\langle e^{i\phi}\rangle_{pq} = \frac{Z}{Z_{pq}}, \tag{2.4.13}$$

where pq refers to the phase quenched theory.

2.4.2 Single Level Model with Positive Chemical Potential

We can truncate the action given in Eq. (2.4.7) in a double scaling limit:

$$\begin{aligned} \beta &\to \infty, \\ \mu &\to \epsilon_0, \\ \exp(\beta(\mu - \epsilon_l)) &= \xi, \end{aligned} \tag{2.4.14}$$

where ϵ_0 is a fixed quark energy level and ξ the effective fugacity.

Only contribution from a single level survives here,

$$S[U] = -\sigma \log\left(1 + \xi U\right). \tag{2.4.15}$$

The effective action on the angle variables include the Vandermonde piece and a Lagrange multiplier.

In the large N limit, the integral over the angles is dominated by a saddle point obtained by solving the equation of motion that follows from the effective action involving Eq. (2.4.15)

$$\frac{\partial S}{\partial \theta_i} = iN\mathcal{N} - \frac{iN\sigma\xi e^{i\theta}}{(1 + \xi e^{i\theta_i})} - \sum_{j(\neq i)}^{N} \cot\left(\frac{\theta_i - \theta_j}{2}\right). \tag{2.4.16}$$

Here also the action is not hermitian, giving rise to the *sign problem* in the presence of a chemical potential. As a result the saddle point configuration will lie out in the complex plane. If we define $z_i = \exp(i\theta_i)$ then in the presence of the non-real potential the z_i will move off the unit circle in the z-plane.

We can explore the nature of eigenvalue distribution on the complex plane for various values of effective fugacity ξ. We find that when ξ is either very small or large, the potential vanishes and so we expect the $\{z_i\}$ to be uniformly distributed around the unit circle. Thus, when μ varies from $\mu \ll \epsilon$ to $\mu \gg \epsilon$ the quark energy level becomes occupied and the effective fermion number jumps by factor σ. In Ref. [21] the authors provide a detailed description of this transition.

Let us look at the various regimes of ξ and see how it affects the eigenvalue distribution, follow-

ing the analytical study given in Ref. [21].

1. *The small ξ confined phase*

   In the small ξ confining phase the effective fermion number vanishes, $\mathcal{N} = 0$, and the Polyakov line expectation values are

$$P = 0, \;\; P^{-1} = \sigma\xi. \tag{2.4.17}$$

   Thus we have $P \neq P^{-1}$, as a result of the complex action.

   As ξ is increased the contour of eigenvalue distribution opens into an arc, just as the matrix model solved by Gross and Witten [19] and Wadia [20, 57].

   The line of phase transitions in the (μ, T) plane corresponds to the straight line

$$\mu = \epsilon - T\Big[(1+\sigma)\log(1+\sigma) - \sigma\log\sigma\Big]. \tag{2.4.18}$$

   Note that is approximation is valid only in the low temperature ($\beta \to \infty$) limit.

2. *The large ξ confined phase*

   In this phase the effective fermion number is

$$\mathcal{N} = \sigma, \tag{2.4.19}$$

   indicating that the level is now occupied.

   The Polyakov line expectation values are

$$P = \frac{\sigma}{\xi}, \;\; P^{-1} = 0. \tag{2.4.20}$$

   Comparing with the previous case the behavior of P and P^{-1} swaps over along the replacement $\xi \to \xi^{-1}$.

The large ξ confined phase persists until the value

$$\xi = \xi_2 = \frac{(1+\sigma)^{1+\sigma}}{\sigma^\sigma}. \tag{2.4.21}$$

For smaller values of ξ the contour of eigenvalue distribution is not closed and the phase does not exist. The points of transition $\xi = \xi_1$ and $\xi = \xi_2$ satisfy $\xi_1\xi_2 = 1$.

In the (μ, T) plane the boundary lies along the straight line

$$\mu = \epsilon + T\Big[(1+\sigma)\log(1+\sigma) - \sigma\log\sigma\Big], \tag{2.4.22}$$

again valid in the low temperature limit.

3. *The deconfined phase*

In the region $\xi_1 \leq \xi \leq \xi_2$, experience with GWW matrix model suggests that the eigenvalue distribution exhibits the shape of an open contour.

In this regime we get a condition

$$\xi = \frac{(\sigma - \mathcal{N})^{\sigma-\mathcal{N}}(1+\mathcal{N})^{1+\mathcal{N}}}{\mathcal{N}^{\mathcal{N}}(1+\sigma-\mathcal{N})^{1+\sigma-\mathcal{N}}}. \tag{2.4.23}$$

This equation determines $\mathcal{N}$ as a function of ξ.

From the above equation it follows that across the transitions at $\xi = \xi_1$ and $\xi = \xi_2$, fermion number density $\mathcal{N}$ and its first derivative $\frac{\partial\mathcal{N}}{\partial\mu}$ are continuous, however higher derivatives are discontinuous. Since $\mathcal{N}$ is the effective fermion number, the first derivative of the grand potential, it follows that the transitions are third order, just as in the original GWW model.

For a single winding, the Polyakov lines are

$$P = \frac{\mathcal{N}}{\sigma+1-\mathcal{N}}\frac{1}{\xi}, \;\; P^{-1} = \frac{\sigma-\mathcal{N}}{1+\mathcal{N}}\xi. \tag{2.4.24}$$

Using complex Langevin dynamics we have simulated the single level matrix model. In Fig. 2.11 we show the eigenvalue distributions of the Polyakov line in the confined and deconfined phases as

a function of the logarithm of the effective fugacity, $\log \xi$, for $SU(N)$ case with $N = N_f = 500$, quark mass $m = 0$ and inverse temperature $\beta = 30$ (low T). We see that the eigenvalue distributions start with a closed contour (confined phase), passes through an open contour (deconfined phase) and again goes into a closed contour. (This figure can be compared with Fig. 12 in Sec. 4.1 of Ref. [21], where it was obtained through analytical methods.)

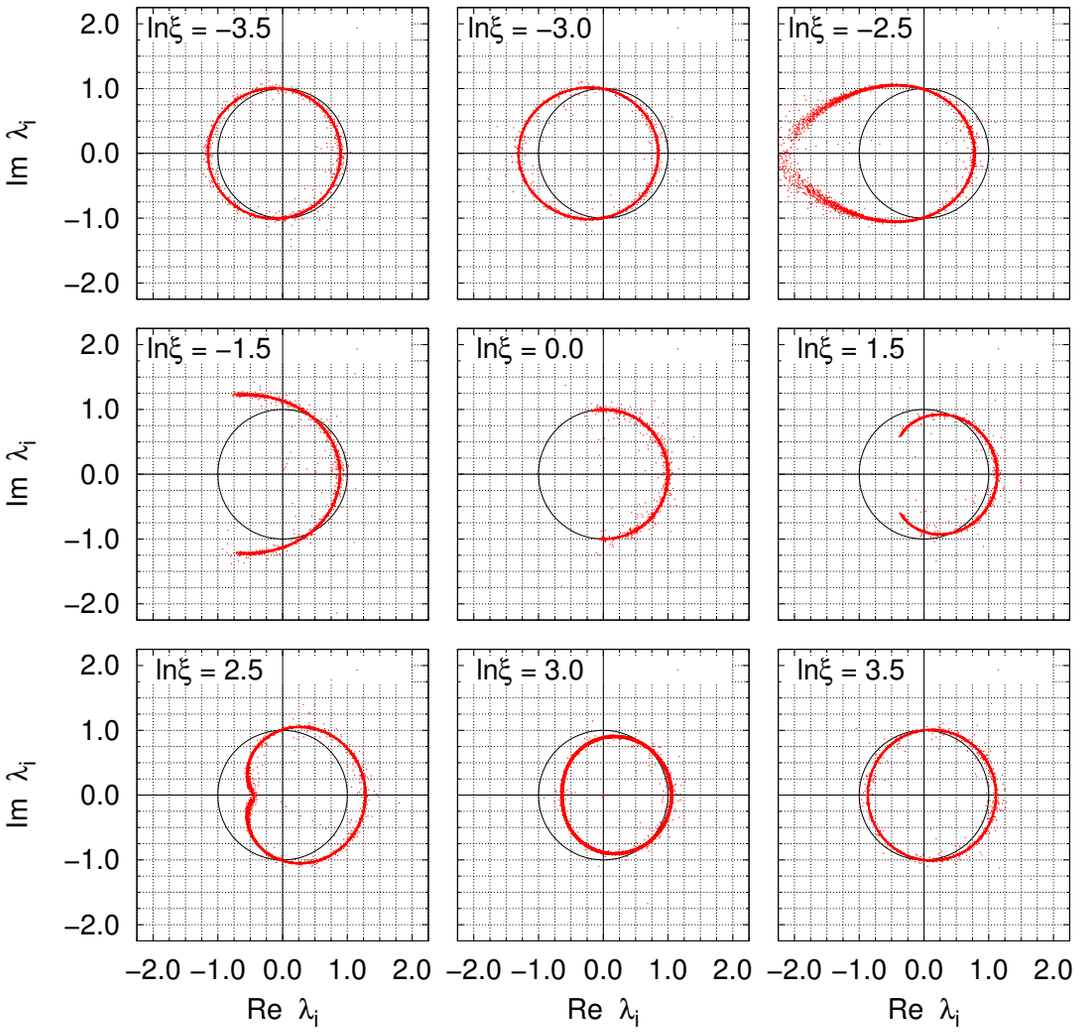

Figure 2.11: The eigenvalue distribution in the confined and deconfined phases as a function of the logarithm of the effective fugacity, $\log \xi$, for single-level $SU(N)$ matrix model with $N = N_f = 500$, quark mass $m = 0$ and inverse temperature $\beta = 30$ (low T). The data are obtained through complex Langevin simulations with Langevin time step $\Delta\tau = 0.000005$, thermalization steps $N_{\rm therm} = 18000$, generation steps $N_{\rm gen} = 2000$ and with measurements performed every 100 steps. The solid unit circles are guide to the eye.

In Fig. 2.12 we provide the (normalized) effective fermion number $\langle f_N \rangle$, and in Fig. 2.13 the Polyakov line expectation value $\langle P \rangle$ and the inverse Polyakov line expectation value $\langle P^{-1} \rangle$ across a pair of GWW transitions from the small ξ confined phase through the deconfined phase to the large ξ confined phase. The transitions from confined/deconfined phases occur when either $\langle P \rangle$ or $\langle P^{-1} \rangle$ vanish. The parameters used are: $N = N_f = 3$ and 500, quark mass $m = 0$ and inverse

temperature $\beta = 30$. The simulations show excellent agreement with the analytical results in the large N.

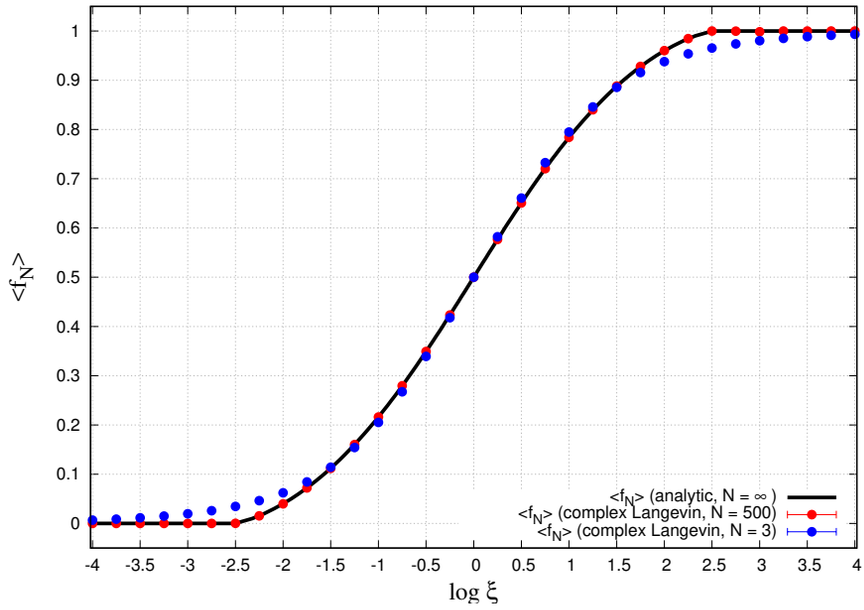

Figure 2.12: The (normalized) effective fermion number $\langle f_N \rangle$ across the pair of GWW transitions from the small ξ confined phase through the deconfined phase to the large ξ confined phase. The solid curve is the analytical result ($N = \infty$). The data points are obtained through complex Langevin simulations. We used Langevin time step $\Delta\tau = 0.000005$, thermalization steps $N_{\text{therm}} = 10000$, generation steps $N_{\text{gen}} = 10000$ and with measurements performed every 100 steps. Here red data points are for $N = N_f = 500$ and blue data points are for $N = N_f = 3$. We used quark mass $m = 0$ and inverse temperature $\beta = 30$ (low T).

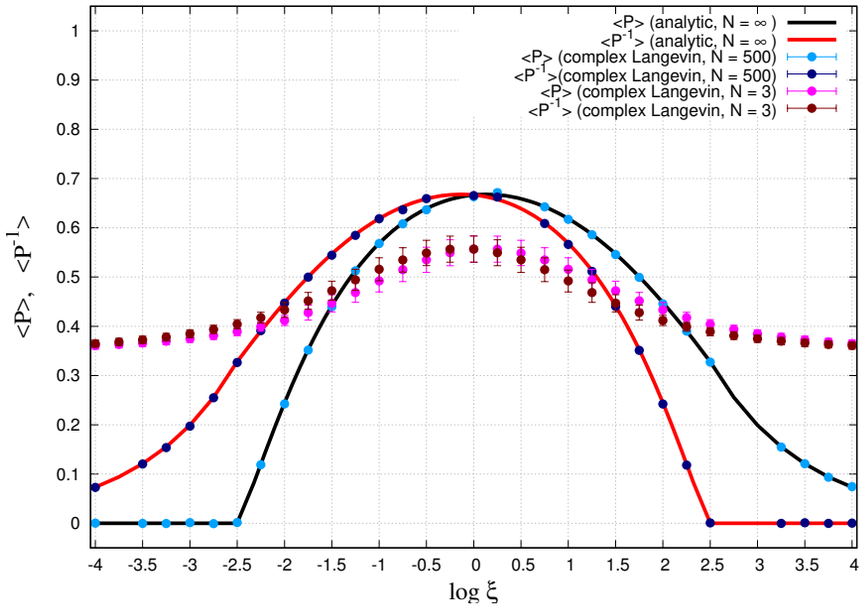

Figure 2.13: The Polyakov line $\langle P \rangle$ and inverse Polyakov line $\langle P^{-1} \rangle$ across the pair of GWW transitions from the small ξ confined phase through the deconfined phase to the large ξ confined phase. The transitions from confined/deconfined phases occur when either $\langle P \rangle$ or $\langle P^{-1} \rangle$ vanish. The solid curves are the analytical results ($N = \infty$). The data points are obtained through complex Langevin simulations. We used Langevin time step $\Delta\tau = 0.000005$, thermalization steps $N_{\text{therm}} = 10000$, generation steps $N_{\text{gen}} = 10000$ and with measurements performed every 100 steps. We simulated the model with $N = N_f = 500$ and $N = N_f = 3$. We used quark mass $m = 0$ and inverse temperature $\beta = 30$ (low T).

In Figs. 2.14 and 2.15 we show the Polyakov lines and fermion number density for a range of simulation parameters: $\beta = \{10, 15, \cdots, 100\}$ and $\mu = \{3.0, 3.025, 3.05, \cdots, 4.0\}$. The quark energy level of the model is fixed to $\epsilon = 3.5$ corresponding to the third level. The Polyakov loops peak around $\mu = 3.5$. In Fig. 2.14 we show the behavior of Polyakov and inverse Polyakov loops for $\beta = \{25, 50, 75, 100\}$. It is clear that the widths of the Polyakov loops decrease as the temperature is reduced (large β) and the behavior of inverse Polyakov line precedes that of the Polyakov line as a function of μ. In Fig. 2.15 we show the behavior of the (normalized) fermion number density $\langle f_N \rangle$ as a function of chemical potential and inverse temperature. The transition in fermion number becomes sharper as the temperature is decreased (high β). The model is in a deconfined phase when $0 < \langle f_N \rangle < 1$.

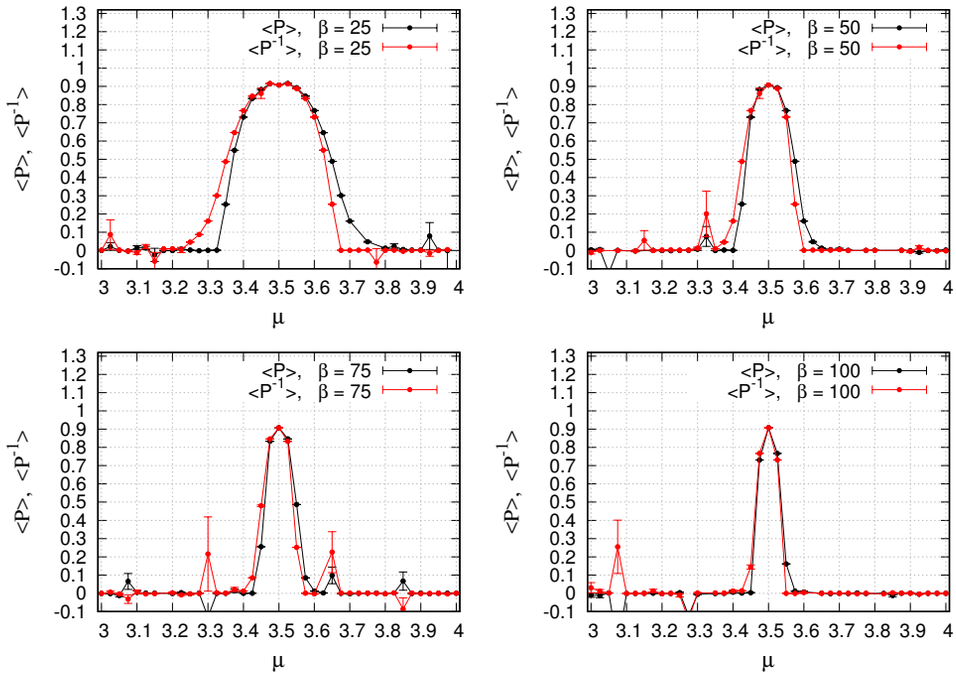

Figure 2.14: Polyakov line $\langle P \rangle$ and inverse Polyakov line $\langle P^{-1} \rangle$ as a function of chemical potential for single level matrix model with quark energy level $\epsilon = 3.5$ and quark mass $m = 0$. Here $N = N_f = 500$ and $\beta = 25, 50, 75, 100$. The data are obtained through complex Langevin simulations with Langevin time step $\Delta\tau = 0.000005$, thermalization steps $N_{\text{therm}} = 5000$, generation steps $N_{\text{gen}} = 5000$ and with measurements performed every 50 steps.

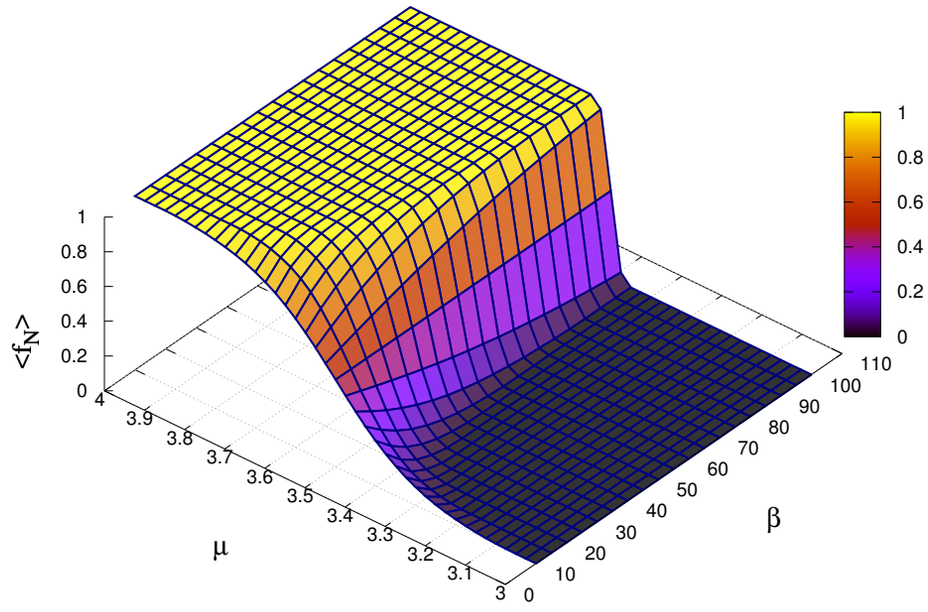

Figure 2.15: The (normalized) fermion number density $\langle f_N \rangle$ as a function of chemical potential μ and inverse temperature β for single-level matrix model with quark energy level $\epsilon = 3.5$ and quark mass $m = 0$. Here $N = N_f = 500$. The model is in a deconfined phase when $0 < \langle f_N \rangle < 1$. The data are obtained through complex Langevin simulations with Langevin time step $\Delta\tau = 0.000005$, thermalization steps $N_{\rm therm} = 5000$, generation steps $N_{\rm gen} = 5000$ and with measurements performed every 50 steps.

When the quark mass is non-vanishing in QCD, the expectation values of bulk observables such as the fermion number density, Polyakov lines and energy, exhibit the 'Silver Blaze' behavior. The bulk observables are nearly zero until onset [65] to a deconfinement transition, which occurs when the chemical potential increases to the value of the lightest quark mass. In our model the onset occurs at $\mu = m$. In Fig. 2.16 (Left) we show the effective fermion number density as a function of chemical potential for large quark mass, near the onset $\mu = m = 25$ for $N = N_f = 100$ and $\beta = 25$ (low T). The Polyakov line as a function of chemical potential is given in Fig. 2.16 (Right). In the large m limit, similar to the $m = 0$ case, the behavior of inverse Polyakov line $\langle P^{-1} \rangle$ precedes that of $\langle P \rangle$ as a function of μ. The transition in μ occurs around onset at m.

2.4.3 Single Level Model with Two Fugacities

In this section we consider the phase diagram of the model given by the action with two effective fugacities

$$S[U] = -\sigma \Big[\log\left(1 + \xi_1 U\ \right) + \log\left(1 + \xi_2 U^\dagger\right) \Big], \tag{2.4.25}$$

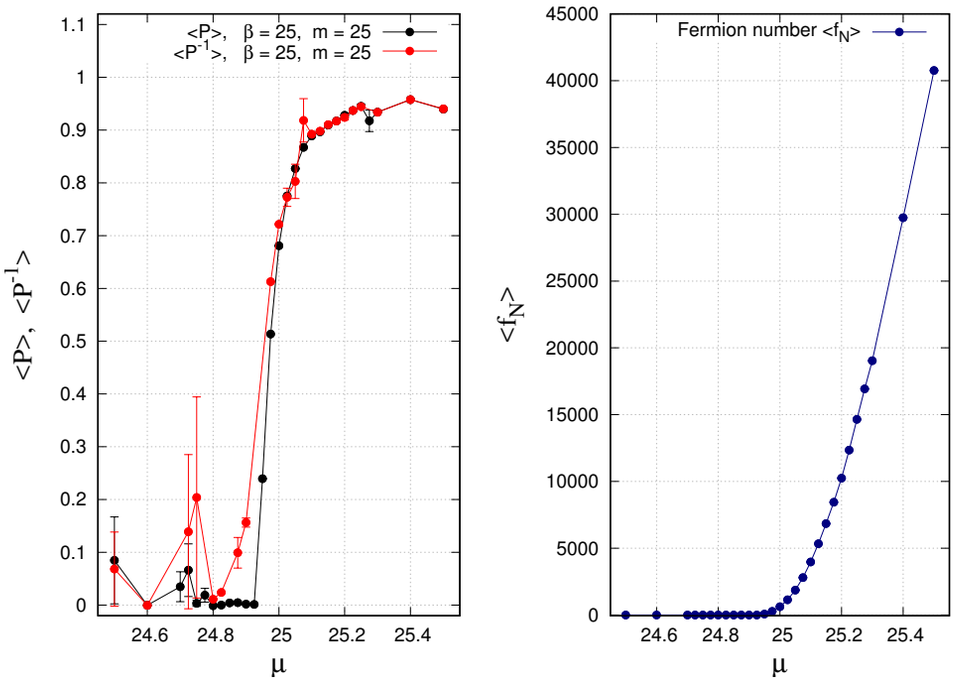

Figure 2.16: The Silver Blaze behavior of observables $\langle f_N \rangle$, $\langle P \rangle$ and $\langle P^{-1} \rangle$ at non-zero quark mass m. (Left) Polyakov line $\langle P \rangle$ and inverse Polyakov line $\langle P^{-1} \rangle$ and (Right) fermion number $\langle f_N \rangle$ as a function of chemical potential for large quark mass near onset at $\mu = m = 25$. Here $N = N_f = 100$ and $\beta = 25$ (low T). The data are obtained through complex Langevin simulations with Langevin time step $\Delta\tau = 0.00005$, thermalization steps $N_{\rm therm} = 5000$, generation steps $N_{\rm gen} = 5000$ and with measurements performed every 50 steps.

where

$$\begin{aligned} \xi_1 &= e^{\beta(\mu-\epsilon)}, \\ \xi_2 &= e^{\beta(-\mu-\epsilon)}. \end{aligned} \tag{2.4.26}$$

Such a model naturally arises from $0+1$-dimensional gauge theory with a fundamental fermion.

In Fig. 2.17 we provide the phase diagram of this model on the (μ, β) plane for the level $l = 1$. (Corresponding to quark energy level $\epsilon = 1.5$ and $\sigma = 4$.) From the behavior of the expectation value of the fermion number density we see that the phase transition from confined to deconfined phase is smooth on the (μ, β) plane even at high temperature ($0.1 \leq \beta \leq 2.0$).

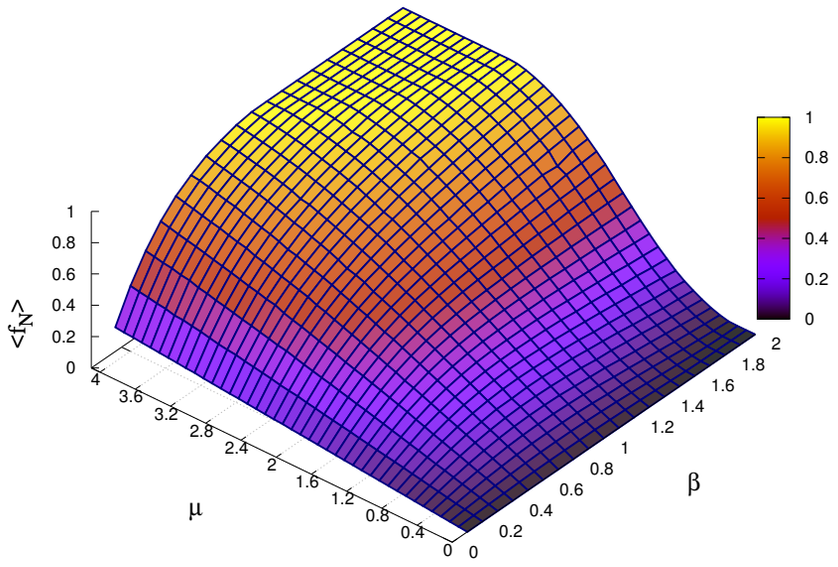

Figure 2.17: The (normalized) fermion number density $\langle f_N \rangle$ as a function of chemical potential μ and inverse temperature β for the matrix model with two effective fugacities. The model has fixed quark energy level $\epsilon = 1.5$, quark mass $m = 0$ and $N = N_f = 100$. The model is in a deconfined phase when $0 < \langle f_N \rangle < 1$. The data are obtained through complex Langevin simulations with Langevin time step $\Delta\tau = 0.00005$, thermalization steps $N_{\rm therm} = 10000$, generation steps $N_{\rm gen} = 50000$ and with measurements performed every 100 steps.

2.4.4 Single Level Model with Interaction

It would be interesting to consider the single-level matrix model with a non-trivial interaction turned on. We take a Polyakov line interaction term of the form

$$S_{\rm int}[U] = g\,(\mathrm{Tr}\,U)(\mathrm{Tr}\,U^{-1}). \tag{2.4.27}$$

Here g denotes a coupling parameter.

Thus we have

$$S[U] = -\sigma \log\left(1 + e^{\beta(\mu-\epsilon)}U\right) + S_{\rm int}[U]. \tag{2.4.28}$$

Here also we take the quark energy level to be fixed at $\epsilon = 3.5$. The action is again not hermitian, giving rise to the sign problem in the presence of a chemical potential. In Figs. 2.18 and 2.19 we plot the fermion number density and the Polyakov lines of the interacting model for various values of the coupling $g = 0, 5, 20, 100$. It is evident that the confinement/deconfinement transition becomes sharper as the interaction strength is increased. The behavior of the Polyakov lines show that the model is in a confined phase for most of the values of the chemical potential.

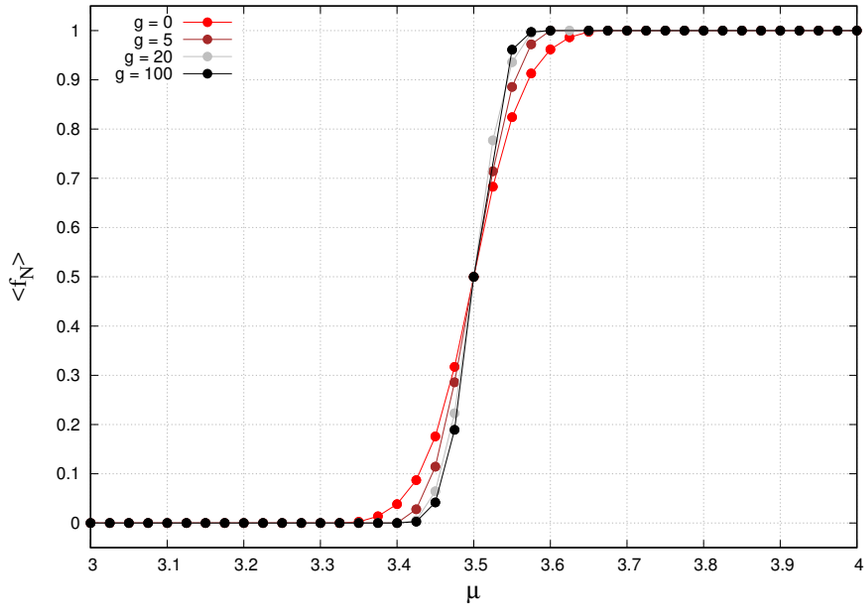

Figure 2.18: The (normalized) fermion number density $\langle f_N \rangle$ as a function of chemical potential μ for interacting single-level matrix model with couplings $g = 0, 5, 20, 100$. We take the quark energy level $\epsilon = 3.5$ and quark mass $m = 0$. Here $N = N_f = 500$. The data are obtained through complex Langevin simulations with Langevin time step $\Delta\tau = 0.000005$, thermalization steps $N_{\text{therm}} = 5000$, generation steps $N_{\text{gen}} = 5000$ and with measurements performed after every 50 steps. The model is in a deconfined phase when $0 < \langle f_n \rangle < 1$. The data show that the phase transition becomes sharper as the interaction strength g is increased.

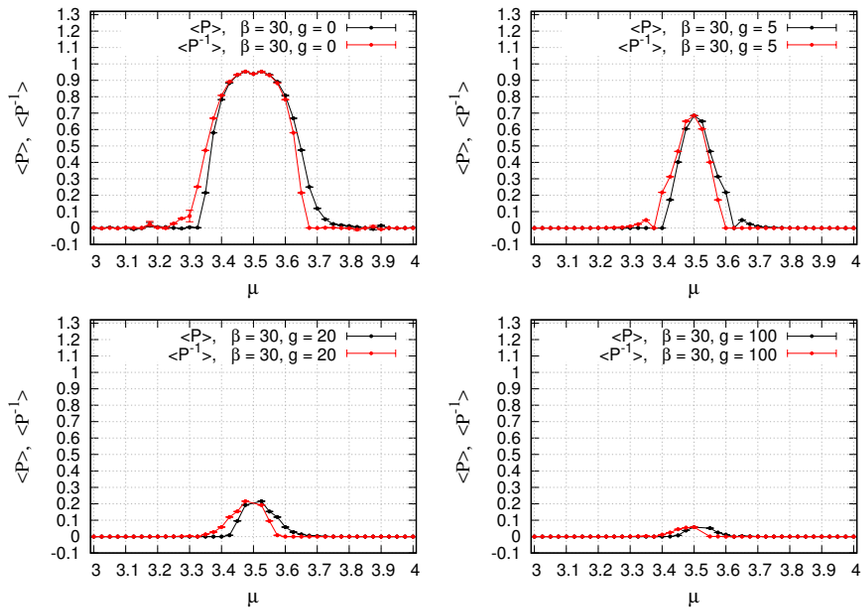

Figure 2.19: The Polyakov line and inverse Polyakov line across a pair of GWW transitions for the interacting single-level matrix model with a fixed quark energy level $\epsilon = 3.5$, quark mass $m = 0$ and $N = N_f = 500$. The data are obtained through complex Langevin simulations with Langevin time step $\Delta\tau = 0.000005$, thermalization steps $N_{\text{therm}} = 5000$, generation steps $N_{\text{gen}} = 5000$ and with measurements performed after every 50 steps. The solid lines are guide to the eye. The plots indicate that the model prefers to stay in a confined phase as the interaction strength g is increased.

2.5 Conclusions and Discussions

In this work we have successfully used complex Langevin dynamics with stochastic quantization to simulate the thermodynamics of a large N unitary matrix models with complex actions. We started with a simple matrix model called the ab-model and investigated its phase structure analytically and numerically. The numerical simulations show excellent match with analytical results. We also studied a model obtained from the effective theory of QCD on $S^1 \times S^3$ at low temperature and finite quark chemical potential. At zero quark mass and low temperature our simulations showed a series of GWW confinement-deconfinement phase transitions as a function of the chemical potential. The phases are characterized by the distribution of eigenvalues of the Polyakov line on the complex plane. In the large quark mass regime we were also able to observe the Silver Blaze behavior in that the bulk observables are roughly zero until the onset transition to the deconfined phase, which occurs at $\mu = m$. We also simulated the model with a simple non-trivial Polyakov line interaction turned on. The model prefers to live in the confined phase as the interaction strength is increased.

We also note that each confinement-deconfinement transition in the Polyakov line is associated with a quark energy level transition. It is interesting to note that the non-monotonic behavior of Polyakov lines have been observed in lattice simulations of QCD with gauge group $SU(2)$ near its saturation density in Ref. [66].

There are several interesting future directions. One could consider complex Langevin simulations of the model with several quark flavors with masses m_f and different chemical potentials μ_f. One could also add other types of non-trivial interaction terms into the model and look for cross-over transitions on the (μ, β) plane [67]. It would also be interesting to see if there exists an AdS/CFT type gravitational dual of the models we studied here. One could ask the question whether the infinite sequence of GWW transitions that we observe in the matrix model be seen in the dual gravitational description.

3

Bound on higher-point Out-of-time-ordered-correlators (OTOCs)

3.1 Commutator, Scrambling and Chaos

A localized disturbance in a chaotic many body quantum system, with time evolution, spreads over the whole phase space, and information associated with the initial perturbation becomes inaccessible to a simple local measurement. This effect is known as scrambling [22, 23]. In practice scrambling is measured by the growth (decay) of an out of time ordered correlator(OTOC) [24],

$$F = \langle V(t)V(0)V(t)V(0)\rangle_\beta \,. \tag{3.1.1}$$

where in Heisenberg's picture $W(t) = e^{-iHt}W(0)e^{iHt}$ and the expectation is a thermal trace. At an initial time this correlator is finite. However due to scrambling the correlator tends to zero as the time translation operator $U(t) = e^{iHt}$ becomes more convoluted with time. At later time, in a chaotic system, we may replace $U(t)$ by a generic unitary matrix, and assuming maximal scrambling, the correlator may be written as matrix average over all possible unitary matrix,

$$F = \int DU \, \langle V(t)V(0)V(t)V(0)\rangle \tag{3.1.2}$$

and asymptotes to zero in a theory with large number of degrees of freedom.

The OTOC is related to the commutator. In the thermal ensemble the commutator is often zero

and one may need to consider the square of it,

$$\begin{aligned} C &= \left\langle [W(t), V(0)]^2 \right\rangle_\beta , \\ &= \mathrm{Tr}\left[e^{-\beta H} [W(t), V(0)]^2 \right] . \end{aligned} \tag{3.1.3}$$

One may expand the commutator square in (3.1.3) in two pieces,

$$C = \left\langle [W(t), V(0)]^2 \right\rangle = -2 \left\langle W(t)W(t)V(0)V(0) \right\rangle + 2 \left\langle W(t)V(0)W(t)V(0) \right\rangle . \tag{3.1.4}$$

The first term in the above expression is a time ordered correlator (TOC) and the second term is an OTOC as in (3.1.1). If we assume something like a large-N factorization, that is if we assume, there is a factorization in the number of degrees of freedom N_d, or in another terms the system has a semi-classical description, where fluctuations are small, then we can factorize the TOC as,

$$\left\langle W(t)W(t)V(0)V(0) \right\rangle \approx 2 \left\langle W(t)V(0) \right\rangle^2 + \left\langle W(t)W(t) \right\rangle \left\langle V(0)V(0) \right\rangle . \tag{3.1.5}$$

The first term in the above expression goes to zero at large time due to usual diffusion/relaxation. At a time scale of the order of diffusion time t_d, we have, $W(t)V(0) \sim e^{-\frac{t}{t_d}}$. Hence diffusion with large N factorization gives thermal factorization of TOCs, i.e. all time ordered thermal correlators factorizes to a product of thermal expectations. For our particular example in hand, we have,

$$\left\langle W(t)W(t)V(0)V(0) \right\rangle \approx \left\langle W(0)W(0) \right\rangle \left\langle V(0)V(0) \right\rangle , \tag{3.1.6}$$

at large time. Hence the large time behavior of the commutator is given by the OTOC (3.1.1).

At a first look, OTOC may apparently seem to have a similar large N factorization as TOC,

$$F \approx 2 \left\langle W(t)V(0) \right\rangle^2 + \left\langle W(t)W(t) \right\rangle \left\langle V(0)V(0) \right\rangle + O(1/N_d) \tag{3.1.7}$$

However, the catch is that the sub-leading part of $F(t)$ grows with time. One may argue that for a system with a large number of degrees of freedom, F tends to zero asymptotically. This could

be understood as following: in an chaotic system, at an intermediate time much larger than the diffusion time $t \gg t_d$, behavior of C is given by

$$C \propto \epsilon e^{2\lambda t}, \tag{3.1.8}$$

where ϵ is a small parameter related to the number of degrees freedom and λ is the Lyapunov exponent. Hence, F at an intermediate time would then behave like,

$$F \approx f_0 - \epsilon f_1 e^{2\lambda t}. \tag{3.1.9}$$

The second term become important at time scale $t_* \sim -\frac{1}{\lambda}\log\epsilon$, which is known as the scrambling time.

It has been proved in [24] using complex analytic techniques that maximum possible value of Lyapunov exponent has an upper bound proportional to the temperature,

$$\lambda_{max} \leq \frac{2\pi}{\beta}. \tag{3.1.10}$$

This maximum value of Lyapunov exponent is also known to saturate in holographic models with gravity ([25, 68, 69, 70]), certain two dimensional CFTs([26, 71]) and also in SYK model ([72, 8, 27, 73]).

Recently there are some interest in OTOCs with more than four insertions ([74, 75, 76, 77, 78, 79, 80, 81, 82]) [*]. Continuing the same logic as that of the previous paragraph, let us consider the following higher power of the commutator,

$$C_n = \left\langle \prod_{i=1}^{n} [V_i(t), V_i(0)] \right\rangle. \tag{3.1.11}$$

When expanded, C_n contains and many other OTOCs and the time ordered correlators. In this expansion, $F_n = \langle (V(T)V(0))^{2n} \rangle$ is the most out of the time ordered OTOC. Here in this work we investigate how analytic properties of an OTOC determines the late time behavior of an OTOC.

[*] Our original motivation to bound higher OTOCs formulated in a discussion with Chethan Krishnan related to his questions about nature of k-point OTOCs in a q-local SYK model [83, 84].

For that purpose we define a generic correlator which not only captures all possible time orderings in (3.1.11) but also is a function of arbitrary temporal variables. After that, we discussed few known examples in the literature and how our results match with them.

3.2 On the growth of generic OTOCs

In this section, we discuss the late time properties of an n-point OTOC. To be well defined a thermal n-point functions needs to be properly regulated. The most generic n-point OTOC with a given scheme of regulation may be expressed as,

$$\mathcal{F}_\beta(t_i,\tau_i) = \mathrm{Tr}\left(e^{-\beta_1\hat{H}}V_1(t_1)e^{-\beta_2\hat{H}}V_2(t_2)\dots e^{-\beta_n\hat{H}}V_n(t_n)\right) \tag{3.2.1}$$

where, $\hat{H}$ is the Hamiltonian of the system, $\beta_i > 0$ are separations between two consecutive operator insertions along the thermal circle, and therefore satisfy the constraint,

$$\sum_{i=1}^{n}\beta_i = \beta \tag{3.2.2}$$

where β is the inverse temperature of the heat bath i.e the circumference of the thermal circle. $\mathcal{F}_\beta(t_i,\tau_i)$ can visualized as shown below in fig. 3.1,

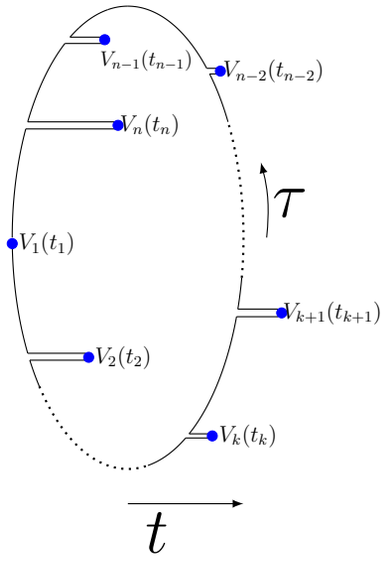

Figure 3.1: Generic n-point correlator on a thermal circle of radius β

where $V_i(t_i)$'s are thermal ordered along τ direction and time is perpendicular to the thermal circle. One can notice from the figure that the lengths of the insertions are not following ascending or descending order, as the correlator is not time-ordered. Various properties of the correlator has been discussed in the appendix 3.5.1.

To proceed we shall assume that each t_i, is some function of one temporal parameter t, i.e $t_i = f_i(t)$. In principle $f_i(t)$ can be an arbitrary function of t, however in this work we restrict ourselves to increasing linear functions.

$$t_i \equiv f_i(t) = \omega_i t \qquad ; \omega_i \geq 0 \tag{3.2.3}$$

We ask the question, how fast the correlators may grow (decay) with the time parameter t. Mathematically it means that we want to put a bound on λ_l, where

$$\frac{\partial}{\partial t}|\mathcal{F}_\beta(t)| \leq \lambda_l |\mathcal{F}_\beta(t)|. \tag{3.2.4}$$

In [24], the authors considered four-point OTOCs and have shown that

$$\lambda_l \leq \frac{2\pi}{\beta}. \tag{3.2.5}$$

The general idea for deriving a chaos bound for generic n-point correlators can be broken into few steps, which closely follows the derivation given in [24]. First, we calculate a differential inequality, and then the chaos bound is established from it under suitable condition.

- First, find the domain of analyticity of the correlator $\mathcal{F}_\beta$ when time t_i is analytically continued from $t \to t + i\tau$. For generic n-point correlator it is an asymmetric half-strip.
- Next, find an appropriate normalization factor $\mathcal{N}_\beta$, such that $g(t) = \mathcal{F}_\beta/\mathcal{N}_\odot \leq 1$ on the analytic domain. This step needs certain amount of care, we would discuss that in details.
- Finally, Schwarz-Pick theorem is used to put a bound on the growth of the correlator at late

times. We find that,

$$\frac{d}{dt}|g|< (1-|g|)\lambda_l \tag{3.2.6}$$

We find that λ_l is inversely proportional to the width (Δ_s) of the asymmetric strip,

$$\lambda_l \leq \frac{\pi}{\Delta_s} \tag{3.2.7}$$

- The (3.2.6) is true for a large class of theories, whereas the chaos bound is derived under the condition that correlators has an expansion in a small parameter ϵ. We assume,

$$g(t) \sim g_o - \epsilon e^{\lambda t} g_1(t), \tag{3.2.8}$$

where importantly ϵ is a small quantity. For example in a large-N theory, ϵ is the string coupling $\frac{1}{N^2}$. Putting the above in (3.2.6) and assuming a boundary condition at some initial time t_i, $g(t_i) = 1$, we see that the bound becomes a bound on Lyapunov index in a time scale determined by the condition $\frac{dg_1}{dt} \leq \lambda g_1$ The boundary condition implies $\mathcal{F}_\beta \sim \mathcal{N}_\odot$ at $t \sim t_i$.

For a large-N theory with dissipation, the initial time scale could be taken as the diffusion time scale, i.e. $t_i \sim t_d$. In a large-N theory we can write,

$$g(t) \sim g_0(t) - \frac{1}{N^2} g_1(t). \tag{3.2.9}$$

Where $g_0(t)$ approaches a constant g_o for a time scale $t \gg t_d$, i.e.,

$$g_0(t) \sim g_o + o(e^{-\frac{t}{t_d}}). \tag{3.2.10}$$

On the other hand, $g_1(t)$ grows exponentially, $g_1(t) \sim \exp(\lambda t)$. The perturbative expansion breaks down when $\lambda t \sim \log(N)$.

3.2.1 Domain of analyticity

Domain of analyticity plays an important role in defining the large time behavior of the OTOCs, as it dictates the bound of the correlators. The question is, once analytically continued to complex time variables $t \to t + i\tau$, what is the domain on which the correlator is well defined. To evaluate that, let's re-express $\mathcal{F}_\beta$ in (3.2.1) by introducing dimensionless quantities $\alpha_i = \beta_i/\beta$, and using Heisenberg picture we can express analytically continued $\mathcal{F}_\beta(t + i\tau, \alpha_i)$ correlator as,

$$\mathcal{F}_\beta(t + i\tau, \alpha_i) = \mathrm{Tr}\left[\rho^{\left(\alpha_1 - \frac{\omega_{n,1}}{\beta}\tau\right)} V_1(t_1)\rho^{\left(\alpha_2 - \frac{\omega_{1,2}}{\beta}\tau\right)} V_2(t_2)\rho^{\left(\alpha_3 - \frac{\omega_{2,3}}{\beta}\tau\right)} \dots \rho^{\left(\alpha_n - \frac{\omega_{n-1,n}}{\beta}\tau\right)} V_n(t_n)\right] \tag{3.2.11}$$

where, $\omega_{i,j} = \omega_i - \omega_j$.

Expressing the trace in the energy basis,

$$\begin{aligned}\mathcal{F}_\beta\left(t + i\tau, \alpha_i\right) = \sum_{m_1, m_2, \cdots, m_n} & e^{-\beta E_{m_1}(\alpha_1 - \frac{\omega_{n,1}}{\beta}\tau)} v^{(1)}_{m_1,m_2} e^{-\beta E_{m_2}(\alpha_i - \frac{\omega_{1,2}}{\beta}\tau)} v^{(2)}_{m_2,m_3} \cdots \\ & \cdots \quad v^{(n-1)}_{m_{n-1},m_n} e^{-\beta E_{m_n}(\alpha_n - \frac{\omega_{n-1,n}}{\beta}\tau)} v^{(n)}_{m_n,m_1}\end{aligned} \tag{3.2.12}$$

where, $v^{(i)}_{a,b}$ are the matrix elements of $V_i(t_i)$ operator. Since, energies E_a are bounded from below for physically sensible theories, the above summations are convergent as long as the coefficient multiplying E_a are positive. When some coefficient, say, without loss of generality $\alpha_1 - \omega_{n,1}\tau = 0$, then the above expression becomes,

$$\begin{aligned}\mathcal{F}_\beta(t + i\tau, \alpha_i) = \sum_{m_2 \cdots, m_n} \sum_{m_1} & \left(v^{(1)}_{m_1,m_2} v^{(n)}_{m_n,m_1}\right) e^{-\beta E_{m_2}\left(\alpha_i - \frac{\omega 1,2}{\beta}\tau\right)} v^{(2)}_{m_2,m_3} \cdots \\ & \cdots \quad v^{(n-1)}_{m_{n-1},m_n} e^{-\beta E_{m_n}\left(\alpha_n - \frac{\omega_{n-1,n}}{\beta}\tau\right)}.\end{aligned} \tag{3.2.13}$$

Now the summation $\sum_{m_1} v^{(n)}_{m_n,m_1} v^{(1)}_{m_1,m_2}$ is not necessarily convergent as it lacks the damping factor $\sim \ e^{-\#E_{m_1}}$ for higher values of m_1 [†].Therefore the correlator is well defined as long as two neighbouring operators $V_i(t_i)$, $V_{i+1}(t_{i+1})$ don't collide with each other along the thermal circle

[†]Here we have assumed discrete spectrum of the Hamiltonian, but similar argument will hold if we consider continuous spectrum as well.

(they need not be at equal times), and that dictates the domain of analyticity. We find that the domain is given by,

$$\tau_- = \text{min.} \left\{ \frac{\alpha_j \beta}{\omega_{j,j-1}} \right\} < \tau < \text{min.} \left\{ \frac{\alpha_i \beta}{\omega_{i-1,i}} \right\} = \tau_+ \tag{3.2.14}$$

Choosing $t_i = 0$ translates to having one $\omega_i = 0$, so the above equation is guaranteed to have solutions and hence $\mathcal{F}_\beta$ is analytic on a half-strip $\mathcal{D} = (0, \infty) \times i(-\tau_-, \tau_+)$.

It should be mentioned that this is the minimum possible domain of analyticity. Depending on the model, the actual domain could be much bigger. It is expected that in a integrable model the domain would be much wider.

3.2.2 Normalization factor

The derivation of chaos bound through the application of Schwarz-Pick theorem, demands a function bounded by unity on the domain $\mathcal{D}$. This means $\mathcal{F}_\beta$ needs to be properly normalized by dividing it with a normalization factor. The normalization factor can be chosen to be greater than the maxima of $\mathcal{F}_\beta$ on domain $\mathcal{D}$ which is finite and independent of $z \in \mathcal{D}$ coordinates. In an unbounded domain using Phragmén-Lindelöf principle, all one needs show that the function $\mathcal{F}_\beta$ is bounded by unity on the boundary and is bounded by a constant $\mathcal{N}_\beta$ in the interior. For us the unbounded domain is an asymmetric half-strip of width Δ_s and $\Re(z) > t_d$, then Phragmén-Lindelöf principle([85, 86]) needs that the function in the interior to be less than $\exp\left(\exp\left(\frac{\pi}{\Delta_s}\Re(z)\right)\right)$, i.e if the constant $\mathcal{N}_\beta < \exp\left(\exp\left(\frac{\pi}{\Delta_s} t_0\right)\right)$ then $|\mathcal{F}_\beta| \leq 1$ in the entire domain.

As we will discuss at the end of this section, there could be some subtleties on how big C could be. This issue is different from the issue of the order of normalization constant and when (3.2.7) could be interpreted as a bound on the lyapunov index, discussed in the beginning of the chapter. If one is does not need to be careful about this constant C then one can simply use the methods of appendix 3.5.3 to put a bound on the correlators to bound a correlator by a product of correlators defined at a higher temperature. In the main text, we will discuss a different method and propose a possible bound on correlators by a product of quantities defined at the same temperature.

To find such a bound, we first look at $\mathcal{F}_\beta$ at $(t, \tau_\pm)$ boundaries. At these boundaries, operators

hit each other on the thermal circle and we have various scenario of that happening,

- first only two operators say V_k, V_{k+1} hit each other then, $\mathcal{F}_\beta$ is of the form,

$$\mathcal{F}_\beta\left(t+i\tau_\pm,\alpha_i\right)=\mathrm{Tr}\left[\rho^{b_1^\pm}V_1(t_1)\rho^{b_2^\pm}V_2(t_2)\ldots\left(\rho^{b_k^\pm}V_k(t_k)V_{k+1}(t_{k+1})\rho^{b_{k+2}^\pm}\right)\ldots\rho^{b_n^\pm}V_{t_n}\right]. \tag{3.2.15}$$

  where,

$$b_i^\pm=\alpha_i\pm\frac{\omega_{i-1,i}}{\beta}\tau_\pm \tag{3.2.16}$$

  and some $b_{k+1}^\pm=0$. It is not necessary that same two operators hit each other on on upper and lower boundary of the strip.

- Many different pairs of operators hit each other

$$\begin{aligned}\mathcal{F}_\beta\left(t+i\tau_\pm,\alpha_i\right)=\mathrm{Tr}\Big[\rho^{b_1^\pm}V_1(t_1)\rho^{b_2^\pm}V_2(t_2)\ldots\left(\rho^{b_k^\pm}V_k(t_k)V_{k+1}(t_{k+1})\rho^{b_{k+2}^\pm}\right)\\ \ldots\left(\rho^{b_j^\pm}V_k(t_j)V_{j+1}(t_{j+1})\right)\ldots\rho^{b_n^\pm}V_{t_n}\Big]\end{aligned} \tag{3.2.17}$$

and a third scenario where more than two operators hitting each other, which can be avoided by slightly changing the regulation scheme, but not changing the domain of analyticity. Therefore it is sufficient to consider the second scenario (3.2.17) as the most general case.

Suppose δ is the smallest positive distance between two neighbouring operators, i.e min. $b_i^\pm>0$, then if we choose some number k such that

$$\frac{1}{2^k}\leq\delta \tag{3.2.18}$$

then we can express the correlator $\mathcal{F}_\beta(t\pm i\tau_\pm,\alpha_i)$ as

$$\mathcal{F}_\beta=\mathrm{Tr}\left(\prod_{i=1}^{2^k}M_i\right) \tag{3.2.19}$$

where M_i could have following forms,

$$M_i = \begin{cases} \rho^{\frac{1}{2^k}} & (3.2.20) \\ \rho^{\frac{1}{2^k}-\eta} V_i(t_i)\rho^{\eta} & (3.2.21) \\ \rho^{\frac{1}{2^k}-\eta'} V_i(t_i)V_{i+1}(t_{i+1})\rho^{\eta'} & (3.2.22) \end{cases}$$

where η, η' are some positive numbers less than $1/2^k$. Using the trace inequality identity for product of 2^k matrices(proof is given in 3.5.3),

$$|\mathcal{F}_\beta| = \left| \mathrm{Tr}\left(\prod_{i=1}^{2^k} M_i \right) \right| \leq \prod_{i=1}^{2^k} \left[\mathrm{Tr}(M_i)^{2^k} \right]^{1/2^k} \tag{3.2.23}$$

we can put a bound on $\mathcal{F}_\beta$(diagrammatic demonstration is in 3.2)

$$\begin{aligned} |\mathcal{F}_\beta(t \pm i\tau_\pm, \alpha_i)| \leq & \prod_{i \in \text{ isolated op.}} \left[\mathrm{Tr}\left(\rho^{\left(\frac{1}{2^{k-1}}-2\eta_i\right)} V_i \rho^{(2\eta_i)} V_i \right)^{2^{k-1}} \right]^{1/2^k} \\ & \times \prod_{j \in \text{ colliding op.}} \left[\mathrm{Tr}\left(\rho^{\left(\frac{1}{2^{k-1}}-2\eta_j\right)} V_j(t_j)V_{j+1}(t_{j+1})\rho^{(2\eta_j)} V_{j+1}(t_{j+1})V_j(t_j) \right)^{2^{k-1}} \right]^{1/2^k} \end{aligned} \tag{3.2.24}$$

trace of operators M_i of the form (3.2.20) will be just one, hence ignored. Index i runs over isolated operator insertions of the form (3.2.21), and these traces are independent of time.Index j runs over all colliding operators of the form (3.2.22)., and we expect them to be finite due to diffusion. For a time t much greater than dissipation time t_d, we have following thermal factorization (with a possible error ε),

$$\begin{aligned} & \left[\mathrm{Tr}\left(\rho^{\left(\frac{1}{2^{k-1}}-2\eta_j\right)} V_j(t_j)V_{j+1}(t_{j+1})\rho^{(2\eta_j)} V_{j+1}(t_{j+1})V_j(t_j) \right)^{2^{k-1}} \right] \\ & \quad \approx \left[\mathrm{Tr}\left(\rho^{\left(\frac{1}{2^{k-1}}-2\eta_j\right)} V_j \rho^{2\eta_j} V_j \right)^{2^{k-1}} \right] \times \left[\mathrm{Tr}\left(\rho^{\left(\frac{1}{2^{k-1}}-2\eta_j\right)} V_{j+1} \rho^{2\eta_j} V_{j+1} \right)^{2^{k-1}} \right] + \varepsilon, \end{aligned} \tag{3.2.25}$$

which is a time independent quantity. Hence, $|\mathcal{F}_\beta|$ on the boundary is bounded by a time indepen-

dent constant,

$$\mathcal{N}_\beta \equiv \prod_{i\in \text{ all ops.}} \left[\text{Tr}\left(\rho^{\frac{1}{2^{k-1}}-2\eta_j} V_j \rho^{2\eta_j} V_j\right)^{2^{k-1}}\right]^{1/2^k} + \varepsilon \tag{3.2.26}$$

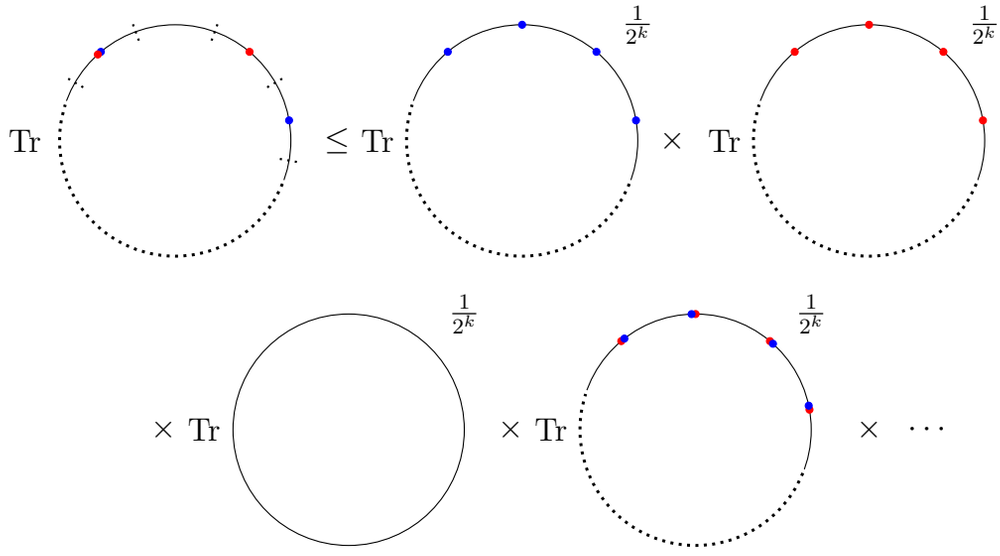

Figure 3.2: Diagrammatic demonstration: Top view of thermal circle, blue/red dots indicate operators at different times.

For any point $z = t + i\tau$ strictly inside the domain $\mathcal{D}$, if we split the thermal circle into 2^k segments with operators $M_i'(z)$, similar to what is done in (3.2.19). If two operators collide in the boundary then we keep them in the same segment. Here, the form of $M_i'(z)$'s will be similar to M_i but in the third line (3.2.22) we will now have some power of ρ inserted between the two colliding operators. For other case (3.2.21), only the insertion of ρ will be different from that in the boundary, whereas M_i' ,the operator itself, would be independent of the real part of time (t).

Now in both of cases the ratios between $M_i'(z)$ and M_i is only a function of τ and is of order one. Therefore Applying Phragmén-Lindelöf principle (as discussed in the beginning of the section) if we normalize $\mathcal{F}_\beta(z)$ with $\mathcal{N}_\beta$, it shall remain bounded by unity in the entire domain $\mathcal{D}$.

In [24] authors have used the contracting properties of y to bound the correlators. This procedure result in an OTOC, where the total sum of the power of y is less than 1. To express such a correlator as a product of thermal quantities we need to introduce ratios of partition functions defined in two different temperatures. For example in the case of a large-N gauge theory, this results in a bound, which is of order e^{N^2}. Hence, technically speaking the particulars of the proof is strictly

valid in a time scale of the $o(\log N) + o(\log(1/\epsilon))$. In a large-$N$ gauge theory $1/\epsilon \sim N^2$. This virtually doubles the time scale. To be mentioned is that it is not entirely unreasonable to assume that bounded correlators remain a $o(1)$ number and actual bound is much less what has been proved. If one is fine to use the contracting properties of y, then one can use the inequality in the appendix 3.5.3 to bound a correlator by a product of correlators defined at a higher temperature.

3.2.3 Bound on growth of the correlator

Continuing from the previous section $g(t + i\tau) = \mathcal{F}_\beta(t + i\tau)/\mathcal{N}_\beta$ is an analytic function and $|g(t + i\tau)| \leq 1$ on the half-strip $\mathcal{D}$. In order to use Schwarz-Pick theorem we conformally map g from $\mathcal{D}$ to a unit disk in complex plane $\mathbb{C}$ using the following transformation

$$z = \frac{1 - \sinh\left[\dfrac{\pi}{(\tau_+ + \tau_-)}\left(t + i\tau - i\left(\dfrac{\tau_+ - \tau_-}{2}\right)\right)\right]}{1 + \sinh\left[\dfrac{\pi}{(\tau_+ + \tau_-)}\left(t + i\tau - i\left(\dfrac{\tau_+ - \tau_-}{2}\right)\right)\right]}. \tag{3.2.27}$$

Above mapping is shown in fig. 3.3, for $(\tau_+ = 2, \tau_- = -1)$. Fixed-time vertical lines at early times begin as semi-circle on right, with endpoint coordinates $[(0, 1), (0, -1)]$ and at late times converge to the point $(-1, 0)$ on the unit disk.

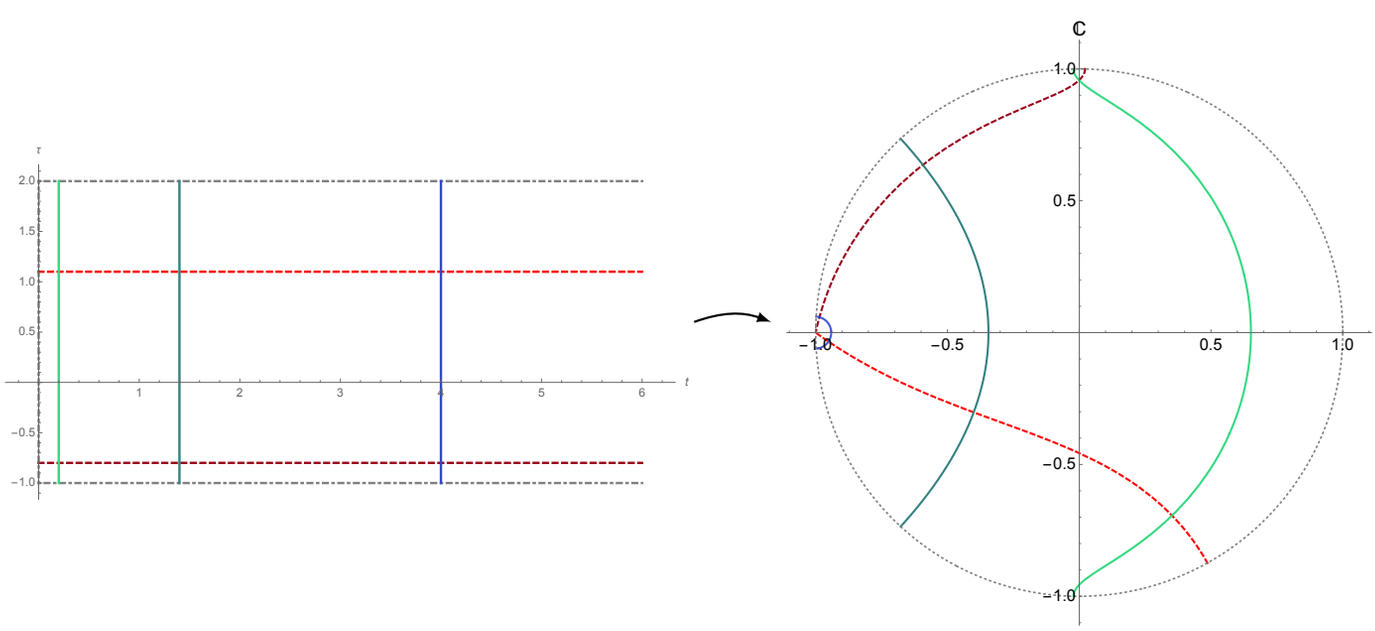

Figure 3.3: Conformal mapping from half-strip $\mathcal{D} = (0, \infty) \times i(-1, 2)$ to unit disk in complex plane $\mathbb{C}$, each line map to its corresponding colored line-segment on the disk.

Let's recall Schwarz-Pick theorem, which states that any conformal mapping $f(z)$ from a unit disk to another unit disk, shall satisfy the following inequality,

$$\frac{|df|}{(1-|f(z)|^2)} \leq \frac{|dz|}{(1-|z|^2)} \tag{3.2.28}$$

where z is the coordinates of the unit disk.

Since $g(z) \leq 1$ on $\mathcal{D}$ (as well as on the unit disk), we can think of $g(z)$ as a conformal mapping from a unit disk to another unit disk, and hence applying Schwarz-Pick theorem for a fixed value of τ, we have

$$\frac{|\partial_t g(t+i\tau)|}{1-|g(t+i\tau)|^2} \leq \frac{\pi}{2\sqrt{2}\Delta_s} \csc\left(\frac{\pi(\tau_+ - \tau)}{\Delta_s}\right) \operatorname{csch}\left(\frac{\pi t}{\Delta_s}\right) \times \left[\cos\left(\frac{\pi}{\Delta_s}(\tau_+ - \tau_- - 2\tau)\right) + \cosh\left(\frac{2\pi t}{\Delta_s}\right)\right]^{\frac{1}{2}} \tag{3.2.29}$$

where, Δ_s is the strip width $(\tau_+ + \tau_-)$. For $t \gg 0$, the above inequality becomes

$$|\partial_t g| \leq \frac{\pi}{2\Delta_s}\left[\csc\left(\frac{\pi}{\Delta_s}(\tau_+ - \tau)\right)\right](1-|g|^2) \tag{3.2.30}$$

Expressing $g(t+i\tau) = u(t+i\tau) + iv(t+i\tau)$, where u, v are real-valued functions and using Cauchy-Schwarz inequality one can easily show that

$$\frac{\partial}{\partial t}|g| \leq \left|\frac{\partial g}{\partial t}\right|. \tag{3.2.31}$$

Using the above relation, $|g| \leq 1$, and choosing the minima of $\csc\left(\frac{\pi(\tau_+ - \tau)}{\Delta_s}\right)$ in the domain, the inequality (3.2.29) becomes

$$\frac{d}{dt}|g| \leq \frac{\pi}{\Delta_s}(1-|g|) \tag{3.2.32}$$

Therefore we have a bound on how $\mathcal{F}_\beta(t)$ decays at late time,

$$|\mathcal{F}_\beta| \lesssim \mathcal{N}_\beta - |\mathcal{F}_\beta(t_0)| e^{\frac{\pi}{\Delta_s} t} \tag{3.2.33}$$

and the Lyapunov exponent can be read-off as $\lambda_L = \dfrac{\pi}{\Delta_s}$ thus, it is just a function of the width of the strip $\mathcal{D}$.

3.3 Examples

In this section, we find out Lyapunov exponents of few correlators. Before considering higher point correlators let's look at a generalization of four-point OTOC considered in [78]

$$f_\gamma(t) = \frac{1}{2} \operatorname{Tr}\left[\hat{\rho}^{(1-\gamma)/2} A(t) \hat{\rho}^{\gamma/2} B(0) \rho^{(1-\gamma)/2} A(t) \hat{\rho}^{\gamma/2} B(0)\right] \tag{3.3.1}$$

Using analytic properties of the correlator and assuming late time behaviour of the correlator(briefly described in ap. 3.5.1) they conclude that the Lyapunov exponent(i.e $\frac{2\pi}{\beta}$) is same as the original four-point OTOC.

Using our approach we can as well derive the same expected Lyapunov bound, as the domain of analyticity for the above correlator $f_\gamma(t)$ lies between

$$\left(-\frac{\beta(1-\gamma)}{2}, \frac{\beta\gamma}{2}\right) \tag{3.3.2}$$

and therefore the strip width $\Delta_s = \beta/2$ which is independent of γ and giving the same Lyapunov exponent.

Next we consider 2n-"Tremolo" correlators mentioned in [76] which is has a form $\langle (V(t)W(0))^n \rangle$. Choosing a equal-spaced regulation scheme,

$$F^n(t) = \operatorname{Tr}\left(\hat{\rho}^{\frac{1}{2n}} V(t) \hat{\rho}^{\frac{1}{2n}} W(0)\right)^n \tag{3.3.3}$$

it is easy to see from our method that the Lyapunov exponent $\lambda_l = \frac{n\pi}{\beta}$. Note that, for the above correlator choosing any other type of regulation scheme would give us a greater Lyapunov expo-

nent, therefore equal-space regulation scheme is the best estimate of chaos bound. The reason being, if we chose unequally spaced regulation scheme, the width of the analytical strip would shrink and therefore the Lyapunov exponent would increase, which would lead to a sub-optimal bound of chaos.

3.4 Conclusion

In this work, we have discussed how complex analytical properties of OTOCs to put constraints on the temporal behavior of OTOCs. In a free or an integrable system, correlators do not grow exponentially with time. Hence, it is natural to ask, whether higher order chaos-bounds for a generic operator ever gets saturated in a given theory. It is known that the four point OTOCs saturate the chaos bounds in gravity and few other large-N theories. One may guess that the growth of the higher point correlators in a black hole back ground also saturate similar bound, and this may be related to the stretching of the geometry discussed in [70]. In this regard, it would be instructive to have a rigorous calculation of higher point correlators in CFTs and in SYK model or in other computable theories.

3.5 Appendix

3.5.1 Properties of Generic n-point correlator

Let's look at few properties of $\mathcal{F}_\beta(t_i, \beta_i)$. In a more conventional way it can be rewritten as,

$$\mathcal{F}_\beta = \mathrm{Tr}\left[\hat{\rho}\left(e^{\tau_1\hat{H}}V_1(t_1)e^{-\tau_1\hat{H}}\right)\left(e^{\tau_2\hat{H}}V_2(t_2)e^{-\tau_2\hat{H}}\right)\ldots\left(e^{\tau_n\hat{H}}V_n(t_n)e^{-\tau_n\hat{H}}\right)\right] \tag{3.5.1}$$

where, $\hat{\rho} = e^{-\beta\hat{H}}/\mathcal{Z}$, is the thermal density matrix,

and $\tau_i \equiv \sum_{j=1}^{i}\beta_j - \beta$. Using Heisenberg picture,

$$A(t) = e^{i\hat{H}t}A(0)e^{-i\hat{H}t} \tag{3.5.2}$$

eqn. (3.5.1) can be compactly expressed as,

$$\begin{aligned}\mathcal{F}_\beta(t_i + i\tau_i) &= \mathrm{Tr}\left[\hat{\rho}\, V_1\left(t_1 + i\tau_1\right) V_2\left(t_2 + i\tau_2\right) \ldots V_n\left(t_n + i\tau_n\right)\right] \\ &= \mathrm{Tr}\left[\hat{\rho} \prod_{i=1}^{n} V_i(t_i + i\tau_i)\right] \end{aligned} \tag{3.5.3}$$

where, $\mathcal{F}_\beta(t_i + i\tau_i)$ is understood as $\mathcal{F}_\beta(t_1 + i\beta_1, t_2 + i\beta_2, \ldots, t_n + i\beta_n)$.

In this way of writing the correlator,

- the time translation invariance, and trace cyclicity gives rise to following relations,

$$\mathcal{F}_\beta(t_i + i\tau_i + c) = \mathcal{F}_\beta(t_i + i\tau_i) \tag{3.5.4}$$

$$\mathcal{F}_\beta(t_i + i\tau_i) = \mathcal{F}_\beta(t_n + i\tau_n - i\beta, t_1 + i\tau_1, \cdots, t_{n-1} + i\tau_{n-1}) \tag{3.5.5}$$

- and its complex conjugate

$$\mathcal{F}^\dagger_\beta(t_1 + i\tau_1, \cdots, t_n + i\beta_n) = \mathcal{F}_\beta(t_n - i\beta_n, t_{n-1} - i\beta_{n-1}, \cdots, t_1 - i\beta_1) \tag{3.5.6}$$

  implies that the generic correlator is not real, unlike the four-point OTOC considered in [24].

- it is straightforward to see the analytic property

$$\left(\frac{\partial}{\partial t_i} + i\frac{\partial}{\partial \tau_i}\right) \mathcal{F}_\beta(t_i + i\tau_i) = 0 \tag{3.5.7}$$

Further if we assume,

$$\mathcal{F}_\beta(t) = \mathcal{F}^0_\beta - \epsilon \mathcal{F}^1_\beta e^{\lambda t}, \tag{3.5.8}$$

where t is suitable linear combination of t_is. Then the above differential equation may be used to bound the maximum value of the Lyapunov exponent λ [79].

3.5.2 Trace Inequalities

Cauchy-Schwarz Inequality for Matrices

Here we give a short proof of *Cauchy-Schwarz Inequality* for matrices,

$$\mathrm{Tr}\big(A^\dagger B\big) \leq [\mathrm{Tr}\big(A^\dagger A\big)]^{1/2}[\mathrm{Tr}\big(B^\dagger B\big)]^{1/2} \tag{3.5.9}$$

where A, B are some generic finite dimensional matrices.

Proof :

Let $[A]_{ij} = a_{ij}$, then $[A^\dagger]_{ij} = a^*_{ji}$, similarly for $[B]_{ij}$, we have b_{ij}. Then

$$\mathrm{Tr}\big(A^\dagger B\big) = \sum_{i,j} a^*_{ki} b_{ki} \tag{3.5.10}$$

If $\vec{v_i} = (a_{1i}, a_{2i}, \dots)$ and $\vec{w_i} = (b_{1i}, b_{2i}, \dots)$, we can write

$$\mathrm{Tr}\big(A^\dagger B\big) = \sum_i \langle v_i | w_i \rangle \tag{3.5.11}$$

Using Cauchy-Schwarz(CS) inequality for $\vec{v_i}, \vec{w_i}$

$$\begin{aligned} \mathrm{Tr}\big(A^\dagger B\big) &\leq \sum_i ||v_i||\ ||w_i|| \\ &= \sum_i \left(\sum_k |a|^2_{ki} \right)^{1/2} \left(\sum_m |b|^2_{mi} \right)^{1/2} \end{aligned} \tag{3.5.12}$$

Now thinking of $p_i = \left(\sum_k a_{ki}^2\right)^{1/2}$, $q_j = \left(\sum_k a_{kj}^2\right)^{1/2}$ as vectors $\vec{p}, \vec{q}$ and using CS inequality

$$\begin{aligned}
\mathrm{Tr}\left(A^\dagger B\right) &\leq \langle p|q\rangle \\
&\leq ||p||\ ||q|| \\
&= (\sum_{i,k} |a_{ki}|^2))^{1/2} (\sum_{j,m} |b_{mj}|^2)^{1/2} \\
&= (\mathrm{Tr}\left(A^\dagger A\right))^{1/2} (\mathrm{Tr}\left(B^\dagger B\right))^{1/2}
\end{aligned} \tag{3.5.13}$$

Therefore, $\mathrm{Tr}\left(A^\dagger B\right) \leq (\mathrm{Tr}\left(A^\dagger A\right))^{1/2} (\mathrm{Tr}\left(B^\dagger B\right))^{1/2}$.

3.5.3 Bound on Trace of Product of Matrices

With the help of above inequality, we put on a bound on the trace of product of matrices,

$$\mathrm{Tr}\left(\prod_{i=1}^{n} M_i\right) \leq \prod_{i=1}^{n} \left[\mathrm{Tr}\left(M_i^\dagger M_i\right)\right]^{1/2} \tag{3.5.14}$$

Proof :

Let,

$$M_{ij} \equiv \prod_{k=i}^{j} V_k \tag{3.5.15}$$

where $i \leq j$, and

$$\begin{aligned}
P_i &\equiv V_i^\dagger V_i \\
P_{j,k} &\equiv \left(V_j V_{j+1} \dots V_k\right)^\dagger \left(V_j V_{j+1} \dots V_k\right) = M_{jk}^\dagger M_{jk}
\end{aligned} \tag{3.5.16}$$

notice that, P's are positive semi-definite matrices.

Applying CS inequality to $\mathrm{Tr}(V_1 V_2 \dots V_n)$,

$$\begin{aligned}
\mathrm{Tr}(V_1 V_2 \dots V_n) &\leq \left[\mathrm{Tr}\left(V_1^\dagger V_1\right)\right]^{1/2} \left[\mathrm{Tr}\left(\left(V_2 V_3 \dots V_n\right)^\dagger \left(V_2 V_3 \dots V_n\right)\right)\right]^{1/2} \\
&= \left[\mathrm{Tr}(P_1)\right]^{1/2} \left[\mathrm{Tr}\left(P_{2,n}\right)\right]^{1/2}
\end{aligned} \tag{3.5.17}$$

to the above inequality, applying CS inequality to $\mathrm{Tr}\,(P_{2,n})$, we have

$$\begin{aligned}\mathrm{Tr}(V_1V_2\dots V_n) &\leq \left[\mathrm{Tr}(P_1)\right]^{1/2}\left[\mathrm{Tr}\,(P_n)^2\right]^{1/4}\left[\mathrm{Tr}\,(P_{2,n-1})^2\right]^{1/4}\\ &\leq \left[\mathrm{Tr}(P_1)\right]^{1/2}\left[\mathrm{Tr}\,(P_n)\right]^{1/2}\left[\mathrm{Tr}\,(P_{2,n-1})\right]^{1/2}\end{aligned} \tag{3.5.18}$$

in the second line we have used the fact that, $\left[\mathrm{Tr}(P^2)\right]^{1/2} \leq \mathrm{Tr}(P)$ for positive semi-definite matrices. Now recursively applying CS inequality to $\mathrm{Tr}(P_{2,k})$'s and using norm-inequality we get the desired bound (3.5.14).

Using the above inequality, the correlator $\mathcal{F}_\beta$ in (3.2.17) is bounded by

$$\begin{aligned}\mathcal{F}_\beta\left(t+i\tau_\pm,\alpha_i\right) \leq \prod_{\{i\in \text{ single op.}\}}&\left[\mathrm{Tr}\Big(\rho^{b_i^\pm}V_i\rho^{b_{i+1}^\pm}V_i\Big)\right]^{1/2}\\ &\prod_{\{j\in \text{ double op.}\}}\left[\mathrm{Tr}\left(\rho^{b_j^\pm}V_j(t_j)V_{j+1}(t_{j+1})\rho^{b_{j+2}^\pm}V_{j+1}(t_{j+1})V_j(t_j)\right)\right]^{1/2}\end{aligned} \tag{3.5.19}$$

here index $i \in \{$ single op.$\}$ runs over all P_i with single operators of the form as in (3.2.21), and index $j \in \{$ double op.$\}$ runs over M_j of the form given in (3.2.22) . It is easy to see that the product of single operator traces are independent of time, but not double operator traces. To have a time-independent normalization factor, we need to find an upper bound on the time dependent part of the above inequality. For that, notice that the individual double operator trace is in fact time ordered, and now setting the initial time t_0 much greater than the dissipation time t_d but much less the scrambling time t_*, (3.5.19) these operators factorize to give a time-independent bound,

$$\begin{aligned}\mathcal{F}_\beta\left(t+i\tau_\pm,\alpha_i\right) \leq \prod_{\{i\in \text{single op.}\}}&\left[\mathrm{Tr}\Big(\rho^{b_i^\pm}V_i\rho^{b_{i+1}^\pm}V_i\Big)\right]^{1/2}\\ &\times\prod_{\{j\in \text{ double op.}\}}\left[\mathrm{Tr}\left(\rho^{b_j^\pm}V_j\rho^{b_{j+2}^\pm}V_j\right)\right]^{1/2}\left[\mathrm{Tr}\left(\rho^{b_j^\pm}V_{j+1}\rho^{b_{j+2}^\pm}V_{j+1}\right)\right]^{1/2}\end{aligned} \tag{3.5.20}$$

Trace Inequality for product of 2^k Matrix

The above inequality is useful for arbitrary number of matrices, but if the number of matrices is a power of 2, say 2^k then there is an interesting inequality

$$\left|\mathrm{Tr}\left(\prod_{i=1}^{2^k} M_i\right)\right| \leq \prod_{i=1}^{2^k} \left[\mathrm{Tr}(M_i)^{2^k}\right]^{1/2^k} \tag{3.5.21}$$

Proof :

Starting with CS inequality for two matrices $A_{1,2}$

$$|\mathrm{Tr}(A_1 A_2)| \leq \left(\mathrm{Tr}\left(A_1^\dagger A_1\right)\mathrm{Tr}\left(A_2 A_2^\dagger\right)\right)^{1/2} = \left(\mathrm{Tr}\left(A_1^2\right)\mathrm{Tr}\left(A_2^2\right)\right)^{1/2} \tag{3.5.22}$$

now if A_i is itself a product of two matrices $B_{2i-1}B_{2i}$, then the above inequality becomes

$$\begin{aligned} |\mathrm{Tr}(B_1 B_2 B_3 B_4)| &\leq \left(\mathrm{Tr}\left(A_1^2\right)\mathrm{Tr}\left(A_2^2\right)\right)^{1/2} \\ &= \left[\mathrm{Tr}\left(B_1^2 B_2^2\right)\mathrm{Tr}\left(B_3^2 B_4^2\right)\right]^{1/2} \\ &\leq \left[\mathrm{Tr}\left(B_1^4\right)\mathrm{Tr}\left(B_2^4\right)\mathrm{Tr}\left(B_3^4\right)\mathrm{Tr}\left(B_4^4\right)\right]^{1/4} \end{aligned} \tag{3.5.23}$$

hence for using the above argument recursively for a product of 2^k matrices M_i, we can show that

$$\left|\mathrm{Tr}\left(\prod_{i=1}^{2^k} M_i\right)\right| \leq \prod_{i=1}^{2^k} \left[\mathrm{Tr}(M_i)^{2^k}\right]^{1/2^k}. \tag{3.5.24}$$

4

ϵ-Expansion in the Gross-Neveu model from Conformal Field Theory

4.1 Introduction

In a recent work of [33] (see also [87]) the techniques of conformal field theory have been used for the computation of leading order anomalous dimensions of composite operators in interacting CFTs defined in terms of epsilon expansions about $d = 3, 4$ spacetime dimensions. The novelty of this technique lies in using conformal symmetry judiciously without taking recourse to any perturbative methods and Feynman diagrams, which has so far been used in such calculations.

The goal of this work is to compute the leading order - in the epsilon expansion - anomalous dimensions of a class of composite operators in the Gross- Neveu model in $2 + \epsilon$ dimensions. Our analysis involves two and three point functions and the OPE of relevant operators, and uses only conformal symmetry. We thus accomplish this without relying on Feynman diagrams and conventional perturbation theory techniques. The analysis follows closely the methods of [33] who first used the method to determine anomalous dimensions of similar operators in the $O(N)$ vector model.

This chapter is organised as follows. We provide the basic set up in section 4.2. In section 4.3 we use methods similar to [33] to compute the anomalous dimensions of the operators ψ and $\bar{\psi}\psi$. The result of this section is in agreement with that available in the literature. After this simple illustration of the technique, we turn to the general case of higher composite operators. In the appendix we compute the required combinatorial coefficients in the free theory OPE using a recursive dia-

grammatic approach [87]. In section 4.4, the two and three point functions, as well as the OPE, of the interacting theory are used and matching with the expected free theory results ultimately leads to a pair of recursion relations involving the leading order anomalous dimensions. The final result for the leading order anomalous dimensions are given in equation (4.4.45). In section 5, we compute the anomalous dimensions of scalars which are not singlet under $U(\tilde{N})$. As far we know, these have not been computed before in the literature and the results of section 4 and 5 are new.

4.2 The Gross-Neveu model

The Gross-Neveu model [88] is a renormalizable field theory in two dimensions. It is described by a $U(\tilde{N})$ symmetric action for $\tilde{N}$ massless self-interacting Dirac fermions $\{\psi^I, \bar{\psi}^I\}$. We will consider the Gross-Neveu model in $2+\epsilon$ dimensions [89]

$$S = \int d^{2+\epsilon}x \left[\bar{\psi}^I \not{\partial} \psi^I + \frac{1}{2} g \mu^{-\epsilon} \left(\bar{\psi}^I \psi^I\right)^2\right], \quad I = 1, ..., \tilde{N}. \tag{4.2.1}$$

Here g is the coupling constant which is dimensionless in two dimensions. This theory has a weakly coupled UV fixed point given by the non-trivial zero of the beta function,

$$\beta(g) = \epsilon g - (N-2)\frac{g^2}{2\pi}, \qquad N = \tilde{N}\,\mathrm{Tr}\{\mathbb{I}\}\,. \tag{4.2.2}$$

Here $\mathrm{Tr}\{\mathbb{I}\}$ is the trace of identity in Dirac fermion space, and in two dimensions $N = 2\tilde{N}$. The fixed point occurs at

$$g_* = \frac{2\pi\epsilon}{N-2} + \mathcal{O}(\epsilon^2)\,. \tag{4.2.3}$$

The special case of $N = 2$ for which the β function vanishes identically corresponds to the Thirring model. In this paper we consider the case for which $N > 2$.

The dimensions of the fermion ψ^I, Δ_1, and composite scalar $\bar{\psi}^I\psi^I$, Δ_2, are given by

$$\begin{aligned} \Delta_1 &= \frac{d-1}{2} + \gamma_1 = \frac{1}{2} + \frac{\epsilon}{2} + \gamma_1\,, \\ \Delta_2 &= d - 1 + \gamma_2 = 1 + \epsilon + \gamma_2\,. \end{aligned} \tag{4.2.4}$$

The anomalous dimensions of the fundamental fermions and the composite scalar in the ϵ-expansion have been computed in perturbation theory using the standard Feynman diagram techniques and, to leading order in ϵ, are given by

$$\gamma_1 = \frac{N-1}{16\pi^2} g_*^2 = \frac{(N-1)\,\epsilon^2}{4\,(N-2)^2}\,,$$
$$\gamma_2 = -\frac{N-1}{2\pi} g_* = -\frac{N-1}{N-2}\epsilon\,. \tag{4.2.5}$$

The purpose of this note is to derive the above expressions, and similar ones for higher dimensional composite operators, using conformal field theory techniques without doing Feynman diagram computations*. For this we assume that the fixed point is a conformal fixed point.

In two dimensions, the fermion propagator is given by

$$\left\langle \psi^I(x)\bar{\psi}^J(y)\right\rangle = \frac{\delta^{IJ}}{2\pi}\frac{\Gamma^\mu(x-y)_\mu}{(x-y)^2}\,. \tag{4.2.6}$$

We normalise our fields

$$\psi^I_{\text{new}} = \sqrt{2\pi}\psi^I, \quad \bar{\psi}^I_{\text{new}} = \sqrt{2\pi}\bar{\psi}^I\,. \tag{4.2.7}$$

In order to simplify the notation in the analysis below, we use the normalised elementary field but denoted by the old variable. In this normalisation, the two point function is

$$\left\langle \psi^I(x)\bar{\psi}^J(y)\right\rangle = \delta^{IJ}\frac{\Gamma^\mu(x-y)_\mu}{(x-y)^2}\,, \tag{4.2.8}$$

and the equation of motions are†

$$\not{\partial}\psi^I = -\frac{g\mu^{-\epsilon}}{2\pi}\psi^I\left(\bar{\psi}^J\psi^J\right)\,, \tag{4.2.9}$$
$$\partial_\mu\bar{\psi}^I\Gamma^\mu = \frac{g\mu^{-\epsilon}}{2\pi}\bar{\psi}^I\left(\bar{\psi}^J\psi^J\right)\,. \tag{4.2.10}$$

In the free theory the fermions satisfy $\not{\partial}\psi^I = 0$, $\partial_\mu\bar{\psi}^I\Gamma^\mu = 0$ which are the shortening conditions

*See [90, 91] for various aspects of the Gross-Neveu model in $2+\epsilon$ dimensions

†In general, for non-integer dimensions, gamma matrices are infinite dimensional and there are infinite number of antisymmetrized products. However for the calculation of anomalous dimensions to the leading order in ϵ, for the class of operators $(\bar{\psi}\psi)^n$ and $\psi(\bar{\psi}\psi)^n$, this complication will not play any role.

for the multiplets $\{\psi^I\}_{\text{free}}$ and $\{\bar{\psi}^I\}_{\text{free}}$. In addition all other bilinears of ψ^I and $\bar{\psi}^I$ are primary operators. At the interacting fixed point $\{\psi^I\}_{\text{fixed pt}}$ and $\{\bar{\psi}^I\}_{\text{fixed pt}}$ are no longer short multiplets. The primary operators in the free theory ψ^I $\left(\bar{\psi}^J\psi^J\right)$ and $\bar{\psi}^I$ $\left(\bar{\psi}^J\psi^J\right)$ now become descendants of the $\{\psi^I\}_{\text{fixed pt.}}$ and $\{\bar{\psi}^I\}_{\text{fixed pt.}}$ respectively. This phenomena of multiplet recombination was observed in ϕ^4-theory [33] where two conformal multiplets in the free theory join and become a single conformal multiplet at the interacting fixed point.

As in [33] we assume that every operator $\mathcal{O}$ in the free theory has a counterpart $V_{\mathcal{O}}$ at the interacting fixed point. The operators $V_{\mathcal{O}}$ and their correlation functions in the interacting theory, approach, respectively, $\mathcal{O}$ and their free correlation function in the $\epsilon \to 0$ limit. In the Gross Neveu model at the IR free point, various operators are constructed out of products of elementary operators ψ and $\bar{\psi}$. We will denote operators in the interacting theory as V_{2p}, V_{2p+1} and $\bar{V}_{2p+1}$ such that in the limit $\epsilon \to 0$ (IR free point)

$$V_{2p} \to (\bar{\psi}\psi)^p, \quad V^I_{2p+1} \to (\bar{\psi}\psi)^p\psi^I\,, \quad \bar{V}^I_{2p+1} \to (\bar{\psi}\psi)^p\bar{\psi}^I\,. \tag{4.2.11}$$

We also require that the multiplet recombination is achieved by

$$\not{\partial} V^I_1 = \alpha V^I_3\,, \quad \partial_\mu \bar{V}^I_1\Gamma^\mu = -\alpha\bar{V}^I_3\,, \tag{4.2.12}$$

for some unknown function $\alpha \equiv \alpha(\epsilon)$ which will be determined below. As an equation of motion, this follows from the Gross-Neveu lagrangian, but in the non-lagrangian approach we follow it is to be interpreted purely as an operator relation indicating that the operator V_3 is, in the interacting theory, a descendant of the primary operator V_1.

Let us illustrate, schematically, how multiplet recombination is used together with the OPE to determine the leading order anomalous dimensions (This is the method developed by [33] and used in later sections here). Suppose the interacting theory has an operator relation of the form $\partial V_O = \alpha V_{O'}$ (as explained above, O's denote operators in the free theory whose counterparts in the interacting theory are the V_O 's). We first find an OPE in the free theory of primary composite

operators $O_p, O_{p'}$ which contains, in the leading terms, O and O' :

$$O_p(x) \times O_{p'}(0) \supset (O + ...) + \rho(O' + ...) + subleading\ terms. \tag{4.2.13}$$

The dots above denote descendant terms (derivatives acing on O) and other subleading terms contain other operators in the spectrum (we have supressed various powers of x). The leading order terms suffice for our purpose. ρ is a combinatorial coefficient, determined by Wick contractions in the free theory (see the appendix). Now in the interacting theory, the corresponding OPE would read:

$$V_{O_p}(x) \times V_{O_{p'}}(0) \supset (V_O + q\,\partial V_O.....) + subleading\ terms. \tag{4.2.14}$$

Note that, using the operator relation, the second term on the right hand side above is proportonal to $V_{O'}$. In the interacting theory, this operator ($V_{O'}$) is a descendant and this crucial fact, together with matching with the free theory in the $\epsilon \to 0$ limit, implies $q\alpha = \rho$. The coefficient q will be determined later in terms of anomalous dimensions of the operators in the OPE and will be seen to be singular in the $\epsilon \to 0$ limit. The coefficient α is determined below (to the required leading order in ϵ) and the above relation will be seen (in section 4.3) to lead to a recursion relation for the leading order anomalous dimensions.

We turn now to the determination of α. We have

$$\left\langle V_1^I(x)\bar{V}_1^J(y)\right\rangle = \delta^{IJ}\frac{\Gamma^\mu(x-y)_\mu}{(x-y)^{2\Delta_1+1}}\,. \tag{4.2.15}$$

Differentiating the above expression and contracting with Γ^μ matrices, we get

$$\left\langle \not{\partial} V_1^I(x)\partial_\sigma\bar{V}_1^J(y)\Gamma^\sigma\right\rangle = \delta^{IJ}\frac{\Gamma^\mu(x-y)_\mu}{(x-y)^{2\Delta_1+3}}h\,, \tag{4.2.16}$$

where, using $\Delta_1 = \frac{d-1}{2} + \gamma_1$, we get

$$h = (2\Delta_1+1)(2-d+2d-2\Delta_1-3) \sim -4\gamma_1\,. \tag{4.2.17}$$

Now requiring that in the limit $\epsilon \to 0$, $\left\langle V_3^I(x)\bar{V}_3^J(y)\right\rangle$ approaches the free theory correlation

function

$$\left\langle \psi^I(\bar{\psi}^K\psi^K)(x)\bar{\psi}^J(\bar{\psi}^L\psi^L)(y)\right\rangle = \delta^{IJ}\frac{\Gamma^\mu(x-y)_\mu(N-1)}{(x-y)^4}\,, \tag{4.2.18}$$

we get the expression for α

$$\alpha = 2\sigma\left(\frac{\gamma_1}{N-1}\right)^{1/2}, \qquad \sigma = \pm 1\,. \tag{4.2.19}$$

4.3 Anomalous dimension of ψ, $\bar{\psi}$ and $\bar{\psi}\psi$

In this section we will compute the anomalous dimensions of the fundamental fermion and the composite scalar. The results of this section are in perfect agreement with the leading order anomalous dimension computed from Feynman diagram techniques. In the next section we will generalise this to higher dimensional operators and derive some new results for the anomalous dimensions.

We consider the OPE between ψ and $\bar{\psi}\psi$ in the free theory. [‡] For this we do not need the full OPE except those terms which are sensitive to the multiplet recombination,

$$\psi^I(x)\times(\bar{\psi}^J\psi^J)(0) \supset \frac{1}{x^2}\{\not{x}\psi^I(0) + x^2\psi^I(\bar{\psi}^J\psi^J)(0) + ..\}\,. \tag{4.3.1}$$

We will compare the above expression for the free OPE with the OPE at the interacting UV fixed point. For this we need the three point function at the interacting fixed point. According to [92], we have[§]

$$\left\langle V_1^I(x_1)\bar{V}_1^K(x_2)V_2(x_3)\right\rangle = \frac{f\not{x}_{13}\not{x}_{23}\delta^{IK}}{(x_{12}^2)^{\Delta_1-\frac{1}{2}\Delta_2}\,(x_{13}^2x_{23}^2)^{\frac{1}{2}\Delta_2+\frac{1}{2}}}\,. \tag{4.3.2}$$

In the above f is a constant. From this we can compute the following OPE

$$V_1^I(x_1)\times V_2(x_3) \supset \frac{f\not{x}_{13}}{(x_{13}^2)^{\frac{1}{2}\Delta_2+\frac{1}{2}}}C(x_{13},\partial_z)V_1^I(z)|_{z=x_3} + ... \tag{4.3.3}$$

[‡] The OPE coefficients are determined in the free theory using Wick's contraction- see the appendix.

[§] As we will explain in the next section, in general conformal invariance requires the presence of another term in the 3-point function. However this extra term does not contribute in the calculation of this section.

Here

$$C(x_{13},\partial_z) = A+\left(B_1 x_{13}^{\mu} + B_2 \not{x}_{13}\Gamma^{\mu}\right)\partial_{\mu}+\left(C_1 x_{13}^{\mu}x_{13}^{\nu} + C_2 x_{13}^{\mu}\not{x}_{13}\Gamma^{\nu} + C_3 x_{13}^2\Gamma^{\mu}\Gamma^{\nu}\right)\partial_{\mu}\partial_{\nu}+..... \tag{4.3.4}$$

It is important to note here that in the above OPE, we have kept only contributions coming from the conformal family of V_1^I which includes V_3 as its descendant. Although the multiplet recombination does not necessarily require a lagrangian description, here our knowledge of the shortening condition follows from the equation of motion (4.2.12). Even though we use different methods, we are dealing with perturbative fixed points which do have a lagrangian description. Thus our analysis is not entirely lagrangian independent[¶].

$A, B_i, C_i, ..$ are functions of conformal dimensions which we determine by considering $x_1 \to x_3$ and expanding (4.3.2) in powers of x_{13},

$$\begin{aligned}\frac{f\not{x}_{13}\not{x}_{23}\delta^{IK}}{(x_{12}^2)^{\Delta_1-\frac{1}{2}\Delta_2}\,(x_{13}^2x_{23}^2)^{\frac{1}{2}\Delta_2+\frac{1}{2}}} &= \frac{f\not{x}_{13}\not{x}_{23}\delta^{IK}}{(x_{13}^2)^{\frac{1}{2}\Delta_2+\frac{1}{2}}(x_{23}^2)^{\Delta_1+\frac{1}{2}}}\Big[1+2\left(\Delta_1-\frac{1}{2}\Delta_2\right)\frac{x_{23}\cdot x_{13}}{x_{23}^2}\\ &\quad -\left(\Delta_1-\frac{1}{2}\Delta_2\right)\frac{x_{13}^2}{x_{23}^2}+\frac{1}{2}(2\Delta_1-\Delta_2)(2+2\Delta_1-\Delta_2)\frac{(x_{23}\cdot x_{13})^2}{(x_{23}^2)^2}+...\Big].\end{aligned} \tag{4.3.5}$$

Comparing with (4.3.3) we can get all the coefficients. We list here the first few coefficients

$$\begin{aligned}&A=-1,\quad B_1=-\frac{\left(\Delta_1-\frac{1}{2}\Delta_2\right)}{\Delta_1+\frac{1}{2}},\quad B_2=\frac{B_1}{2\Delta_1+1-d},\\ &C_1=-\frac{(2\Delta_1-\Delta_2)\,(2+2\Delta_1-\Delta_2)}{2\,(2\Delta_1+1)\,(2\Delta_1+3)}\,,\\ &C_2=\frac{2C_1}{2\Delta_1+1-d},\quad C_3=\frac{1}{2\Delta_1+1-d}\left[C_1+\frac{\left(\Delta_1-\frac{1}{2}\Delta_2\right)}{2\Delta_1+1}\right].\end{aligned} \tag{4.3.6}$$

Now we consider the following free correlators in the limit $|x_1|<<|x_2|$,

$$\begin{aligned}&\left\langle\psi^I(x_1)(\bar\psi^J\psi^J)(0)\bar\psi^K(x_2)\right\rangle \sim \frac{\not{x}_1}{x_1^2}\left\langle\psi^I(0)\bar\psi^K(x_2)\right\rangle\,,\\ &\left\langle\psi^I(x_1)(\bar\psi^J\psi^J)(0)\bar\psi^K(\bar\psi^L\psi^L)(x_2)\right\rangle \sim \left\langle\psi^I(\bar\psi^J\psi^J)(0)\bar\psi^K(\bar\psi^L\psi^L)(x_2)\right\rangle\,.\end{aligned} \tag{4.3.7}$$

[¶]Presumably the shortening condition can be used for more general fixed points to fix values of anomalous dimensions. It would be very interesting to understand the phenomena of multiplet recombination more generally.

Using the OPE (4.3.3), we have

$$\left\langle V_1^I(x_1)V_2(0)\bar{V}_1^K(x_2)\right\rangle \sim \frac{Af\not{x}_1}{(x_1^2)^{\frac{1}{2}\Delta_2+\frac{1}{2}}}\left\langle V_1^I(0)\bar{V}_1^K(x_2)\right\rangle \,. \tag{4.3.8}$$

This will match with the free correlator if $f \to -1$ in the limit $\epsilon \to 0$. Next we compare the correlation function with the insertion of the descendant operator $\bar{V}_3^I$,

$$\left\langle V_1^I(x_1)V_2(0)\bar{V}_3^I(x_2)\right\rangle \sim \frac{f\not{x}_1}{(x_1^2)^{\frac{1}{2}\Delta_2+\frac{1}{2}}}C(x_1,\partial_\mu)\left\langle V_1^I(0)\bar{V}_3^K(x_2)\right\rangle \,. \tag{4.3.9}$$

Here $\bar{V}_3^K$ is the descendant of $\bar{V}_1^K$ defined in (4.2.12) and the derivative acts on the first insertion. It is very easy to see that the first two terms containing A, B_1 in the expansion of C on the right hand side go to zero as we take $\epsilon \to 0$,

$$\left\langle V_1^I(0)\bar{V}_3^K(x_2)\right\rangle = -\frac{1}{\alpha}\left\langle V_1^I(0)\partial_\mu\bar{V}_3^K(x_2)\right\rangle\Gamma^\mu = -\frac{\delta^{IK}}{(z^2)^{\Delta_1+\frac{1}{2}}}\frac{\sqrt{\gamma_1(N-1)}}{2\pi\sigma}\,. \tag{4.3.10}$$

Now we see that the contribution to (4.3.9) will come from the term with B_2. In fact using the expansion we get

$$\begin{aligned}\left\langle V_1^I(x_1)V_2(0)\bar{V}_3^K(x_2)\right\rangle &\sim \frac{f\not{x}_1}{(x_1^2)^{\frac{1}{2}\Delta_2+\frac{1}{2}}}B_2(\not{x}_1\,\Gamma^\mu\partial_\mu)\left\langle V_1^I(0)\bar{V}_3^K(x_2)\right\rangle \,,\\ &= \frac{fB_2\alpha}{(x_1^2)^{\frac{1}{2}\Delta_2-\frac{1}{2}}}\left\langle V_3^I(0)\bar{V}_3^K(x_2)\right\rangle \,.\end{aligned} \tag{4.3.11}$$

In the above we used the equation of motion for the primary field (4.2.12). Thus we see that it will go to the free correlator if $fB_2\alpha \sim \mathcal{O}(1)$ in the limit $\epsilon \to 0$. Since f goes to constant and α goes to zero, B_2 must diverge. We also see from (4.3.6) that B_2 has a chance of blowing up. If we define

$$\delta = \frac{d-1}{2}, \quad \Delta_1 = \delta+\gamma_1, \quad \Delta_2 = 2\delta+\gamma_2\,, \tag{4.3.12}$$

then

$$B_2 \sim -\frac{(\gamma_1-\frac{1}{2}\gamma_2)}{2\gamma_1(\delta+\gamma_1+\frac{1}{2})}\,. \tag{4.3.13}$$

Thus B_2 will blow up if γ_1 vanishes as at least $\mathcal{O}(\epsilon^2)$

Now we write

$$\gamma_1 \sim y_{1,2}\epsilon^2, \quad \gamma_2 \sim y_{2,1}\epsilon\,. \tag{4.3.14}$$

Then we get

$$fB_2\alpha \sim \frac{y_{2,1}\sigma\, f}{2\sqrt{y_{1,2}(N-1)}} \to 1\,. \tag{4.3.15}$$

Using that $f \to -1$, we get

$$y_{2,1} = -2\sigma\sqrt{y_{1,2}(N-1)}\,. \tag{4.3.16}$$

Also in the interacting theory, the conformal dimension Δ_3 of the descendant $V_3^I(x_1)$ is related to Δ_1 of $V_1^I(x_1)$ by

$$\begin{aligned}
&\Delta_3 = \Delta_1 + 1 \Rightarrow 3\delta + \gamma_3 = \delta + \gamma_1 + 1,\\
&\gamma_3 = \gamma_1 - \epsilon \Rightarrow y_{3,1} = -1\,.
\end{aligned} \tag{4.3.17}$$

We will show this by explicit computation in the next section.

Now we are interested in finding the OPE between V_3^I and V_2. This can be obtained from (4.3.3) by acting with a derivative and using (4.2.12).

$$V_3^I(x_1) \times V_2(x_3) \supset \frac{\tilde{f}}{\alpha(x_{13}^2)^{\frac{1}{2}\Delta_2+\frac{1}{2}}}\tilde{C}(x_{13},\partial_z)V_1^I(z)|_{z=x_3} + ... \tag{4.3.18}$$

Here

$$\tilde{C}(x_{13},\partial_z) = \tilde{A} + \left(\tilde{B}_1 x_{13}^\mu + \tilde{B}_2 \not{x}_{13}\Gamma^\mu\right)\partial_\mu + \left(\tilde{C}_1 x_{13}^\mu x_{13}^\nu + \tilde{C}_2 x_{13}^\mu \not{x}_{13}\Gamma^\nu + \tilde{C}_3 x_{13}^2\Gamma^\mu\Gamma^\nu\right)\partial_\mu\partial_\nu + ... \tag{4.3.19}$$

where

$$\begin{aligned}
&\tilde{f} = (d-\Delta_2-1)f, \quad \tilde{A} = A, \quad \tilde{B}_1 = \frac{d-\Delta_2+1}{d-\Delta_2-1}B_1,\\
&\tilde{B}_2 = \frac{1-\Delta_2}{d-\Delta_2-1}B_2 - \frac{B_1}{d-\Delta_2-1}\,.
\end{aligned} \tag{4.3.20}$$

In order to compare with the free correlator, we also need the following OPE

$$\psi_i(\bar{\psi}_k\psi_k)(x_1)\times(\bar{\psi}_j\psi_j)(0)\supset\frac{1}{x_1^2}\{(N-1)\psi_i(0)+\not{x}_1\psi_i(\bar{\psi}_j\psi_j)(0)+..\} \tag{4.3.21}$$

$$\begin{aligned}\left\langle\psi_i(\bar{\psi}_k\psi_k)(x_1)(\bar{\psi}_j\psi_j)(0)\bar{\psi}_l(x_2)\right\rangle&\sim\frac{(N-1)}{x_1^2}\left\langle\psi_i(0)\bar{\psi}_l(x_2)\right\rangle\,,\\ \left\langle\psi_i(\bar{\psi}_k\psi_k)(x_1)(\bar{\psi}_j\psi_j)(0)\bar{\psi}_l(\bar{\psi}_l\psi_l)(x_2)\right\rangle&\sim\frac{\not{x}_1}{x_1^2}\left\langle\psi_i(\bar{\psi}_j\psi_j)(0)\bar{\psi}_l(\bar{\psi}_l\psi_l)(x_2)\right\rangle\,.\end{aligned} \tag{4.3.22}$$

Proceeding as before, we find that for $|x_1|<<|x_2|$, we have

$$\left\langle V_3^I(x_1)V_2(0)\bar{V}_3^K(x_2)\right\rangle\sim\frac{\tilde{f}\tilde{B}_2\not{x}_1}{(x_1^2)^{\frac{1}{2}\Delta_2+\frac{1}{2}}}\left\langle V_3^I(0)\bar{V}_3^K(x_2)\right\rangle\,. \tag{4.3.23}$$

Thus in order to match with the free correlator, we require $\tilde{f}\tilde{B}_2\to 1$. Now using that $f\to-1$, we get

$$(1-\Delta_2)B_2-B_1=-1\,. \tag{4.3.24}$$

Using (4.3.12) and (4.3.14), to leading order in ϵ, we get

$$y_{2,1}+y_{2,1}^2=4y_{1,2}\,. \tag{4.3.25}$$

Using further (4.3.16), we get

$$2y_{1,2}(N-2)=\sigma\sqrt{y_{1,2}(N-1)}\,, \tag{4.3.26}$$

which implies

$$\sigma=+1,\quad y_{1,2}=\frac{(N-1)}{4(N-2)^2},\quad y_{2,1}=-\frac{N-1}{N-2}\,. \tag{4.3.27}$$

Therefore the anomalous dimensions are

$$\gamma_1=\frac{(N-1)}{4(N-2)^2}\epsilon^2,\quad \gamma_2=-\frac{N-1}{N-2}\epsilon\,. \tag{4.3.28}$$

These results are in agreement with results in [89, 93].

4.4 Anomalous dimensions of $(\bar{\psi}\psi)^p$ and $(\bar{\psi}\psi)^p\psi$

In this section we will compute the leading order anomalous dimensions of a class of higher dimensional composite operators in the interacting theory described by the UV fixed point of the Gross-Neveu Model. In the free theory limit ($\epsilon \to 0$) these operators are of the form $(\bar{\psi}\psi)^p$ and $\psi(\bar{\psi}\psi)^p$ with $p > 1$. Let us denote these operators in the interacting theory as V_{2p} and V_{2p+1} such that in the limit $\epsilon \to 0$ (axiom)

$$V_{2p} \to (\bar{\psi}\psi)^p, \quad V^I_{2p+1} \to (\bar{\psi}\psi)^p\psi^I\,. \tag{4.4.1}$$

4.4.1 The structure of the OPEs

We will need the following OPEs in the free theory

$$\left(\bar{\psi}\psi\right)^p(x_1) \times \left(\bar{\psi}\psi\right)^p\psi^I(0) \supset \frac{f_{2p}}{(x_1^2)^p}\left\{\psi^I(0) + \not{x}_1\rho_{2p}\left(\bar{\psi}\psi\right)\psi^I(0)\right\}\,, \tag{4.4.2}$$

$$\left(\bar{\psi}\psi\right)^p\psi^I(x_1) \times \left(\bar{\psi}\psi\right)^p\left(\bar{\psi}\psi\right)(0) \supset \frac{f_{2p+1}}{(x_1^2)^{p+1}}\left\{\not{x}_1\psi^I(0) + x_1^2\rho_{2p+1}\left(\bar{\psi}\psi\right)\psi^I(0)\right\}\,. \tag{4.4.3}$$

where I is an $U(\bar{N})$ index. f_{2p}, f_{2p+1} and ρ_{2p}, ρ_{2p+1} are combinatorial coefficients. Counting all possible Wick contractions gives their values to be

$$f_{2p} = \prod_{i=1}^{p} i(N-i), \quad f_{2p+1} = (p+1)\prod_{i=1}^{p} i(N-i)\,, \tag{4.4.4}$$

$$\rho_{2p} = -\frac{p}{N-1}, \quad \rho_{2p+1} = \frac{N-p-1}{N-1}\,. \tag{4.4.5}$$

See the appendix for details of the calculation. Now let us consider the corresponding OPEs in the interacting theory. The most general structure of the OPE, in the first case where the free theory limit is eq. (4.4.2), is

$$V_{2p}(x_1) \times V^I_{2p+1}(0) \supset \left(\frac{1}{(x_{12}^2)^a}C(x_{12},\partial_2)V_1^I(x_2) + \frac{\not{x}_{12}}{(x_{12}^2)^b}D(x_{12},\partial_2)V_1^I(x_2) + ...\right)_{x_2=0}\,. \tag{4.4.6}$$

The dots indicate other primary operators that can appear in the OPE. Here

$$a = (\Delta_{2p} + \Delta_{2p+1} - \Delta_1)/2\,, \tag{4.4.7}$$

$$b = (\Delta_{2p} + \Delta_{2p+1} - \Delta_1 + 1)/2\,. \tag{4.4.8}$$

The differential operators $C(x_{12}, \partial_2)$ and $D(x_{12}, \partial_2)$ have the general form

$$C(x_{12}, \partial_2) = A_0 + B_0 x_{12}^\mu \partial_{2\mu} + B_1 \not{x}_{12} \not{\partial}_{2\mu} + ... \tag{4.4.9}$$

$$D(x_{12}, \partial_2) = A_0' + B_0' x_{12}^\mu \partial_{2\mu} + B_1' \not{x}_{12} \not{\partial}_{2\mu} + ... \tag{4.4.10}$$

For the OPE of two generic primary operators (one bosonic and the other fermionic) both of these structures can occur. However now we will show that, for the $V_{2p}(x_1)V^I_{2p+1}(0)$ OPE, only the first structure in eq. (4.4.6) is consistent with our axiomatic requirement that in the limit $\epsilon \to 0$ correlators of the interacting theory should match with corresponding correlators in the free theory.

For this consider the 3 pt. function $\left\langle V_{2p}(x_1)V^I_{2p+1}(x_2)\bar{V}_3^J(x_3)\right\rangle$. Then using the OPE - eq. (4.4.6) - we have,

$$\begin{aligned}\left\langle V_{2p}(x_1)V^I_{2p+1}(0)\bar{V}_3^J(x_3)\right\rangle_{|x_1|\ll|x_3|} \sim &\left\{\frac{1}{(x_{12}^2)^a}\left(A_0 + B_0 x_{12}^\mu \partial_{2\mu}\right)\left\langle V_1^I(x_2)\bar{V}_3^J(x_3)\right\rangle + ...\right\}_{x_2=0} \\ &+\left\{\frac{\not{x}_{12}}{(x_{12}^2)^b}\left(A_0' + B_0' x_{12}^\mu \partial_{2\mu}\right)\left\langle V_1^I(x_2)\bar{V}_3^J(x_3)\right\rangle + ...\right\}_{x_2=0} \\ &+\alpha\left\{\frac{B_1 \not{x}_{12}}{(x_{12}^2)^a}\left\langle V_3^I(x_2)\bar{V}_3^J(x_3)\right\rangle + \frac{B_1' x_{12}^2}{(x_{12}^2)^b}\left\langle V_3^I(x_2)\bar{V}_3^J(x_3)\right\rangle\right\}_{x_2=0}\end{aligned} \tag{4.4.11}$$

In the free theory the OPE, eq. (4.4.2) gives,

$$\left\langle \left(\bar{\psi}\psi\right)^p(x_1)\left(\bar{\psi}\psi\right)^p\psi^I(0)\left(\bar{\psi}\psi\right)\bar{\psi}^J(x_3)\right\rangle \underset{|x_1|\ll|x_3|}{\sim} \left(\frac{\not{x}_{12}}{(x_{12}^2)^p} f_{2p}\rho_{2p}\left\langle \left(\bar{\psi}\psi\right)\psi^I(x_2)\left(\bar{\psi}\psi\right)\bar{\psi}^J(x_3)\right\rangle\right)_{x_2=0}$$

Now since in the $\epsilon \to 0$ limit we require

$$\left\langle V_{2p}(x_1)V^I_{2p+1}(x_2)\bar{V}_3^J(x_3)\right\rangle \to \left\langle \left(\bar{\psi}\psi\right)^p(x_1)\left(\bar{\psi}\psi\right)^p\psi^I(x_2)\left(\bar{\psi}\psi\right)\bar{\psi}^J(x_3)\right\rangle\,. \tag{4.4.12}$$

and,

$$\left\langle V_3^I(x_2)\bar{V}_3^J(x_3\right\rangle \to \left\langle \left(\bar{\psi}\psi\right)\psi^I(x_2)\left(\bar{\psi}\psi\right)\bar{\psi}^J(x_3)\right\rangle \,. \tag{4.4.13}$$

Hence we clearly see that only the first structure in eqn. (4.4.6) needs to be considered. In other words all the coefficients appearing in $D(x_{12},\partial_2)$ can be set to zero in this case.

Next consider the OPE of V^I_{2p+1} and V_{2p+2}. Again just on grounds of conformal symmetry we can write down an expression similar to eq. (4.4.6). But once again it is easy to show using the free theory OPE, eq. (4.4.3) that our axiom

$$\left\langle V^I_{2p+1}(x_1)V_{2p+2}(x_2)\bar{V}_3^J(x_3)\right\rangle \to \left\langle \left(\bar{\psi}\psi\right)^p\psi^I(x_1)\left(\bar{\psi}\psi\right)^p(\bar{\psi}\psi)(x_2)\left(\bar{\psi}\psi\right)\bar{\psi}^J(x_3)\right\rangle \,. \tag{4.4.14}$$

allows only the second structure of eq. (4.4.6) for the OPE of V^I_{2p+1} and V_{2p+2}.

Note that the above distinction is important when both operators involved in the OPE are primary operators. When one of the operators is a descendant the structure of the OPE simply follows by acting with derivatives on the OPE of the primary operators. For example when $p=1$ the OPE of V_2 and V_3^I can be obtained from the OPE of V_1^I and V_2 by differentiating the latter.

4.4.2 Determining the coefficients in the OPE

We will now obtain the expression for the coefficients in eq. (4.4.9). The method for doing this is simple. The form of the 3 pt. function which is fixed in the usual way by conformal invariance is matched against the form obtained by taking the OPE of the first two operators within the 3-pt. function. We start with the following 3 pt. function,

$$\left\langle V_{2p}(x_1)V^I_{2p+1}(x_2)\bar{V}_1^J(x_3)\right\rangle = g_1\frac{\not{x}_{12}\not{x}_{13}\delta^{IJ}}{(x_{12}^2)^{a+1/2}(x_{23}^2)^b(x_{31}^2)^{c+1/2}} + g_2\frac{\not{x}_{23}\delta^{IJ}}{(x_{12}^2)^a(x_{23}^2)^{b+1/2}(x_{31}^2)^c}\,. \tag{4.4.15}$$

where

$$\begin{aligned} a &= \frac{(\Delta_{2p}+\Delta_{2p+1}-\Delta_1)}{2}, \quad b = \frac{(\Delta_{2p+1}+\Delta_1-\Delta_{2p})}{2}\,, \\ c &= \frac{(\Delta_1+\Delta_{2p}-\Delta_{2p+1})}{2}\,. \end{aligned} \tag{4.4.16}$$

The form is determined by conformal invariance which allows for both the above structures[‖]. Now using the OPE

$$V_{2p}(x_1)\times V^I_{2p+1}(0)\supset\left(\frac{1}{(x_{12}^2)^a}C(x_{12},\partial_2)V_1^I(x_2)\right)_{x_2=0}. \tag{4.4.17}$$

we get,

$$\begin{aligned}\left\langle V_{2p}(x_1)V^I_{2p+1}(0)\bar V_1^J(x_3)\right\rangle_{|x_1|\ll|x_3|} &\sim \left(\frac{1}{(x_{12}^2)^a}C(x_{12},\partial_2)\left\langle V_1^I(x_2)\bar V_1^J(x_3)\right\rangle\right)_{x_2=0}\\ &= \frac{A_0(-\not{x}_3)\delta^{IJ}}{(x_1^2)^a(x_3^2)^{\Delta_1+1/2}}+\frac{B_0\delta^{IJ}}{(x_1^2)^a(x_3^2)^{\Delta_1+1/2}}\Big(\left(\frac12-\Delta_1\right)x_3^2\not{x}_1\\ &\quad-\left(\frac12+\Delta_1\right)\not{x}_3\not{x}_1\not{x}_3\Big)+\frac{B_1(D-2\Delta_1-1)\not{x}_1\delta^{IJ}}{(x_3^2)^{\Delta_1+1/2}(x_1^2)^a}\end{aligned} \tag{4.4.18}$$

In obtaining the second line above we have used the following results:

$$\left\langle V_1^I(x_2)\bar V_1^J(x_3)\right\rangle=\frac{\not{x}_{23}}{(x_{23}^2)^{\Delta_1+1/2}}, \tag{4.4.19}$$

$$x_{12}^\mu\partial_{2\mu}\left(\frac{\not{x}_{23}}{(x_{23}^2)^{\Delta_1+1/2}}\right)=\frac{1}{(x_{23}^2)^{\Delta_1+3/2}}\left(\not{x}_{12}x_{23}^2(\frac12-\Delta_1)-(\Delta_1+\frac12)\not{x}_{23}\not{x}_{12}\not{x}_{23}\right) \tag{4.4.20}$$

$$\not{x}_{12}\not{\partial}_2\left(\frac{\not{x}_{23}}{(x_{23}^2)^{\Delta_1+1/2}}\right)=\frac{(D-2\Delta_1-1)\not{x}_{12}}{(x_{23}^2)^{\Delta_1+1/2}}. \tag{4.4.21}$$

But from eqn. (4.4.16),

$$\begin{aligned}\left\langle V_{2p}(x_1)V^I_{2p+1}(0)\bar V_1^J(x_3)\right\rangle_{|x_1|\ll|x_3|} &= g_1\frac{\not{x}_1\not{x}_3}{(x_1^2)^{a+1/2}(x_3^2)^{b+1/2+c}}\left[1+\left(c+\frac12\right)\frac{(\not{x}_1\not{x}_3+\not{x}_3\not{x}_1)}{x_3^2}+\ldots\right]\\ &\quad+g_2\frac{\not{x}_{13}}{(x_1^2)^a(x_3^2)^{b+c+1/2}}\left[1+c\frac{(\not{x}_1\not{x}_3+\not{x}_3\not{x}_1)}{x_3^2}+\ldots\right].\end{aligned} \tag{4.4.22}$$

Comparing the above equation with eq. (4.4.18) we get,

$$\begin{aligned}A_0&=g_2,\\ B_0\left(\frac12-\Delta_1\right)+B_1\left(D-2\Delta_1-1\right)&=-cg_2,\\ B_0\left(\frac12+\Delta_1\right)&=cg_2.\end{aligned} \tag{4.4.23}$$

[‖]See, for example, [94]. Contrast this with Petkou's result [92] where only the first term appears.

Since the tensor structure of the first term in eq. (4.4.22) does not have any matching with the tensor structures appearing in eq. (4.4.18), we can set $g_1 = 0$. Finally we have,

$$B_0 = \frac{(\Delta_1 + \Delta_{2p} - \Delta_{2p+1})\, A_0}{(2\Delta_1 + 1)}, \qquad B_1 = \frac{B_0}{(2\Delta_1 + 1 - D)}\,. \tag{4.4.24}$$

Next we consider the following 3 pt. function

$$\left\langle V^I_{2p+1}(x_1) V_{2p+2}(x_2) \bar{V}_1^J(x_3) \right\rangle = g'_1 \frac{\not{x}_{12}\not{x}_{32}\delta^{IJ}}{(x^2_{12})^{a'+1/2}(x^2_{23})^{b'+1/2}(x^2_{31})^{c'}} + g'_2 \frac{\not{x}_{13}\delta^{IJ}}{(x^2_{12})^{a'}(x^2_{23})^{b'}(x^2_{31})^{c'+1/2}}\,, \tag{4.4.25}$$

where,

$$\begin{aligned} a' &= \frac{(\Delta_{2p+1} + \Delta_{2p+2} - \Delta_1)}{2}\,, \\ b' &= \frac{(\Delta_{2p+2} + \Delta_1 - \Delta_{2p+1})}{2}\,, \\ c' &= \frac{(\Delta_1 + \Delta_{2p+1} - \Delta_{2p+2})}{2}\,. \end{aligned} \tag{4.4.26}$$

In this case using the OPE we get

$$V^I_{2p+1}(x_1) \times V_{2p+2}(0) \supset \left(\frac{\not{x}_{12}}{(x^2_{12})^{a'}} D(x_{12}, \partial_2) V_1^I(x_2) \right)_{x_2 = 0}\,. \tag{4.4.27}$$

Therefore,

$$\begin{aligned} \left\langle V^I_{2p+1}(x_1) V_{2p+2}(0) \bar{V}_1^J(x_3) \right\rangle_{|x_1| \ll |x_3|} &\sim \left(\frac{1}{(x^2_{12})^{a'}} D(x_{12}, \partial_2) \left\langle V_1^I(x_2) \bar{V}_1^J(x_3) \right\rangle \right)_{x_2 = 0}\,, \\ &= \frac{A'_0(-\not{x}_1\not{x}_3)\delta^{IJ}}{(x_1^2)^{a'}(x_3^2)^{\Delta_1 + 1/2}} + \frac{\not{x}_1 B'_0 \delta^{IJ}}{(x_1^2)^{a'}(x_3^2)^{\Delta_1+1/2}} \Big(\left(\frac{1}{2} - \Delta_1 \right) x_3^2 \not{x}_1 \\ &\quad - \left(\frac{1}{2} + \Delta_1 \right) \not{x}_3 \not{x}_1 \not{x}_3 \Big) + \frac{\delta^{IJ} B'_1 (D - 2\Delta_1 - 1) x_1^2}{(x_3^2)^{\Delta_1 + 1/2}(x_1^2)^{a'}} \end{aligned} \tag{4.4.28}$$

In the limit $|x_1| \ll |x_3|$ eq. (4.4.25) becomes

$$\left\langle V^I_{2p+1}(x_1) V_{2p+2}(0) \bar{V}_1^J(x_3) \right\rangle_{|x_1| \ll |x_3|} = g'_1 \frac{\not{x}_1 \not{x}_3}{(x_1^2)^{a'+1/2}(x_3^2)^{b'+1/2+c'}} \left[1 + c' \frac{(\not{x}_1 \not{x}_3 + \not{x}_3 \not{x}_1)}{x_3^2} + \ldots \right]$$

$$+ g_2' \frac{\not{x}_{13}}{(x_1^2)^{a'}(x_3^2)^{b'+c'+1/2}} \left[1 + \left(c' + \frac{1}{2}\right) \frac{(\not{x}_1 \not{x}_3 + \not{x}_3 \not{x}_1)}{x_3^2} + ...\right] . \tag{4.4.29}$$

Comparing the above equation with eq. (4.4.28), we obtain,

$$\begin{aligned} A_0' &= -g_1 \,, \\ B_0' \left(\frac{1}{2} - \Delta_1\right) + B_1 \left(D - 2\Delta_1 - 1\right) &= c' g_1' \,, \\ B_0 \left(\frac{1}{2} + \Delta_1\right) &= -c' g_1' \,. \end{aligned} \tag{4.4.30}$$

This gives,

$$B_0' = \frac{\left(\Delta_1 + \Delta_{2p+1} - \Delta_{2p+2}\right) A_0'}{(2\Delta_1 + 1)}, \qquad B_1' = \frac{B_0'}{(2\Delta_1 + 1 - D)} \,. \tag{4.4.31}$$

Here, similar arguments as above would set $g_2' = 0$. This again shows that in the 3 pt. function of two primary fermion operators and a primary scalar operator in general one must keep both tensor structures. Which structure contributes in a specific case depends upon the particular primary operators under consideration. When one of the operators involved in the 3 pt. function is a descendant, the allowed structure is of course determined by the correlator of primary operators.

4.4.3 Recursion relations for the leading order anomalous dimensions

In the $\epsilon \to 0$ limit, the OPEs of the interacting theory should go over to the free theory OPEs - eqs. (4.4.2, 4.4.3) - and the corresponding 3 pt. functions must match as well. This matching gives

$$A_0 = f_{2p}, \quad B_1 \alpha = f_{2p} \rho_{2p} \,. \tag{4.4.32}$$

$$\Rightarrow \frac{\left(\Delta_1 + \Delta_{2p} - \Delta_{2p+1}\right)}{(2\Delta_1 + 1)\left(2\Delta_1 + 1 - D\right)} \alpha = \rho_{2p} \,. \tag{4.4.33}$$

We use the following relations

$$\Delta_1 = \frac{1+\epsilon}{2} + \gamma_1 \,, \tag{4.4.34}$$

$$\Delta_{2p} = 2p\left(\frac{1+\epsilon}{2}\right) + \gamma_{2p} \,, \tag{4.4.35}$$

$$\Delta_{2p+1} = (2p+1)\left(\frac{1+\epsilon}{2}\right) + \gamma_{2p+1} \,, \tag{4.4.36}$$

$$\alpha = 2\sigma\left(\frac{\gamma_1}{N-1}\right)^{1/2} . \tag{4.4.37}$$

to get

$$\frac{(\gamma_{2p}-\gamma_{2p+1})}{2\gamma_1}\sigma\left(\frac{\gamma_1}{N-1}\right)^{1/2} = -\frac{p}{N-1} \,. \tag{4.4.38}$$

Writing $\gamma_k(\epsilon) = y_{k,1}\epsilon + y_{k,2}\epsilon^2 + ...$ we get,

$$y_{2p+1,1} - y_{2p,1} = 2\sigma p\left(\frac{y_{1,2}}{N-1}\right)^{1/2} . \tag{4.4.39}$$

Using $y_{1,2} = \frac{N-1}{4(N-2)^2}$ this gives,

$$y_{2p+1,1} - y_{2p,1} = \sigma\frac{p}{N-2} \,. \tag{4.4.40}$$

Similarily we get for the other case,

$$A_0' = f_{2p+1}, \quad B_1'\alpha = f_{2p+1}\rho_{2p+1} \,, \tag{4.4.41}$$

$$\Rightarrow \frac{(\Delta_1 + \Delta_{2p+1} - \Delta_{2p+2})}{(2\Delta_1+1)\,(2\Delta_1+1-D)}\alpha = \rho_{2p+1} \,, \tag{4.4.42}$$

$$\Rightarrow \frac{(\gamma_{2p+1}-\gamma_{2p+2})}{2\gamma_1}\sigma\left(\frac{\gamma_1}{N-1}\right)^{1/2} = \frac{N-p-1}{N-1} \,, \tag{4.4.43}$$

which gives

$$y_{2p+1,1} - y_{2p+2,1} = \sigma\left(\frac{N-p-1}{N-2}\right) . \tag{4.4.44}$$

Solving the recursion relations eqs. (4.4.40) and (4.4.44) (with $\sigma = 1$) we get our desired result,

$$y_{2p,1} = -\frac{p(N-p)}{(N-2)}\,, \qquad y_{2p+1,1} = -\frac{p(N-p-1)}{(N-2)}\,. \tag{4.4.45}$$

Thus we have for the scaling dimensions of these composite operators,

$$\Delta_{(\bar\psi\psi)^p} \equiv \Delta_{2p} = p + p\epsilon - \frac{p(N-p)}{(N-2)}\epsilon + O(\epsilon^2)\,, \tag{4.4.46}$$

$$\Delta_{(\bar\psi\psi)^p\psi} \equiv \Delta_{2p+1} = (p+\frac{1}{2}) + (p+\frac{1}{2})\epsilon - \frac{p(N-p-1)}{(N-2)}\epsilon + O(\epsilon^2)\,. \tag{4.4.47}$$

Note, in particular, that the classically marginal operator $(\bar\psi\psi)^2$ receives corrections to its conformal dimension only at $O(\epsilon^2)$, since for $p = 2$ the second and third terms in the expression for $\Delta_{(\bar\psi\psi)^p}$cancel. This is analogous to the bosonic case treated in [33] where the classically marginal operator $(\phi.\phi)^2$ has the same property.

4.5 Other scalar primaries

In this section we will consider a scalar primary which is not a singlet under the symmetry group $U(\tilde N)$ and calculate its anomalous dimension. In the free theory we consider a scalar of the form

$$\mathcal{O}^{(IJ)} = \bar\psi^I\psi^J - \frac{\delta^{IJ}}{\tilde N}\bar\psi^K\psi^K\,. \tag{4.5.1}$$

In order to calculate the OPE we need the following correlation functions in the free theory:

$$\left\langle \psi^K(x)\bar\psi^I\psi^J(0)\bar\psi^L(z)\right\rangle = -\frac{\delta^{KI}\delta^{JL}\not{x}\not{z}}{x^2z^2}\,, \tag{4.5.2}$$

$$\left\langle \psi^K(x)\bar\psi^I\psi^J(0)\bar\psi^L(\bar\psi^P\psi^P)(z)\right\rangle = -\frac{(\delta^{IK}\delta^{JL} - 2\delta^{KL}\delta^{IJ})\Gamma^\mu(x-z)_\mu}{(x-z)^2z^2}\,. \tag{4.5.3}$$

Therefore for $x \sim 0$, we get

$$\begin{aligned}\left\langle \psi^K(x)\mathcal{O}^{(IJ)}(0)\bar\psi^L(z)\right\rangle &= -\frac{(\delta^{KI}\delta^{JL} - \frac{1}{\tilde N}\delta^{IJ}\delta^{KL})\not{x}\not{z}}{x^2z^2}\,,\\ \left\langle \psi^K(x)\mathcal{O}^{(IJ)}(0)\bar\psi^L(\bar\psi^P\psi^P)(z)\right\rangle &= \frac{(\delta^{KI}\delta^{JL} - \frac{1}{\tilde N}\delta^{IJ}\delta^{KL})\not{z}}{z^4}\,.\end{aligned} \tag{4.5.4}$$

Thus we get the following OPE in the free theory,

$$\psi^K(x)\times\mathcal{O}^{(IJ)}(0)\supset\frac{(\delta^{KI}\delta^{JL}-\frac{1}{\bar{N}}\delta^{IJ}\delta^{KL})}{x^2}\left\{\not{x}\psi^L(0)+\frac{x^2}{1-N}\psi^L(\bar{\psi}^P\psi^P)(0)+\right\}\tag{4.5.5}$$

Now we proceed as before. We assume that there exists an operator $V_{\mathcal{O}^{(LM)}}(x)$ at the fixed point corresponding to the operator $\mathcal{O}^{(LM)}(x)$. Based on the symmetries, the 3-point function involving the scalar at the fixed point is given by

$$\left\langle V_1^I(x_1)\bar{V}_1^K(x_2)V_{\mathcal{O}^{(LM)}}(x_3)\right\rangle=\frac{\tilde{f}'\not{x}_{13}\not{x}_{23}(\delta^{IL}\delta^{KM}-\frac{1}{\bar{N}}\delta^{LM}\delta^{IK})}{(x_{12}^2)^{\Delta_1-\frac{1}{2}\Delta_{(LM)}}(x_{13}^2x_{23}^2)^{\frac{1}{2}\Delta_{(LM)}+\frac{1}{2}}}\tag{4.5.6}$$

The OPE obtained in (4.3.3) should hold in the case of scalar fields. All the corresponding coefficients are given in (4.3.6) except that Δ_2 is replaced by $\Delta_{(LM)}$. Thus in this case,

$$V_1^I(x_1)\times V_{\mathcal{O}^{(LM)}}(x_3)\supset\frac{\tilde{f}\not{x}_{13}(\delta^{IL}\delta^{MK}-\frac{1}{\bar{N}}\delta^{ML}\delta^{IK})}{(x_{13}^2)^{\frac{1}{2}\Delta_{(LM)}+\frac{1}{2}}}\tilde{E}(x_{13},\partial_z)V_1^K(z)|_{z=x_3}+..\tag{4.5.7}$$

with

$$\tilde{E}(x_{13},\partial_z)=A'+\left(B_1'x_{13}^\mu+B_2'\not{x}_{13}\Gamma^\mu\right)\partial_\mu+\left(C_1'x_{13}^\mu x_{13}^\nu+C_2'x_{13}^\mu\not{x}_{13}\Gamma^\nu+C_3'x_{13}^2\Gamma^\mu\Gamma^\nu\right)\partial_\mu\partial_\nu+.....\tag{4.5.8}$$

where the relevant coefficients are

$$A'=-1,\quad B_1'=-\frac{\left(\Delta_1-\frac{1}{2}\Delta_{(LM)}\right)}{\Delta_1+\frac{1}{2}},\quad B_2'=\frac{B_1'}{2\Delta_1+1-d},\tag{4.5.9}$$

We proceed as in previous cases. We find that $\tilde{f}$ should approach -1 in the limit $\epsilon\to 0$. Furthermore the 3-point function with the descendant has the form

$$\begin{aligned}\left\langle V_1^I(x)V_{\mathcal{O}^{(LM)}}(0)\bar{V}_3^P(z)\right\rangle\quad&\sim\quad\frac{\tilde{f}\not{x}(\delta^{IL}\delta^{KM}-\frac{1}{\bar{N}}\delta^{LM}\delta^{IK})}{(x^2)^{\frac{1}{2}\Delta_{(LM)}+\frac{1}{2}}}B_2'(\not{x}\,\Gamma^\mu\partial_\mu)\left\langle V_1^K(0)\bar{V}_3^P(z)\right\rangle\,,\\&=\frac{\tilde{f}(\delta^{IL}\delta^{KM}-\frac{1}{\bar{N}}\delta^{LM}\delta^{IK})B_2'\alpha}{(x^2)^{\frac{1}{2}\Delta_{(LM)}-\frac{1}{2}}}\left\langle V_3^K(0)\bar{V}_3^P(z)\right\rangle\,.\end{aligned}\tag{4.5.10}$$

Now comparing with the free correlator, we find that

$$\tilde{f}B_2'\alpha = -\frac{1}{N-1}\,. \tag{4.5.11}$$

and

$$B_2' = \frac{\pi\big(\gamma_1 - \frac{1}{2}\gamma_{(LM)}\big)}{\gamma_1}, \quad \gamma_1 \sim y_{1,2}\epsilon^2, \quad \gamma_{(LM)} \sim y_{(LM),1}\epsilon\,. \tag{4.5.12}$$

which implies that

$$y_{(LM),1} = \frac{1}{N-2}\,. \tag{4.5.13}$$

Therefore the leading order anomalous dimension is

$$\gamma_{\mathcal{O}^{(IJ)}} = \frac{1}{N-2}\epsilon\,. \tag{4.5.14}$$

We could not find a check for this result in the literature. It would be interesting to compare this new result against a perturbative computation of the anomalous dimension.

4.6 Discussion

In this note we have computed, to first order in the epsilon expansion, the anomalous dimensions of a class of composite operators in the Gross-Neveu model. As emphasised earlier, we have done the computation without using the usual perturbative techniques. The primary input was conformal symmetry, which fixed for us the two and three point functions and the required OPEs. The main results, which, to our knowledge, have not been known before, are given in eq. (4.4.45), . It is to be emphasised that the methods used here can fix only the *leading* order anomalous dimensions. It would be interesting to extend the computations to second order in ϵ. As discussed in [33] for the case of the $O(N)$ bosonic vector model, two and three point functions would not suffice for the higher order computation and one would require conformal bootstrap of the four point functions to extract further information.

4.7 Appendix

4.7.1 Computation of f_{2p} and ρ_{2p}

Here we follow the diagrammatic method [87] to compute the combinatorial factors appearing in the OPEs (4.4.2), (4.4.3). A typical diagram will look like

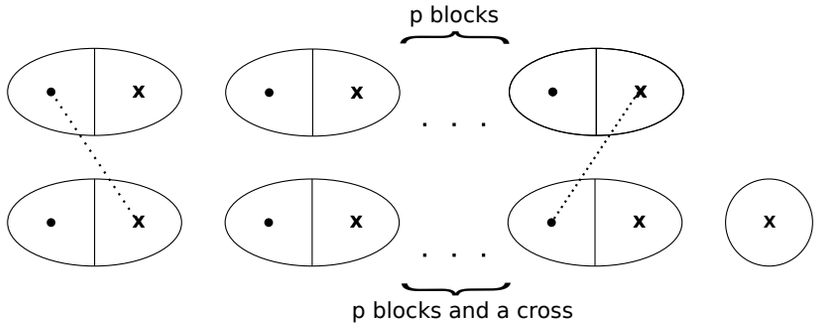

where each block refers to a $\overline{\psi}.\psi$ pair, $\overline{\psi}$ is denoted by $\bullet$ and ψ by $\times$, and each line denotes a contraction. Further we follow the convention that the top row corresponds to the operator at x and the lower one corresponds to the operator at origin. In order to compute the combinatorial factors we need to count all possible contractions, carefully picking up (-1) factors whenever we move a fermionic operator through the other operator. To compute the combinatorial factors our strategy will be to set up recursion relations. For this we contract one block at a time from the top row with the blocks at the bottom row. The contribution of a given contraction is given by following rules:

1. While contracting we always keep the block at the position x on the left of the block at the origin.

2. A diagram involving a complete loop will give a factor of $+N$ to the combinatorial factor.

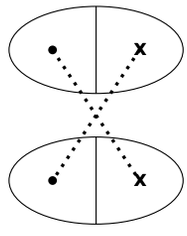

3. Two blocks contracting to the same block results in one block with -1 factor.

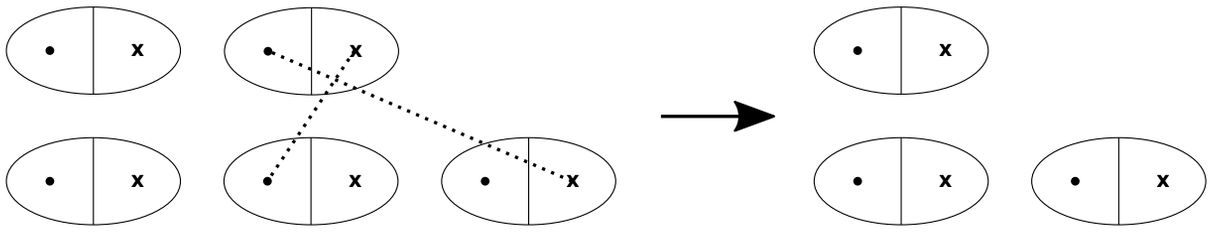

To compute f_{2p} we need to contract p pairs of ψ's and finally leave ψ^I. We will get the following three diagrams. In these diagrams the top row has p blocks at x and bottom row has p blocks together with one $\times$ at origin.

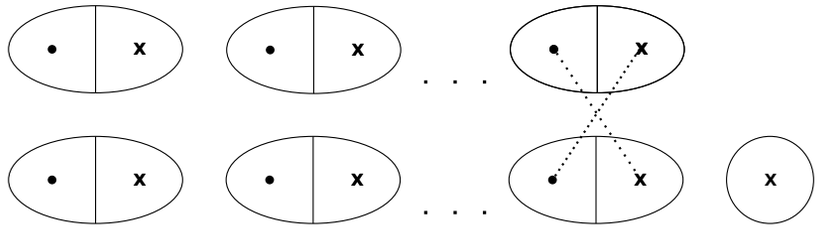

The contribution of the above diagram is $p\tilde{N}\,\mathrm{Tr}\{\mathbb{I}\} = pN$.

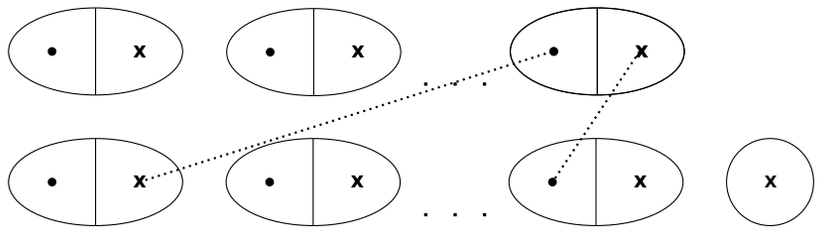

The contribution of the above diagram is just $-p(p-1)$,

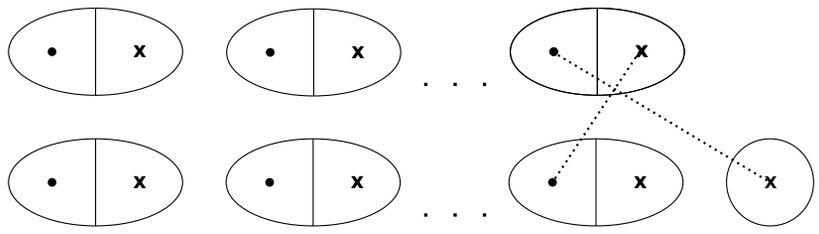

The contribution of this diagram is just $-p$. Therefore the recursion relation is

$$f_{2p} = [pN - p(p-1) - p]f_{2(p-1)} = [pN - p^2]f_{2(p-1)} \tag{4.7.1}$$

For $p = 1$, we can see that $f_2 = (N - 1)$, so

$$f_{2(p)} = \prod_{i=1}^{p} i(N - i)\,. \tag{4.7.2}$$

To get a recursion relation for $f_{2p}\rho_{2p}$, the strategy is to first draw one line, and then proceed recursively by drawing two lines. To draw one line, we have three diagrams, but the first two diagrams

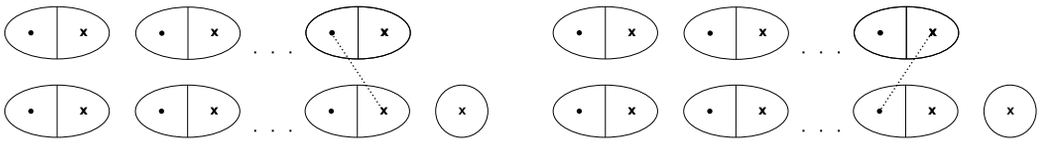

cancel each other, and only the third diagram

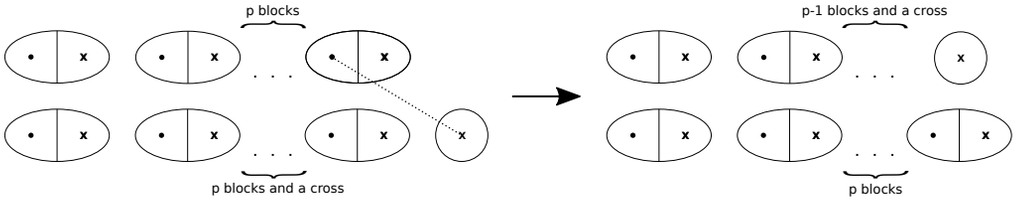

will contribute as $-p$. Next we need to compute the contribution, g_{2p}, from the new diagram,

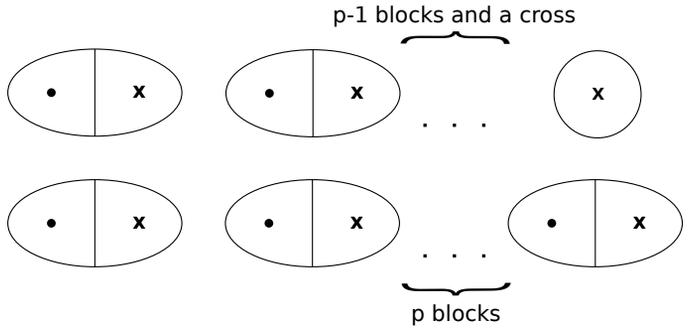

which can be recursively reduced by contracting one block on the top and bottom row, by drawing two lines,

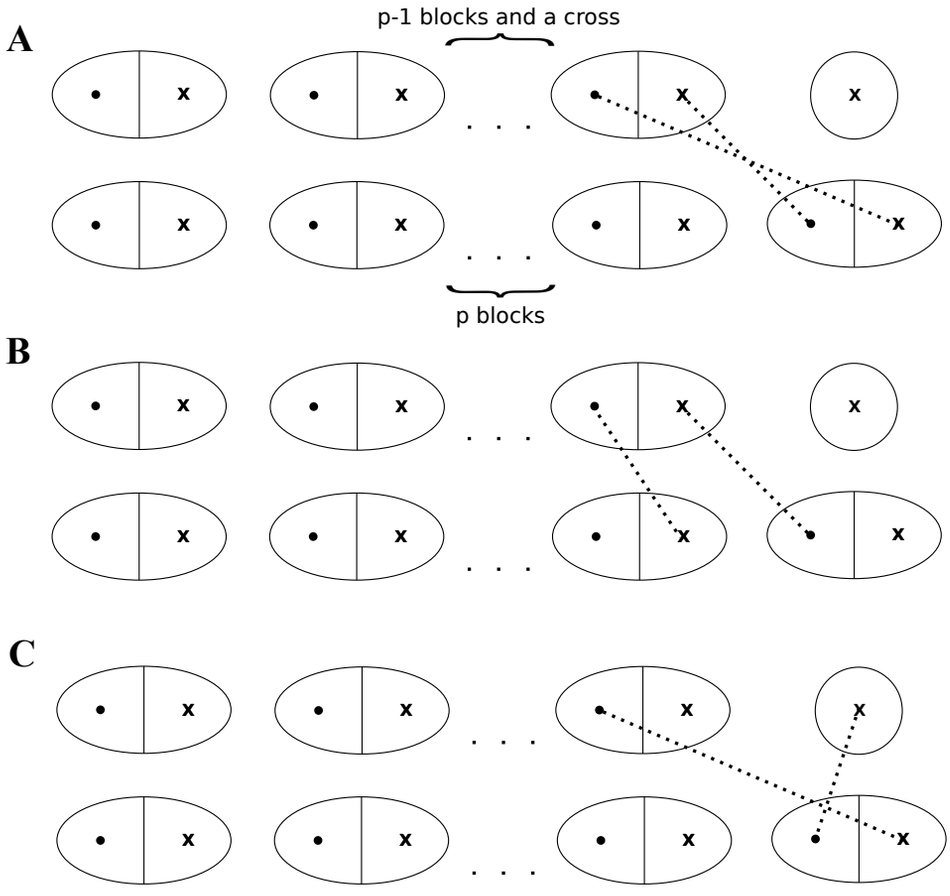

The contribution from **A** is pN, from **B** is $-p(p-1)$ and from **C** is $-p$. Therefore the recursion relation for g_{2p} is

$$g_{2p} = \left(pN - p^2\right) g_{2(p-1)} \,. \tag{4.7.3}$$

Knowing $g_2 = 1$,

$$g_{2p} = \prod_{i=2}^{p} i\,(N-i) \,. \tag{4.7.4}$$

Since, $f_{2p}\rho_{2p} = -p(g_{2p})$, we get

$$\rho_{2p} = \frac{-p(g_{2p})}{f_{2p}} = -\frac{p}{N-1} \,. \tag{4.7.5}$$

4.7.2 Computation of f_{2p+1} and ρ_{2p+1}

The setup is,

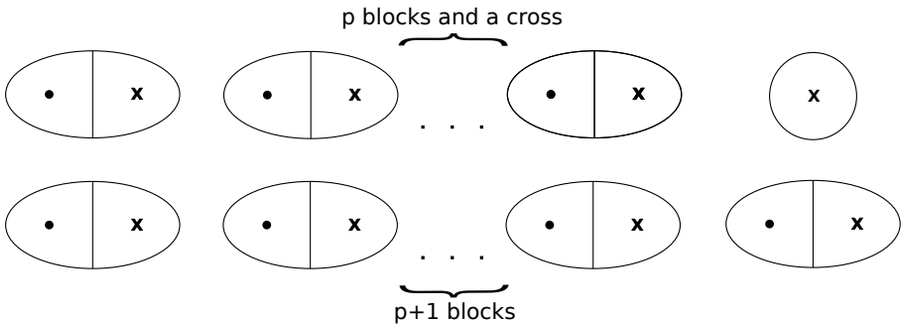

and we need to draw $(2p+1)$ lines. Analogous to the ρ_{2p} computation, we first contract one line involving the cross, to give a factor of $+(p+1)$ and the diagram

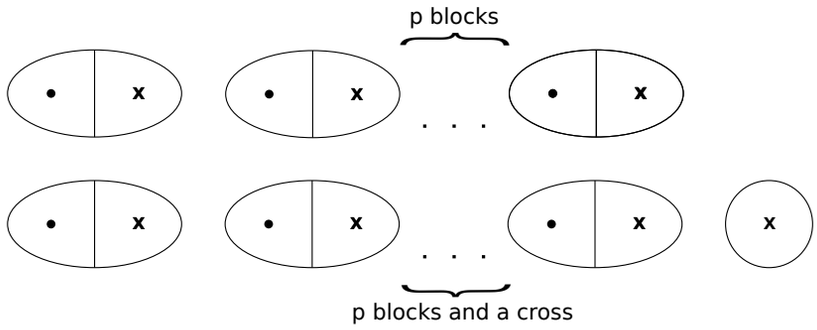

which is nothing but f_{2p}. Therefore,

$$f_{2p+1} = (p+1) f_{2p} = (p+1) \prod_{i=1}^{p} i(N-i)\,. \tag{4.7.6}$$

For the computation of $f_{2p+1}\rho_{2p+1} = \tilde{g}_{2p+1}$, we notice that the diagram is exactly same as that for $g_{2(p+1)}$. Therefore,

$$\tilde{g}_{2p+1} = g_{2(p+1)} = \prod_{i=2}^{p+1} i(N-i)\,. \tag{4.7.7}$$

So,

$$\rho_{2p+1} = \frac{\tilde{g}_{2p+1}}{f_{2p+1}} = \frac{N-(p+1)}{N-1}\,. \tag{4.7.8}$$

Summary and Future Work

To summarize, this thesis presents few approaches to understand open QFTs. Repeating myself, Open QFTs are extremely difficult problems, and the work presented here is just few humble approaches, to study them. In future, these technologies can be extended for deeper insights into the problem. Based on the thesis, I am currently working along the following directions :

- A computationally more efficient way of studying complex actions is needed. Also the physical world being $3+1$ d, it is not always possible to reduce it to a simple matrix theory. One needs to simulate complex actions on $R^{3,1}$ manifold, and one such approach is using Thimbles. Using thimbles, we can also study dynamical symmetry breaking and dimensional reduction higher dimensional QFTs.

- To further study the MSS conjecture of bound on quantum chaos, it is interesting to compute Lyapunov exponent for higher-point OTOC in Black Hole geometry and SYK model and see if the conjectured value satisfies in these cases. For this one can consider, multiple shock waves in a black hole background and see if it's saturating the bound mentioned in [2]. Similarly, considering higher point correlators in SYK model, and computing it's late-time behaviour could be studied. For instance, a full analytic expression for six-point correlator in SYK model, could be computed and the Lyapunov exponent can be extracted in the maximally out-of-time-ordered configuration.

- To study analytically higher order anomalous dimensions of CFTs, it turns out Mellin-space representation is quite useful. Although(at the time of writing this thesis) lot of work has been done in scalar field theories, not much has been done in Fermionic CFTs. It would be interesting to develop Mellin-space representation for generic Fermionic CFTs.

References

[1] Pallab Basu, Kasi Jaswin, and Anosh Joseph. Complex langevin dynamics in large n unitary matrix models. 2018.

[2] Pallab Basu and Kasi Jaswin. Higher point otocs and the bound on chaos. 2018.

[3] Sudip Ghosh, Rajesh Kumar Gupta, Kasi Jaswin, and Amin A. Nizami. -expansion in the gross-neveu model from conformal field theory. *Journal of High Energy Physics*, 2016(3), mar 2016.

[4] Juan Martin Maldacena. The Large N limit of superconformal field theories and supergravity. *Int. J. Theor. Phys.*, 38:1113–1133, 1999. [Adv. Theor. Math. Phys.2,231(1998)].

[5] Edward Witten. Anti-de Sitter space and holography. *Adv. Theor. Math. Phys.*, 2:253–291, 1998.

[6] S.S. Gubser, I.R. Klebanov, and A.M. Polyakov. Gauge theory correlators from non-critical string theory. *Physics Letters B*, 428(1-2):105–114, May 1998.

[7] A. Kitaev. A simple model of quantum holography. http://online.kitp.ucsb.edu/online/entangled15/kitaev/,http://online.kitp.ucsb.edu/online/entangled15/kitaev2/. Talks at KITP, April 7, 2015 and May 27, 2015.

[8] Subir Sachdev and Jinwu Ye. Gapless spin fluid ground state in a random, quantum Heisenberg magnet. *Phys. Rev. Lett.*, 70:3339, 1993.

[9] Edward Witten. An syk-like model without disorder.

[10] Razvan Gurau. A review of the 1/n expansion in random tensor models.

[11] Igor R. Klebanov and Grigory Tarnopolsky. Uncolored random tensors, melon diagrams, and the syk models.

[12] J. R. Klauder. STOCHASTIC QUANTIZATION. *Acta Phys. Austriaca Suppl.*, 25:251–281, 1983.

[13] G. Parisi. ON COMPLEX PROBABILITIES. *Phys. Lett.*, 131B:393–395, 1983.

[14] Gert Aarts and Ion-Olimpiu Stamatescu. Stochastic quantization at finite chemical potential. *JHEP*, 09:018, 2008.

[15] Cengiz Pehlevan and Gerald Guralnik. Complex Langevin Equations and Schwinger-Dyson Equations. *Nucl. Phys.*, B811:519–536, 2009.

[16] Yuta Ito and Jun Nishimura. The complex Langevin analysis of spontaneous symmetry breaking induced by complex fermion determinant. *JHEP*, 12:009, 2016.

[17] Gert Aarts. Can stochastic quantization evade the sign problem? The relativistic Bose gas at finite chemical potential. *Phys. Rev. Lett.*, 102:131601, 2009.

[18] Gert Aarts and Frank A. James. Complex Langevin dynamics in the SU(3) spin model at nonzero chemical potential revisited. *JHEP*, 01:118, 2012.

[19] D. J. Gross and Edward Witten. Possible Third Order Phase Transition in the Large N Lattice Gauge Theory. *Phys. Rev.*, D21:446–453, 1980.

[20] Spenta R. Wadia. A Study of U(N) Lattice Gauge Theory in 2-dimensions. 2012.

[21] Simon Hands, Timothy J. Hollowood, and Joyce C. Myers. QCD with Chemical Potential in a Small Hyperspherical Box. *JHEP*, 07:086, 2010.

[22] Patrick Hayden and John Preskill. Black holes as mirrors: Quantum information in random subsystems. *JHEP*, 09:120, 2007.

[23] Yasuhiro Sekino and Leonard Susskind. Fast Scramblers. *JHEP*, 10:065, 2008.

[24] Juan Maldacena, Stephen H. Shenker, and Douglas Stanford. A bound on chaos. *JHEP*, 08:106, 2016.

[25] Stephen H. Shenker and Douglas Stanford. Black holes and the butterfly effect. *JHEP*, 03:067, 2014.

[26] Daniel A. Roberts and Douglas Stanford. Two-dimensional conformal field theory and the butterfly effect. *Phys. Rev. Lett.*, 115(13):131603, 2015.

[27] Juan Maldacena and Douglas Stanford. Remarks on the Sachdev-Ye-Kitaev model. *Phys. Rev.*, D94(10):106002, 2016.

[28] Riccardo Rattazzi, Vyacheslav S. Rychkov, Erik Tonni, and Alessandro Vichi. Bounding scalar operator dimensions in 4D CFT. *JHEP*, 12:031, 2008.

[29] Sheer El-Showk, Miguel F. Paulos, David Poland, Slava Rychkov, David Simmons-Duffin, and Alessandro Vichi. Solving the 3d Ising Model with the Conformal Bootstrap II. c-Minimization and Precise Critical Exponents. *Journal of Statistical Physics*, 157:869, 2014.

[30] Sheer El-Showk, Miguel F. Paulos, David Poland, Slava Rychkov, David Simmons-Duffin, and Alessandro Vichi. Solving the 3d ising model with the conformal bootstrap. *Phys. Rev. D*, 86:025022, Jul 2012.

[31] Sheer El-Showk, Miguel F. Paulos, David Poland, Slava Rychkov, David Simmons-Duffin, and Alessandro Vichi. Solving the 3d ising model with the conformal bootstrap ii.

$$c$$

c -minimization and precise critical exponents. *Journal of Statistical Physics*, 157(4-5):869–914, Jun 2014.

[32] Rajesh Gopakumar, Apratim Kaviraj, Kallol Sen, and Aninda Sinha. Conformal Bootstrap in Mellin Space. *Phys. Rev. Lett.*, 118(8):081601, 2017.

[33] Slava Rychkov and Zhong Ming Tan. The ϵ-expansion from conformal field theory. *J. Phys.*, A48(29):29FT01, 2015.

[34] Shin Muroya, Atsushi Nakamura, Chiho Nonaka, and Tetsuya Takaishi. Lattice QCD at finite density: An Introductory review. *Prog. Theor. Phys.*, 110:615–668, 2003.

[35] Philippe de Forcrand. Simulating QCD at finite density. *PoS*, LAT2009:010, 2009.

[36] John R. Klauder. Coherent State Langevin Equations for Canonical Quantum Systems With Applications to the Quantized Hall Effect. *Phys. Rev.*, A29:2036–2047, 1984.

[37] Marco Cristoforetti, Francesco Di Renzo, and Luigi Scorzato. New approach to the sign problem in quantum field theories: High density QCD on a Lefschetz thimble. *Phys. Rev.*, D86:074506, 2012.

[38] H. Fujii, D. Honda, M. Kato, Y. Kikukawa, S. Komatsu, and T. Sano. Hybrid Monte Carlo on Lefschetz thimbles - A study of the residual sign problem. *JHEP*, 10:147, 2013.

[39] Francesco Di Renzo and Giovanni Eruzzi. Thimble regularization at work: from toy models to chiral random matrix theories. *Phys. Rev.*, D92(8):085030, 2015.

[40] Yuya Tanizaki, Yoshimasa Hidaka, and Tomoya Hayata. Lefschetz-thimble analysis of the sign problem in one-site fermion model. *New J. Phys.*, 18(3):033002, 2016.

[41] Hirotsugu Fujii, Syo Kamata, and Yoshio Kikukawa. Monte Carlo study of Lefschetz thimble structure in one-dimensional Thirring model at finite density. *JHEP*, 12:125, 2015. [Erratum: JHEP09,172(2016)].

[42] Andrei Alexandru, Gök çe Başar, and Paulo Bedaque. Monte carlo algorithm for simulating fermions on lefschetz thimbles. *Phys. Rev. D*, 93:014504, Jan 2016.

[43] John R. Klauder. A Langevin Approach to Fermion and Quantum Spin Correlation Functions. *J. Phys.*, A16:L317, 1983.

[44] J. Berges and I. O. Stamatescu. Simulating nonequilibrium quantum fields with stochastic quantization techniques. *Phys. Rev. Lett.*, 95:202003, 2005.

[45] J. Berges, Sz. Borsanyi, D. Sexty, and I. O. Stamatescu. Lattice simulations of real-time quantum fields. *Phys. Rev.*, D75:045007, 2007.

[46] Juergen Berges and Denes Sexty. Real-time gauge theory simulations from stochastic quantization with optimized updating. *Nucl. Phys.*, B799:306–329, 2008.

[47] J. Bloch, J. Glesaaen, J. J. M. Verbaarschot, and S. Zafeiropoulos. Complex Langevin Simulation of a Random Matrix Model at Nonzero Chemical Potential. 2017.

[48] Gert Aarts. Complex Langevin dynamics at finite chemical potential: Mean field analysis in the relativistic Bose gas. *JHEP*, 05:052, 2009.

[49] Gert Aarts and K. Splittorff. Degenerate distributions in complex Langevin dynamics: one-dimensional QCD at finite chemical potential. *JHEP*, 08:017, 2010.

[50] Yuta Ito and Jun Nishimura. Spontaneous symmetry breaking induced by complex fermion determinant — yet another success of the complex Langevin method. *PoS*, LATTICE2016:065, 2016.

[51] Konstantinos N. Anagnostopoulos, Takehiro Azuma, Yuta Ito, Jun Nishimura, and Stratos Kovalkov Papadoudis. Complex Langevin analysis of the spontaneous symmetry breaking in dimensionally reduced super Yang-Mills models. *JHEP*, 02:151, 2018.

[52] G. Parisi and Yong-shi Wu. Perturbation Theory Without Gauge Fixing. *Sci. Sin.*, 24:483, 1981.

[53] Poul H. Damgaard and Helmuth Huffel. Stochastic Quantization. *Phys. Rept.*, 152:227, 1987.

[54] Gert Aarts, Erhard Seiler, and Ion-Olimpiu Stamatescu. The Complex Langevin method: When can it be trusted? *Phys. Rev.*, D81:054508, 2010.

[55] Gert Aarts, Frank A. James, Erhard Seiler, and Ion-Olimpiu Stamatescu. Complex Langevin: Etiology and Diagnostics of its Main Problem. *Eur. Phys. J.*, C71:1756, 2011.

[56] Gert Aarts, Pietro Giudice, and Erhard Seiler. Localised distributions and criteria for correctness in complex Langevin dynamics. *Annals Phys.*, 337:238–260, 2013.

[57] Spenta R. Wadia. N = Infinity Phase Transition in a Class of Exactly Soluble Model Lattice Gauge Theories. *Phys. Lett.*, 93B:403–410, 1980.

[58] P. V. Buividovich, Gerald V. Dunne, and S. N. Valgushev. Complex Path Integrals and Saddles in Two-Dimensional Gauge Theory. *Phys. Rev. Lett.*, 116(13):132001, 2016.

[59] Marcos Marino. Les Houches lectures on matrix models and topological strings. 2004.

[60] https://dlmf.nist.gov/4.13.

[61] Bo Sundborg. The Hagedorn transition, deconfinement and N=4 SYM theory. *Nucl. Phys.*, B573:349–363, 2000.

[62] Ofer Aharony, Joseph Marsano, Shiraz Minwalla, Kyriakos Papadodimas, and Mark Van Raamsdonk. The Hagedorn - deconfinement phase transition in weakly coupled large N gauge theories. *Adv. Theor. Math. Phys.*, 8:603–696, 2004. [,161(2003)].

[63] Luis Alvarez-Gaume, Cesar Gomez, Hong Liu, and Spenta Wadia. Finite temperature effective action, AdS(5) black holes, and 1/N expansion. *Phys. Rev.*, D71:124023, 2005.

[64] Luis Alvarez-Gaume, Pallab Basu, Marcos Marino, and Spenta R. Wadia. Blackhole/String Transition for the Small Schwarzschild Blackhole of AdS(5)x S**5 and Critical Unitary Matrix Models. *Eur. Phys. J.*, C48:647–665, 2006.

[65] Thomas D . Cohen. Functional integrals for QCD at nonzero chemical potential and zero density. *Phys. Rev. Lett.*, 91:222001, 2003.

[66] Simon Hands, Seyong Kim, and Jon-Ivar Skullerud. A Quarkyonic Phase in Dense Two Color Matter? *Phys. Rev.*, D81:091502, 2010.

[67] Pallab Basu and Anindya Mukherjee. Dissolved deconfinement: Phase Structure of large N gauge theories with fundamental matter. *Phys. Rev.*, D78:045012, 2008.

[68] Daniel A. Roberts, Douglas Stanford, and Leonard Susskind. Localized shocks. *JHEP*, 03:051, 2015.

[69] Stephen H. Shenker and Douglas Stanford. Multiple Shocks. *JHEP*, 12:046, 2014.

[70] Stephen H. Shenker and Douglas Stanford. Stringy effects in scrambling. *JHEP*, 05:132, 2015.

[71] Gustavo Turiaci and Herman Verlinde. On CFT and Quantum Chaos. *JHEP*, 12:110, 2016.

[72] A Kitaev. Hidden correlations in the hawking radiation and thermal noise. http://online.kitp.ucsb.edu/online/joint98/kitaev/options.html, 2014. talk given at Fundamental Physics Prize Symposium, Nov. 10, 2014.

[73] Joseph Polchinski and Vladimir Rosenhaus. The Spectrum in the Sachdev-Ye-Kitaev Model. *JHEP*, 04:001, 2016.

[74] Felix M. Haehl, R. Loganayagam, Prithvi Narayan, and Mukund Rangamani. Classification of out-of-time-order correlators. 2017.

[75] Felix M. Haehl, R. Loganayagam, Prithvi Narayan, Amin A. Nizami, and Mukund Rangamani. Thermal out-of-time-order correlators, KMS relations, and spectral functions. *JHEP*, 12:154, 2017.

[76] Felix M. Haehl and Moshe Rozali. Fine Grained Chaos in AdS_2 Gravity. *Phys. Rev. Lett.*, 120(12):121601, 2018.

[77] Felix M. Haehl and Moshe Rozali. Effective Field Theory for Chaotic CFTs. 2018.

[78] Naoto Tsuji, Philipp Werner, and Masahito Ueda. Exact out-of-time-ordered correlation functions for an interacting lattice fermion model. *Phys. Rev.*, A95(1):011601, 2017.

[79] Naoto Tsuji, Tomohiro Shitara, and Masahito Ueda. Bound on the exponential growth rate of out-of-time-ordered correlators. 2017.

[80] Nicole Yunger Halpern, Brian Swingle, and Justin Dressel. Quasiprobability behind the out-of-time-ordered correlator. *Phys. Rev. A*, 97:042105, Apr 2018.

[81] Justin Dressel, José Raúl González Alonso, Mordecai Waegell, and Nicole Yunger Halpern. Strengthening weak measurements of qubit out-of-time-order correlators. *Phys. Rev. A*, 98:012132, Jul 2018.

[82] Nicole Yunger Halpern, Anthony Bartolotta, and Jason Pollack. Reconciling two notions of quantum operator disagreement: Entropic uncertainty relations and information scrambling, united through quasiprobabilities. 2018.

[83] Chethan Krishnan, Sambuddha Sanyal, and P. N. Bala Subramanian. Quantum Chaos and Holographic Tensor Models. *JHEP*, 03:056, 2017.

[84] Chethan Krishnan, K. V. Pavan Kumar, and Sambuddha Sanyal. Random Matrices and Holographic Tensor Models. *JHEP*, 06:036, 2017.

[85] E. Pharagmén and Ernst Lindelöf. Sur une extension d'un principe classique de l'analyse et sur quelques propriétés des fonctions monogènes dans le voisinage d'un point singulier. *Acta Math.*, 31:381–406, 1908.

[86] Paul Garrett. *Modern Analysis of Automorphic Forms By Example*, volume 1, Appendix 3.B of *Cambridge Studies in Advanced Mathematics*. Cambridge University Press, 2018.

[87] Pallab Basu and Chethan Krishnan. ϵ-expansions near three dimensions from conformal field theory. *Journal of High Energy Physics*, 2015(11):40, 2015.

[88] David J. Gross and André Neveu. Dynamical symmetry breaking in asymptotically free field theories. *Phys. Rev. D*, 10(10):3235–3253, November 1974.

[89] Moshe Moshe and Jean Zinn-Justin. Quantum field theory in the large n limit: a review.

[90] Proof of the absence of multiplicative renormalizability of the Gross-Neveu model in the dimensional regularization d =2+2 ε | SpringerLink. https://link.springer.com/article/10.1007/BF02634015.

[91] A. N. Vasil'ev and M. I. Vyazovsky. Proof of the absence of multiplicative renormalizability of the Gross-Neveu model in the dimensional regularizationd=2+2ε. *Theor Math Phys*, 113(1):1277–1288, October 1997.

[92] Anastasios C. Petkou. Operator product expansions and consistency relations in a O(N) invariant fermionic CFT for $2 < d < 4$. *Physics Letters B*, 389(1):18–28, December 1996.

[93] Alessandro Bondi, Guiseppe Curci, Giampiero Paffuti, and Paolo Rossi. Metric and central charge in the perturbative approach to two dimensional fermionic models. *Annals of Physics*, 199(2):268–339, May 1990.

[94] Conformal Quantum Field Theory in D-dimensions | E.S. Fradkin | Springer. https://www.springer.com/gp/book/9780792341581.